NUMERICAL MODELING OF THE TEST PIT FOR FALLING WEIGHT DEFLECTOMETER

FHWA/MT-21-010/9921-806

Final Report

prepared for
THE STATE OF MONTANA
DEPARTMENT OF TRANSPORTATION

in cooperation with
THE U.S. DEPARTMENT OF TRANSPORTATION
FEDERAL HIGHWAY ADMINISTRATION

December 2021

prepared by
Mohammadhossein Sadeghiamirshahidi, Ph.D., A.M. ASCE.
Marvin Speece, Ph.D.

Montana
Technological
University
Butte, MT

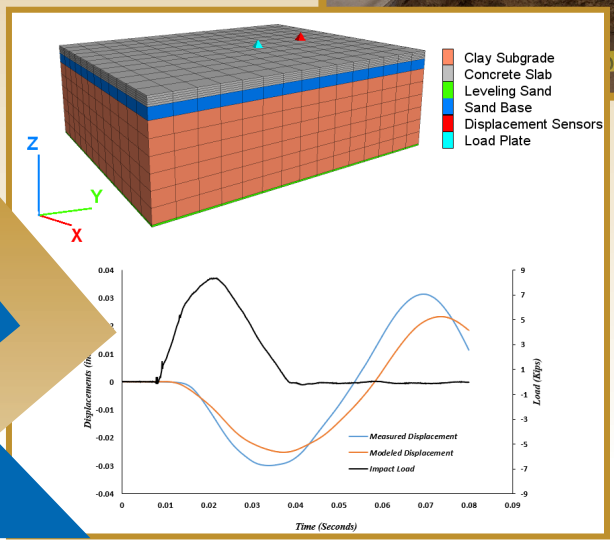

RESEARCH PROGRAMS

MONTANA
Department of Transportation

Numerical Modeling of the Test Pit for Falling Weight Deflectometer Calibration

Final Report

by

Mohammadhossein Sadeghiamirshahidi, Ph.D., A.M. ASCE.
Assistant Professor, Geological Engineering
Marvin Speece, Ph.D.
Professor, Geophysics

Affiliation
Montana Technological University

Submitted to:

Montana Department of Transportation
2701 Prospect Avenue
P.O. Box 201001
Helena, MT 59620-1001

11/24/2021

TECHNICAL REPORT DOCUMENTATION PAGE

1. Report No. FHWA/MT-21-010/9921-806	**2. Government Accession No.**	**3. Recipient's Catalog No.**
4. Title and Subtitle Numerical Modeling of the Test Pit for Falling Weight Deflectometer Calibration		**5. Report Date** November 24, 2021 **6. Performing Organization Code**
7. Author(s) Mohammadhossein Sadeghiamirshahidi, Ph.D., A.M. ASCE. https://orcid.org/0000-0002-5266-3522 Marvin Speece, Ph.D.		**8. Performing Organization Report No.**
9. Performing Organization Name and Address Montana Technological University, 1300 West Park Street Butte, MT 59701		**10. Work Unit No.** **11. Contract or Grant No.** Contract # 9921-806
12. Sponsoring Agency Name and Address Research Programs Montana Department of Transportation (SPR) 2701 Prospect Avenue PO Box 201001		**13. Type of Report and Period Covered** Final report (November 19, 2020-November 24, 2021) **14. Sponsoring Agency Code** 5401

15. Supplementary Notes
Conducted in cooperation with the U.S. Department of Transportation, Federal Highway Administration. This report can be found at https://www.mdt.mt.gov/research/projects/tpfwdc.aspx.

Recommended Citation: Mohammadhossein Sadeghiamirshahidi (0000-0002-5266-3522) and Marvin Speece. Numerical Modeling of the Test Pit for Falling Weight Deflectometer Calibration. United States. Montana Department of Transportation. Montana Technological University https://doi.org/10.21949/1518319.

16. Abstract
Montana Department of Transportation (MDT) planned to replace the soft clay layer of their test pit for Falling Weight Deflectometer (FWD) calibration with a geofoam layer hoping to increase the operational lifetime of the test pit. In this research, the possibility of replacing the clay layer with a geofoam layer was investigated using dynamic response analyses. A three-dimensional explicit finite volume model was developed and calibrated using the results of previous calibration tests conducted by MDT. The model was then used to determine if the geofoam can be used instead of clay as the soft layer in the FWD calibration test pit. Based on the results of the numerical models, it was concluded that geofoam can be used instead of the clay layer. In fact, 30 different setups were designed using two types of geofoam, i.e., EPS 19 and EPS 29. A decision matrix analyses approach was proposed to rank these designs from best to worst based on five criteria, i.e., AASHTO R32-11 maximum deflection requirements, reducing the possible noise, proper damping, construction cost, and variability. Based on the proposed decision matrix analyses it was determined that the best 12 ft wide-15 ft long geofoam setup would be composed of a 28 (in.) thick geofoam EPS 19, overlaying 3 (in.) of sand at the bottom of the test pit, and 23 (in.) of sand above the geofoam layer. A 5 (in.) thick concrete slab would be placed on the top of this setup.

17. Key Words Falling Weight Deflectometers, Numerical Analysis, Polystyrene (Geofoam)	**18. Distribution Statement** No restrictions. This document is available through the National Technical Information Service, Springfield, VA 22161.		
19. Security Classif. (of this report) Unclassified	**20. Security Classif. (of this page)** Unclassified	**21. No. of Pages** 125	**22. Price**

Form DOT F 1700.7 (8-72) Reproduction of completed page authorized

TABLE OF CONTENTS

1. LIST OF TABLES

2. LIST OF FIGURES

3. PROBLEM STATEMENT

Evaluation of pavement sections is commonly conducted using the deflection data from Falling Weight Deflectometer (FWD) tests. The reliability of these evaluations is highly dependent on the accuracy of the measured deflections. Therefore, to ensure the desired accuracy of measured deflections, FWDs undergo annual calibration and monthly relative calibrations. These calibrations are conducted according to AASHTO R32-11 [1]. The calibration tests are conducted on an indoor test pit made of a concrete slab underlaid by a base and a soft subgrade.

The calibration facility operated by the Montana Department of Transportation (MDT) has used a 12 ft wide, 15 ft long, and 5 in thick concrete slab overlying a 6-in thick sandy base and a 4-ft thick clay subgrade (R32 design, Figure 1). The measured deflections during calibration tests conducted by MDT on this test pit met the deflection requirements laid out by AASHTO R32-11 for a few years, after which the test area needed to be replaced. Because rebuilding the test area is both costly and time-consuming, the MDT was interested in a new design that could operate over longer periods. MDT designed an alternative to the R32 design, using geofoam instead of the clay layer as the soft subgrade (Figure 2).

Figure 1. Schematic as-built cross-section of the MDT's original testing area (not to scale).

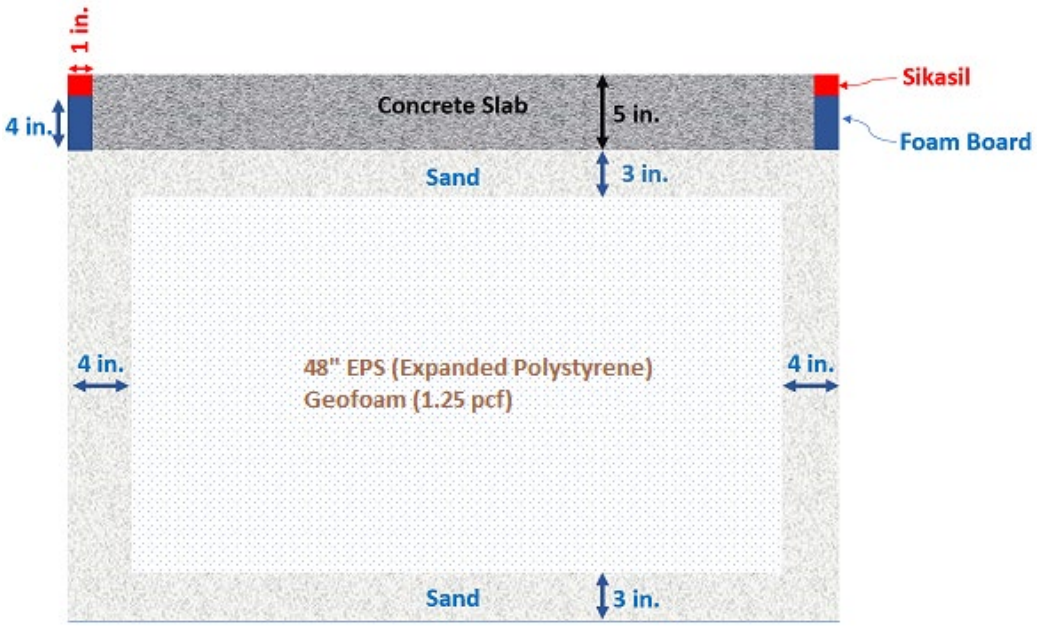

Figure 2. Schematic as-built cross-section of the MDT's preliminary alternative testing area (not to scale).

The alternative calibration test pit (geofoam test pit) was designed based on static analyses. The designed test area was constructed, and several FWD calibration tests were conducted. The new setup did not meet all the AASHTO R32-11 deflection requirements. According to AASHTO R32-11, a deflection of 0.012 (in.) or more due to a 16 (kip) impact load is required for preliminary screening of a potential test area. Therefore, the recorded 0.024 (in.) maximum deflection of the original clay setup due to a 15.14 (kip) impact load was considered acceptable. It is worth noting that this deflection was twice the minimum required deflection suggested by AASHTO R32-11. However, the recorded 0.042 (in.) maximum deflection of the geofoam setup due to a 15.14 (kip) impact load, which is twice the recorded deflection of the clay setup and four times the minimum deflection required by AASHTO R32-11, was considered excessive. Also, some deflections (noise) upon initiation of the falling weight (before the weight actually hits the plate) were detected by the accelerometers during the calibration tests conducted on the geofoam test pit. The purpose of this study is to use dynamic response analyses to investigate the possibility of using geofoam instead of the clay layer in the test pit. If the results of the investigation reveal that geofoam can in fact be used, the next goal of this study will be to modify the preliminary alternative design and provide recommendations to improve the performance of the test area to where it meets the AASHTO R32-11 deflection requirements.

4. BACKGROUND AND LITERATURE REVIEW

Management of pavement systems, at the project or network level, relies on the structural evaluation of pavements which entails approximating the remaining pavement life, estimating load-supporting capacity, and calculating the required thickness of structural overlays. Deflection data from Falling Weight Deflectometers (FWDs) are the basis of such evaluations [2]. For example, one of the key inputs in deterministic physical models used in pavement structural analyses is the moduli of elasticity of the pavement layers [3]. The pavement deflection measured from FWD tests is used to back-calculate the layers' moduli [4–11]. The reliability of the back-calculated moduli, and any analyses conducted based on those moduli, directly depends on the accuracy of the measured deflections. Annual calibration and monthly relative calibrations of the FWDs are therefore necessary to ensure the desired accuracy of the measured deflections. These calibrations are conducted according to AASHTO R32-11 [1] to establish calibration factors for correcting FWD measurements.

AASHTO R32-11 requires the calibration facility to be an indoor space with a constant temperature between 50 and 100°F, heated, but not necessarily air-conditioned. The calibration tests are conducted on a concrete slab with a smooth and crack-free surface. The concrete slab does not have to be isolated from the surrounding floor provided that the deflection characteristics and other requirements for the facility are met. The suggested dimensions for the concrete slab by AASHTO R32-11 are 12 ft by 15 ft (with an 8 ft wide clear zone around the perimeter).

The required deflections in the concrete slab, i.e., 0.012 in or more due to a 16,000-lb load, is generally achieved by using a 5 in thick Portland cement concrete slab underlaid by 8 in of open-graded crushed aggregate base and relatively weak subgrade (subgrade modulus < 12,000 psi when the bedrock is deeper than 25 ft., and subgrade modulus < 7500 psi when the bedrock is between 10 to 25 ft deep, and areas with bedrock located shallower than 10 ft are not recommended).

The calibration facility operated by MDT has used a test pit setup shown in Figure 1. Although the AASHTO's deflection requirements were met using this setup, the short lifetime of the test pit inspired a new more durable test pit design. In their first attempt at designing such a setup, MDT designed an alternative to the R32 design based on static analysis, where they used geofoam instead of the clay subgrade (Figure 2). When tested, the new geofoam test area did not meet the AASHTO R32-11 deflection requirements. Static analyses usually neglect the slab mass and subgrade's damping, despite their importance in the dynamic response of structural elements [12]. Three-dimensional dynamic models, on the other hand, are able to incorporate these crucial factors. For example, one such model has been developed by Kuo et al. [13] and was used to calibrate the back-calculation of pavement layers' stiffnesses. Their model confirmed that subgrade damping and self-weight of the slab which are ignored in static analyses have in fact a significant effect on the results. According to their findings, boundary conditions are another significant factor in modeling FWD deflections. In other research, Foinquinos et al., [14] studied the response of pavements under deflection basin tests (e.g., FWD) and wave propagation tests (e.g., Spectral Analysis of Surface Waves test). Their results confirmed that the magnitude and shape of the deflection basins developed by the FWD tests are affected by the dynamic response of the pavement system and are significantly different from the basins developed by static conditions.

Mallela and George [15] developed a three-dimensional finite element model to study the behavior of pavements under dynamic loading. They first conducted several model runs to evaluate the effects of mesh size and boundary conditions on the results of such models. They concluded that a boundary located at a depth greater than 12.2-m (40-ft) deep does not significantly affect the deflections estimated at the surface. Furthermore, lateral boundaries beyond 9.1 m (30 ft) from the loading area showed negligible effects on the simulation results. It is worth mentioning that they treated the pavement-shoulder interface as a discontinuity, i.e., the shoulder did not provide any structural support to the pavement [15]. They used elastic analysis for all the layers in their models based on the fact that the practical loads applied on the pavements are not likely to exceed the elastic limits of layers. They also found that a fine mesh (element size of 75 mm) around the loaded area with a larger element size farther from the loaded area helps create a nonreflective (quiet) boundary.

Shoukry et al., [16] used finite element models to investigate the effects of doweled or undoweled joints and the spacing between the transverse joints of concrete slabs on the behavior of rigid pavement layers during FWD tests. They compared the deflection basin created in their model with the actual basin measured in experiments which showed the ability of finite element models to simulate the FWD tests. Their results also confirmed that neglecting the dynamic loading condition could lead to unreliable deflection estimates and backcalculation procedures. As in Mallela and George [15], linear elastic behavior was assumed for all layers in this study [16].

William [17] used dynamic finite element models to simulate flexible, rigid, and composite pavement models. They used quiet boundaries at the bottom of all three models. They concluded that a refined mesh is necessary for layers that experience higher stresses (concrete slabs) while a coarser mesh can be used for the base and subgrade. They also added a steel loading plate to their model to increase the accuracy of the loading condition.

Park and Chang [18] applied a two-dimensional plane strain finite element model to investigate the behavior of a flexible pavement structure with Expanded Polystyrene (EPS) geofoam subgrade. Their model consisted of asphalt pavement with a base of crushed rock, subbase of open-aggregate and sand, concrete capping slab, and geofoam subgrade. Their numerical results along with some experimental tests indicated that EPS geofoam can be used as a subgrade in flexible pavements. The deformations predicted by their finite element model were in good agreement with those predicted by AASHTO's flexible pavement design method.

In summary, the published research confirms that dynamic models should be used instead of static models to simulate the behavior of FWD tests. They mostly agree that linear elastic behavior can be assumed for all material in the dynamic model. Mesh size and boundary condition were also shown to be key parameters affecting the results of the models.

5. DATA COLLECTION (TASK 1)

In FWD field tests as well as the indoor calibration tests, pavement (concrete slab in calibration tests) deflections caused by the impact from a falling mass are recorded with geophones at different points. The first step in the three-dimensional dynamic modeling of these tests is to determine the falling weight impact loads applied to the concrete. Various magnitudes of impact loads can be induced by FWDs with loading durations of about 20 to 40 milliseconds and a peak at about 10 to 25 milliseconds. A typical curve illustrating the impact load-time relations (impact load time history) is shown in Figure 3. The curve was developed based on the data reported by previous researchers [13,15–17,19]. Because various impact loads can be generated depending on the weight and height of the drop, the normalized stress (stress at any point in time divided by maximum stress) is shown on the y-axis of the plot.

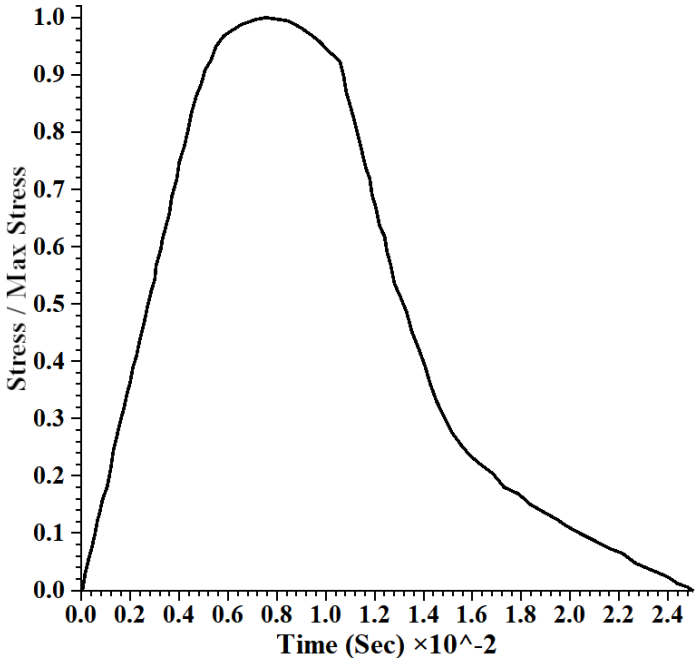

Figure 3. Typical impact load/stress-time relations caused by the weight drop in FWD calibration tests.

The impact stress time histories collected during three calibration tests conducted by MDT in December 2019 are shown in Figure 4. These tests were conducted on the geofoam test pit. The general trend recorded in these calibration tests follows that of published data. The corresponding displacements recorded during the aforementioned calibration tests conducted by MDT are also shown in Figure 5.

Unfortunately, the impact load time history data and corresponding displacements recorded during the calibration tests conducted on the clay test pit in 2016 are not available. Some displacement history data from calibration tests conducted on the clay test pit in January 2018 is available but unfortunately, the corresponding impact load time history data is not available. The issue was discussed with MDT staff, and Dr. David Orr (Cornell University), and it was determined that the impact load-time history data for the clay test pit was not recorded. However, the data containing the maximum load and maximum displacement caused by those loads exist for calibration tests conducted in January 2018. Some of these data are shown in Table 1. Since

the impact load time history is very consistent for FWD calibration tests, it was decided in the second meeting to use the existing maximum load and maximum displacement data for the first step of our modeling. The typical impact load-time relation with the collected maximum loads will be assumed for the tests in the model and the maximum displacements predicted by the model will be compared to the collected data in the tests.

Table 1. Some of the maximum load-Maximum Deflection data collected in January 2018 by MDT

Force (kip)	Deflection (mils)
9.01	14.13125
9.01	14.13125
11.94	18.98625
11.98	19.0525
15.1	24.0775
15.14	24.075

Also, the exact location of the weight drop for each one of these tests is not known. This information is required for the modeling. Mr. Amestoy has provided us with an approximate location (within a couple of inches) of the weight drop for the tests conducted on the clay pit in January. It was suggested by the MDT staff to conduct a new set of calibration tests on the geofoam test pit so that the exact location of the weight drop and any other missing data can be collected and be used in the models.

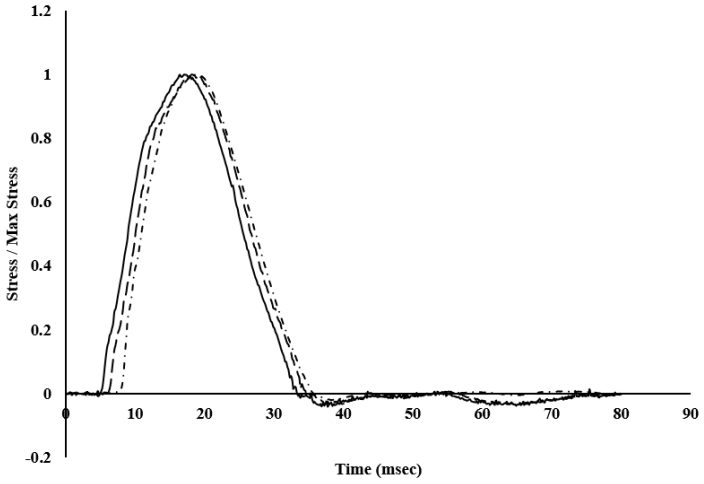

Figure 4. Impact stress-time curves of three calibration tests conducted by MDT in December 2019.

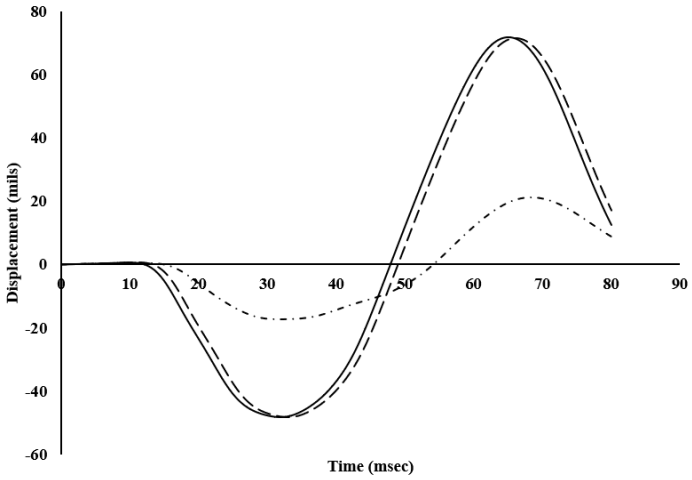

Figure 5. Corresponding displacements recorded in the same three calibration tests conducted by MDT in December 2019.

The next important parameter that is required for three-dimensional dynamic modeling of FWD tests is the mechanical damping of the material. Any natural dynamic system has some degree of damping which is due to the energy loss caused by the internal friction in the intact material. Additionally, in nonintact material, damping could also occur due to the slippage along interfaces. In numerical modeling of systems, the magnitude and form of these energy losses should be produced by damping [20]. The natural damping in soils and rocks is mainly independent of the frequency, i.e., damping is hysteretic [20–22]. The numerical formulation of the hysteretic damping is based on modulus reduction curves which imply a nonlinear stress/strain curve. Some examples of the modulus reduction curves for clay, sand, and concrete are shown in Figure 6 [23–27].

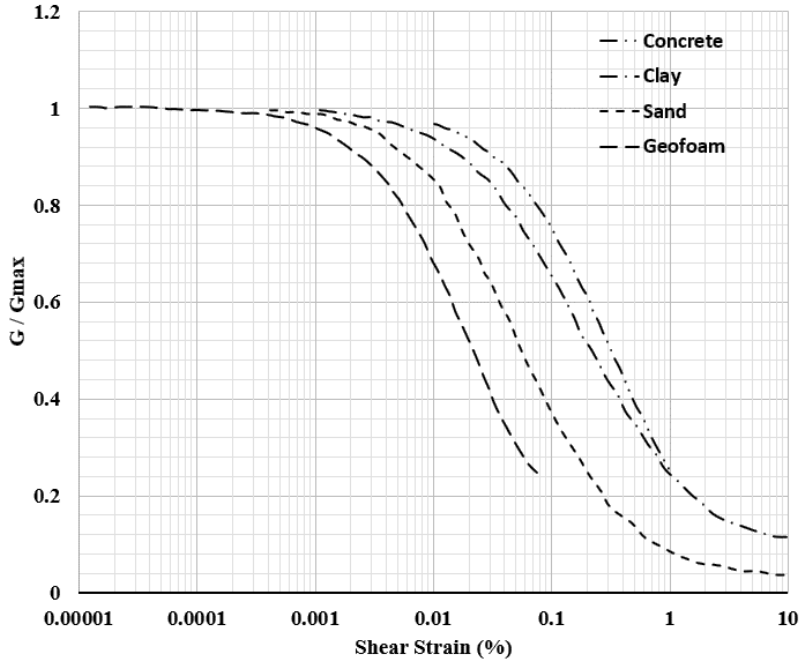

Figure 6. Some examples of the modulus reduction curves for clay, sand, and concrete (data from [23–27]).

Other important data required for modeling the calibration tests conducted by MDT have also been collected (from MDT or typical values) and summarized in Table 2.

Table 2. Summary of Material Properties Collected for Numerical Modeling

Material	Unit weight (pcf)	Elastic Modulus (psi)	Poisson's Ratio
Concrete	70-150	2.5E6-4.5E6	0.1-0.2
Sand Base and Leveling Sand	109-124	1.38E3-2.77E4	0.25-0.4
Clay Subgrade	87-112	6.94E1-2.77E4	0.1-0.5
Geofoam (ESP19)	1.15	5.8E2	0.05

The next step in this project is to develop a model based on the original design (clay setup) and use the results of the previous calibration tests, i.e., deflection characteristics of the concrete slab, to validate the model. After validating the model developed in this step, the model will be adjusted to simulate the behavior of the preliminary alternative test area (geofoam set up). This model will also be validated using the results of calibration tests conducted on the geofoam setup. The final model will then be used to determine whether or not the use of geofoam instead of the clay layer is practically possible. If the results indicate that the replacement is possible, the model will be utilized to modify the preliminary alternative test area design to achieve deflection amplitudes that are in the acceptable range suggested by AASHTO R32-11.

6. NUMERICAL MODELING-ORIGINAL SETUP (TASK 2)

In this stage, a three-dimensional explicit finite volume model was developed based on the original design (i.e., clay set up as shown in Figure 1). As mentioned before, the deflection requirements by AASHTO R32 were met during the calibration tests conducted by MDT using this setup. FLAC3D (Fast Lagrangian Analysis of Continua in 3 Dimensions) software from Itasca Consulting Group, Inc. was used to create the model. The FISH script (code) developed in FLAC3D for this stage of modeling (Task 2) is presented in Appendix A.

6.1 Model Geometry and Initial Conditions

Four 12-ft-wide (in X-direction) and 15-ft-long (in Y-direction) blocks with different thicknesses (in Z-direction) were created for modeling the original test pit. Based on the original design, the thicknesses of the concrete slab, base sand, clay subgrade, and the leveling sand in the model were assigned as 5 in., 6 in., 48 in., and 1 in., respectively. The geometry of the test pit in the model is shown in Figure 7.

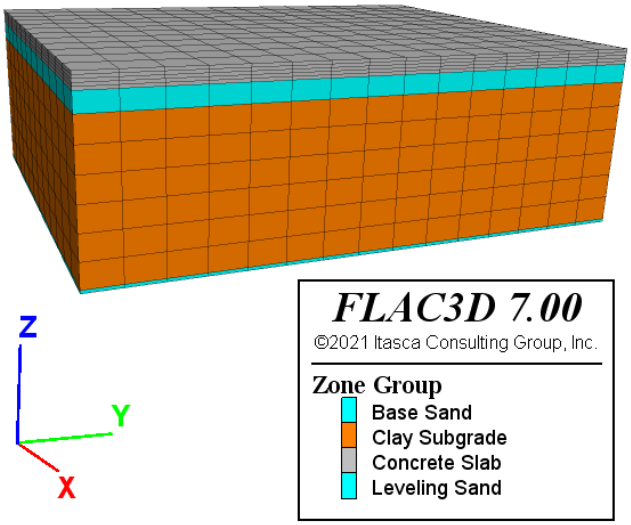

Figure 7. The geometry of the test pit model (original design) in FLAC3D.

The initial stress conditions, i.e., stress at any depth caused by the weight of overburden, were developed in the model and are shown in Figure 8.

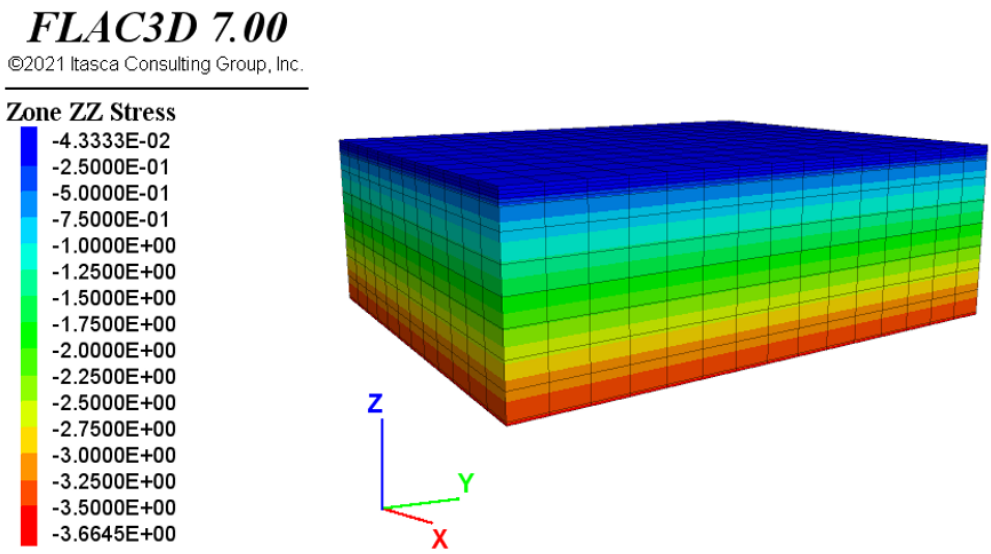

Figure 8. Initial stress conditions (in psi) of the model.

6.2 Boundary Conditions

In numerical modeling of the dynamic behavior of material, wave reflection at model boundaries could adversely affect the results of the model. This negative impact can be reduced by using free-field boundary conditions (also known as quiet or viscous boundaries) instead of fixed boundary conditions. Using these quiet boundaries in the modeling of the FWD tests on pavements (in the field) usually improves the predicted deflections by the model (e.g., [15,17]). In FWD calibration tests, however, the boundaries of the test pit are not completely under free-field conditions. In other words, there are actual physical boundaries around the test pit which means that the test pit is not continuously connected to the surrounding ground. This is especially the case for the clay subgrade where a liner is placed between the subgrade and the surrounding ground. To understand the effects of this discontinuity, both fixed and quiet boundary conditions were used in the model and the results were compared. In the model, free boundary conditions at the surface (top) of the model and fixed boundary conditions at the base (bottom) were used. All other four faces of the model, i.e., North, East, South, and West faces, were fixed in x and y directions and were free to move in the z-direction. Quiet boundaries were also examined at the base and the other four faces of the model (except the surface). As was expected, due to the actual physical boundaries around the test pit, the fixed boundary conditions better simulated the calibration test pit behavior.

6.3 Material Constitutive Models and Material Properties

As mentioned before, different load magnitudes used in FWD calibration tests are within the elastic limits of all layers and linear elastic behavior has been commonly used in dynamic modeling of FWD tests [15,16,19]. Non-linear viscoelastic-plastic models and non-linear elastic material models with a Mohr-Coulomb yield have also been used for dynamic modeling of FWD tests ([4,17,28]). In this study, both linear elastic behavior with structural damping (hysteretic damping) and elastoplastic material behavior with a Mohr-Coulomb yield model were examined. Material properties used in both models are summarized in Table 3. The linear elastic model

with structural damping (hysteretic damping) simulated the behavior of the test pit more precisely.

Table 3. Material Properties Used in the Model

Material	Unit weight (pcf)	Elastic Modulus (psi)	Poisson's Ratio	Cohesion (psi)	Friction Angle (degrees)
Concrete	149.8	3.5E6	0.15	337	46
Sand Base and leveling Sand	120	4.9E3	0.4	0	35
Clay Subgrade	100	8.7E2	0.2	7	29

As mentioned before, material damping was also considered in our models. Hysteretic damping was used based on the modulus reduction curves shown in Figure 6. Based on the modulus reduction curves, the following incremental constitutive relation for the shear strain can be derived [29]:

$$\bar{\tau} = M_s \gamma \tag{1}$$

$$M_t = \frac{d\bar{\tau}}{d\gamma} = M_s + \frac{dM_s}{d\gamma} \tag{2}$$

where, $\bar{\tau}$ is normalized shear stress, γ is the shear strain, M_s is the normalized secant modulus, and M_t is the normalized tangent modulus. The incremental shear modulus at any strain, G_γ, in the model is then calculated by:

$$G_\gamma = G_{max} M_t \tag{3}$$

$$G_{max} = \frac{E}{2(1+v)} \tag{4}$$

where, G_{max} is the maximum shear modulus (at zero strain), E is Young's modulus, and v is Poisson's ratio. In FLAC3D, different formulas can be used to fit the best curve to the actual modulus reduction curves from which the M_t (or M_s) at any strain is calculated during the modeling steps. The constants of the fitting formula are then given as inputs in FLAC3D. The following fitting formula, known as the sigma-3 fitting formula [29], was used in our model.

$$M_s = \frac{a}{1 + \exp(-\frac{L - x_0}{b})} \tag{5}$$

In Equation 5, L is the $\log_{10}(\gamma)$, and a, b, and x_0 are fitting constants. Table 4 summarizes the fitting constants for different layers used in our model.

Table 4. Fitting Constant Used for Material Damping in the Model

Material	Constant a	Constant b	Constant x_0
Concrete	1.07	-0.55	-0.4
Sand Base and leveling Sand	1.05	0.5	-1.15
Clay Subgrade	1.07	-0.6	-0.63

6.4 Impact Loads and Corresponding Displacements

As discussed before, the impact load time history data and corresponding displacements recorded during the calibration tests conducted on the clay test pit in 2016 are not available. The typical impact load time history shown in Figure 3 was therefore used in the model. The displacements (deflections) at the location of the sensors rack were then recorded at every step. For simplicity, a square area was used instead of a circular area to apply the impact loads in the model. Figure 9 shows the location of applied impact loads and the displacement sensors rack.

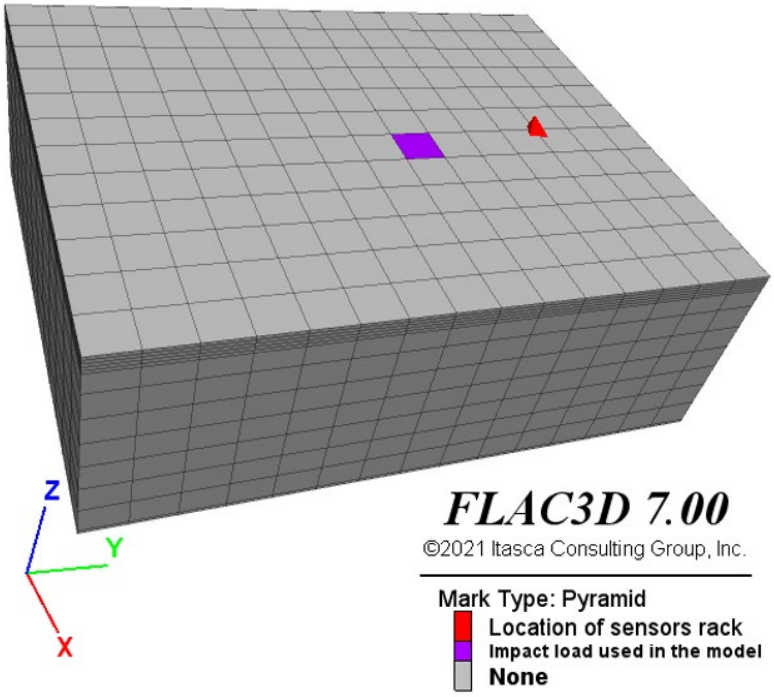

Figure 9. Location of applied impact loads and the displacement sensors rack.

6.5 Results and Discussion

As explained before, the linear elastic models better simulated the behavior of the test pit. Therefore, only the results of linear elastic models with fixed boundary conditions are presented here. The displacement histories at the location of the sensors rack for all different impact loads are shown in Figure 10. The figure shows that the model's deflection history is consistent with the typical deflection patterns seen in the FWD calibration tests. The stress distribution and vertical displacement in the model 8 milliseconds after the weight drop are shown in Figure 11 and Figure 12, respectively.

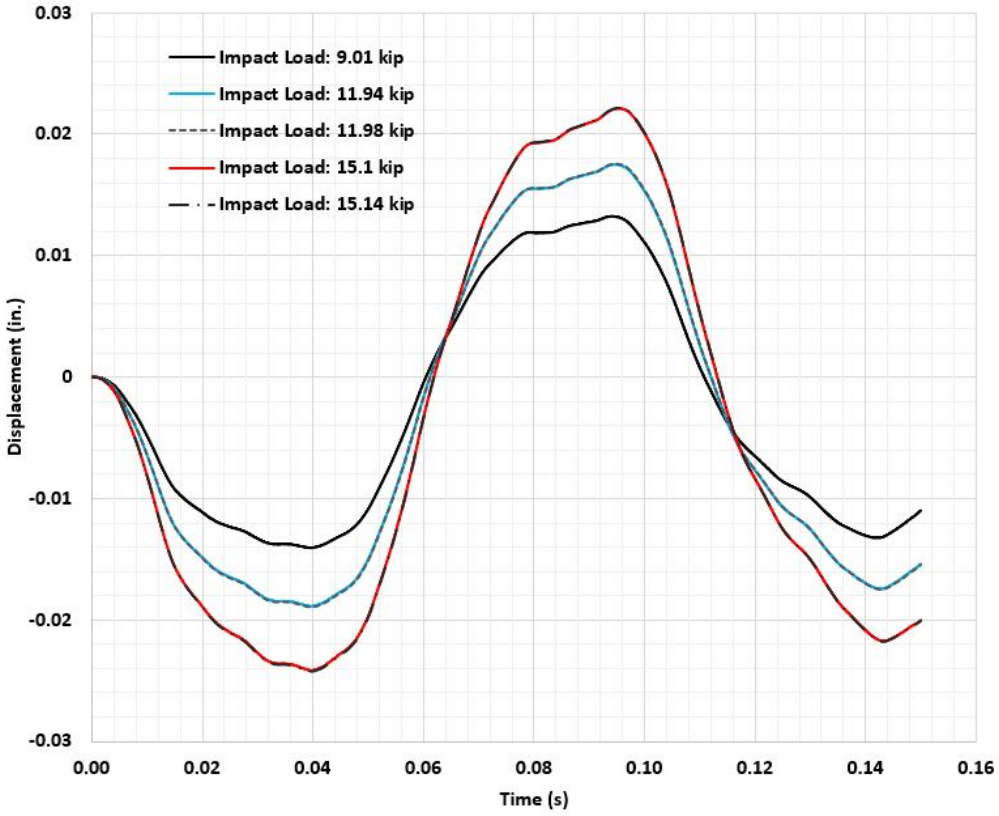

Figure 10. Displacement histories at the location of the sensors rack for five different impact loads.

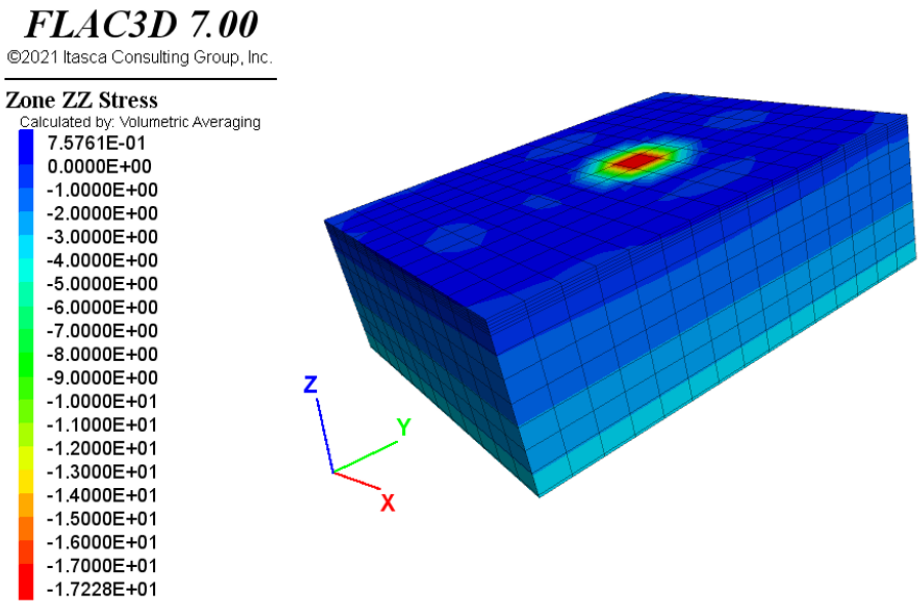

Figure 11. Stress distribution in the model (in psi), 8 milliseconds after the weight drop (for max impact load of 11.94 kip).

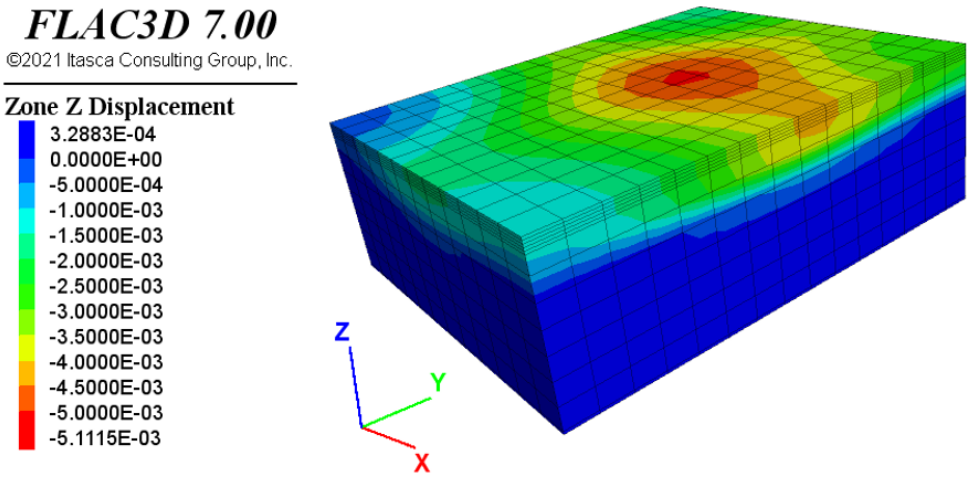

Figure 12. Vertical displacement of the model (in.), 8 milliseconds after the weight drop (for max impact load of 11.94 kip).

The maximum deflections predicted by the model for different load magnitudes, along with the recorded maximum deflections during the calibration tests are shown in Table 5.

Table 5. Summary of Recorded and Predicted Deflections

Force (kip)	Maximum Stress (psi)	Recorded Deflection (in)	Predicted Deflection in the Model (in)	Difference between Recorded and Predicted Deflections (in)	Error (%)
9.01	79.665891	0.01413125	0.01406478	-0.00006647	-0.47
11.94	105.572779	0.01898625	0.01887952	-0.00010673	-0.56
11.98	105.926457	0.0190525	0.01894595	-0.00010655	-0.56
15.1	133.513314	0.0240775	0.02416509	0.00008759	0.36
15.14	133.866991	0.024075	0.02423262	0.00015762	0.65

As can be seen from the table, all the predicted deflections by the model are within 1% of recorded deflections during MDT's FWD tests. It is worth mentioning that the deflections predicted by the model are sensitive to the impact load time history used in the model. Although the impact load time histories are very consistent, a slight change in the form or the location of the peak of the history could change the predicted deflection histories. The model is also sensitive to the material properties as well as the location of the weight drop with respect to the location of the rack of sensors. The next step of this project is to modify the model developed in this step to simulate the behavior of the alternative calibration test pit (geofoam test pit). The main difference between the original clay setup (modeled in this step) and the alternative geofoam setup is that the clay subgrade is replaced with a geofoam subgrade that has significantly different elastic modulus and unit weight. Therefore, the sensitivity of the current model to the elastic modulus of the subgrade is of interest.

To achieve this goal, the model with the maximum impact load of 15.1 (kip) was rerun multiple times, each time with a different elastic modulus for the clay subgrade. All the other properties of the model were kept the same for this sensitivity analysis. The results of this sensitivity analysis are shown in Figure 13.

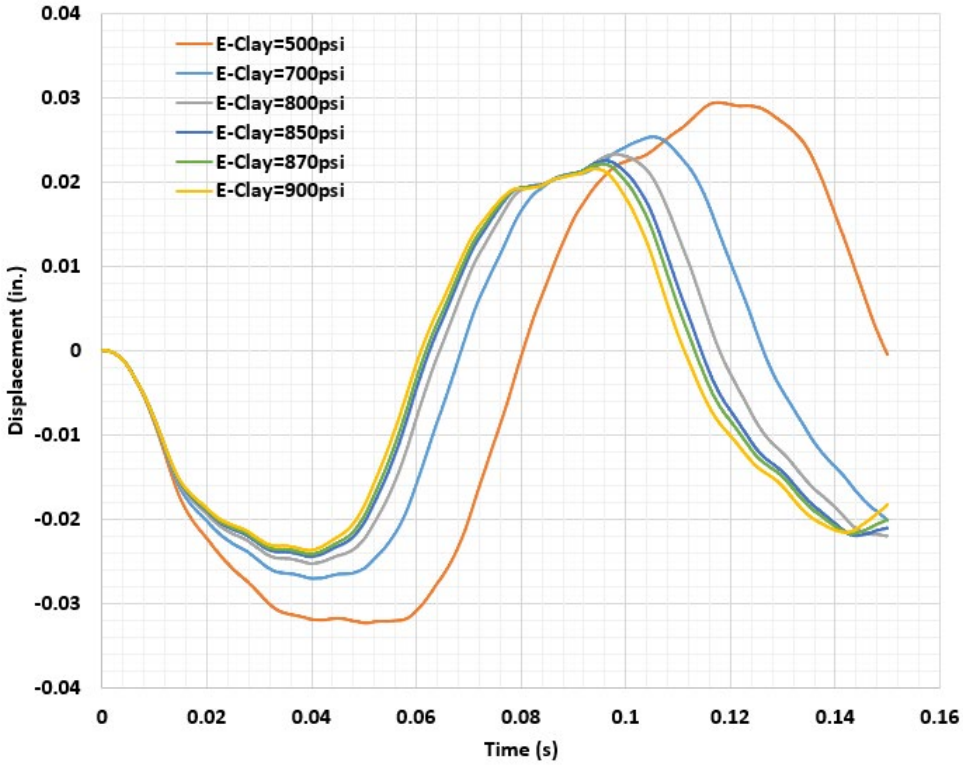

Figure 13. Sensitivity of the models predicted deflection histories to the elastic modulus of the clay subgrade.

As can be seen from Figure 13, reducing the elastic modulus of the subgrade increases the deflections of the model. This partly explains the excessive deflections observed in the MDT's geofoam test pit because the elastic modulus of geofoam is less than clay. The geometry of the MDT's alternative geofoam test pit is also slightly different from the original clay test pit, and the more precise analysis of its behavior will be investigated in the next step of this project.

6.6 Conclusions-Task 2

The results of the second phase of this project (Task 2) were to show the capability of the developed model in predicting the deflections with reasonable accuracy. The sensitivity of the model to the elastic modulus of the subgrade layer shows that the model is very likely capable of simulating the behavior of the alternative geofoam test pit. The behavior of the model can be assessed even better in the next step when both the impact load time history and measured deflection time history at the location of the sensors are known. This allows us to compare the predicted deflection time histories with the measured time histories instead of just comparing the maximum predicted and observed deflections.

7. NUMERICAL MODELING-ALTERNATIVE SETUP (TASK 3)

In the numerical modeling of the test pit conducted in Task 2 (i.e., clay set up) the stresses caused by the weight of the truck were not included in the models. These stresses are transferred onto the concrete slab at three locations, i.e., at the locations of the two sets of dual tires as well as on the loading plate before the calibration test starts. As these stresses could affect the measured displacements, they should also be included in the model. To include these stresses in the model, the loads induced by the weight of the truck at the locations of the dual tires as well as at the location of the loading plate just before the calibration tests started were measured by MDT staff (John Amestoy) on April 15, 2021. The stresses were then calculated from these loads. The model for the original test pit (clay set up) was modified to include these stresses and the results were compared to the previous model. A three-dimensional model was then developed based on the alternative test pit design (geofoam setup) for Task 3. The stresses caused by the weight of the truck were also included in the geofoam setup model. As mentioned before, the impact load time history data and the corresponding deflection time histories for the geofoam setup are available. These available data were measured, however, without bolting down the displacement sensor rack to the concrete slab. After discussing this issue in a meeting with the MDT staff, it was decided to conduct the tests again with the sensor rack bolted down to the concrete slab. The new tests with the sensors rack bolted down were conducted on April 15, 2021, and the results of these calibration tests were used to validate the models developed for Task 3. The FISH script (code) developed in FLAC3D for this stage of modeling (Task 3) is presented in Appendix B.

7.1 Preliminary Calibration Test Pit (Clay Setup) Reconsideration

In this stage, the clay setup model (discussed in section 7) was modified to include the stresses caused by the weight of the truck. The weight of dual tires and the loading plate before the tests started were 2200 lbs and 1500 lbs, respectively. The initial stress conditions, i.e., stress at any depth caused by the weight of overburden and the stresses caused by the weight of the truck, are shown in Figure 14.

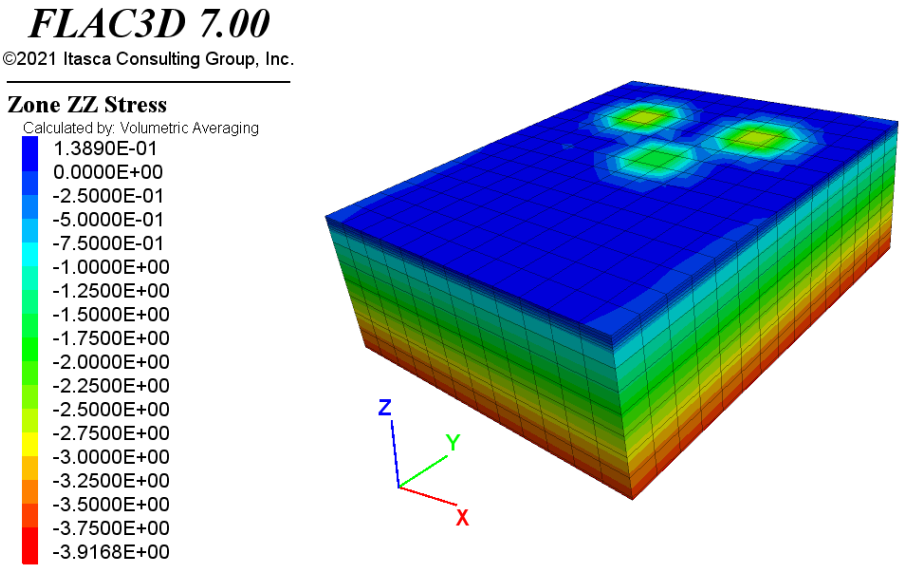

Figure 14. Initial stress conditions, including the stresses caused by the weight of the truck (clay setup).

As mentioned before, due to the lack of impact load time history data and corresponding displacements for the clay setup, only the maximum deflections predicted by the model for different load magnitudes were compared to those recorded during the calibration tests.

Table 6 summarizes the recorded and predicted deflections for the clay set up using the new model where the stresses caused by the weight of the truck are considered. Comparing the results presented in Table 5 and Table 6 shows that including the weight of the truck does not have a significant effect on the predicted deflections by the model for the clay setup.

Table 6. Summary of Recorded and Predicted Deflections after Considering the Weight of the Truck in the Model

Force (kip)	Maximum Stress (psi)	Recorded Deflection (in)	Predicted Deflection in the Model (in)	Difference between Recorded and Predicted Deflections (in)	Error (%)
9.01	79.665891	0.01413125	0.01400926	-0.000121989	0.86
11.94	105.572779	0.01898625	0.01884702	-0.000139230	0.73
11.98	105.926457	0.0190525	0.01891366	-0.000138840	0.72
15.1	133.513314	0.0240775	0.02416271	0.000085209	-0.35
15.14	133.866991	0.024075	0.02423087	0.000155870	-0.64

7.2 Model Geometry and Initial Conditions (Geofoam Setup)

The geometry of the alternative setup (geofoam setup) model created in FLAC3D is shown in Figure 15. The model was created based on the dimensions shown in Figure 2. Because the geofoam layer is surrounded by a sand layer it cannot be seen in a complete plot of the geometry (Figure 15A). Therefore, a cut was made through the geometry (Figure 15B) to show the geofoam layer.

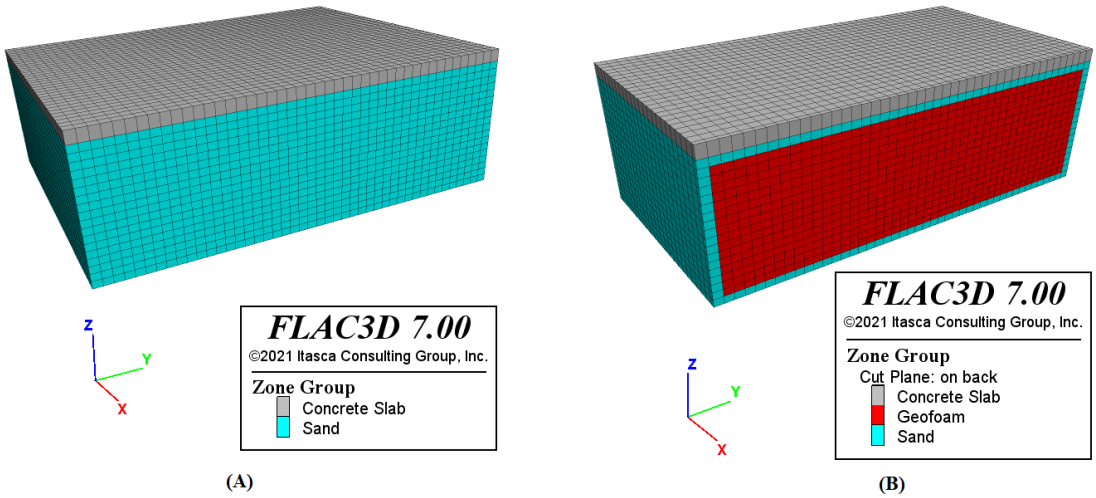

Figure 15. The geometry of the test pit model (alternative design) in FLAC3D.

The initial stress conditions, i.e., stress at any depth caused by the weight of overburden and the weight of the truck, were developed in the model and are shown in Figure 16.

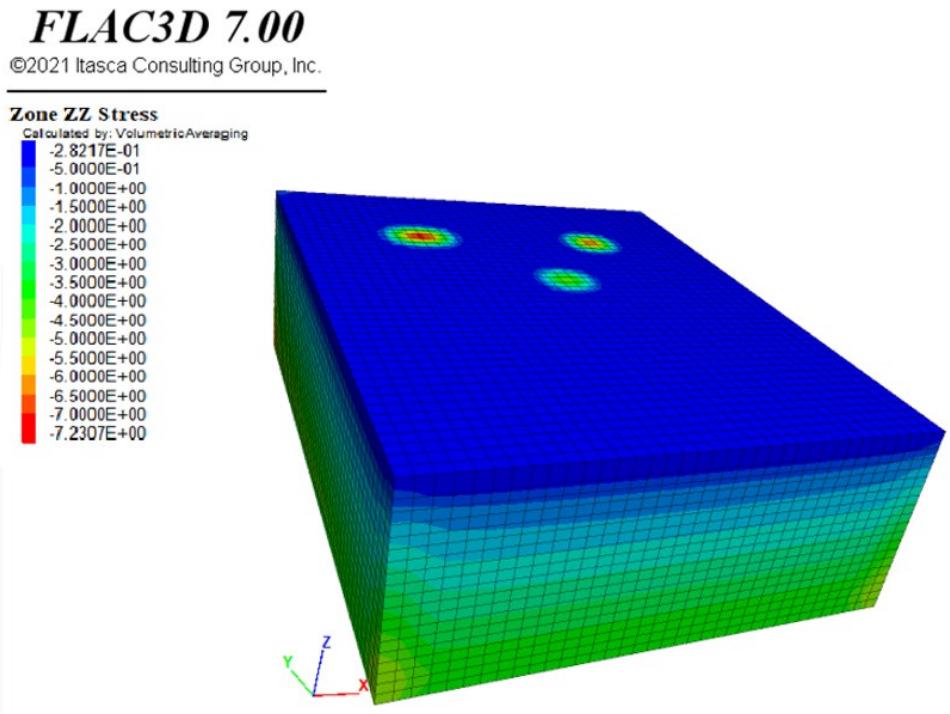

Figure 16. Initial stress conditions including the stresses caused by the weight of the truck (geofoam setup).

7.3 Boundary Conditions, Material Constitutive Models, and Material Properties (Geofoam Setup)

In the model, free boundary conditions at the surface (top) of the model and fixed boundary conditions at the base (bottom) were used. All other four faces of the model, i.e., North, East, South, and West faces, were fixed in x and y directions and were free to move in the z-direction. As for the clay setup, linear elastic behavior with structural damping (hysteretic damping) was used for all the layers. Material properties used in the model are summarized in Table 7, and the structural damping's fitting constants used in the geofoam setup are presented in Table 8.

Table 7. Material Properties Used in the Model (Geofoam Setup)

Material	Unit Weight (pcf)	Elastic Modulus (psi)	Poisson's Ratio
Concrete	149.8	3. 5E6	0.15
Sand	120	4.9E3	0.4
Geofoam	1.15	5.8E2	0.1

Note that for the concrete slab and the sand layers, the same values of unit weight, elastic modulus, Poisson's ratio, and structural damping's fitting constants were used in both the clay setup model and the geofoam setup model.

Table 8. Fitting Constant Used for Material Damping in the Model (Geofoam Setup)

Material	Constant a	Constant b	Constant x_0
Concrete	1.07	-0.55	-0.4
Sand	1.05	0.5	-1.15
Geofoam	1.1	-0.6	-1.5

7.4 Impact Loads and Corresponding Displacements for Alternative Calibration Test Pit (Geofoam Setup)

The impact load time history data and corresponding displacements recorded during the calibration tests conducted on the geofoam test on April 15, 2021, are shown in Figure 17 and Figure 18, respectively.

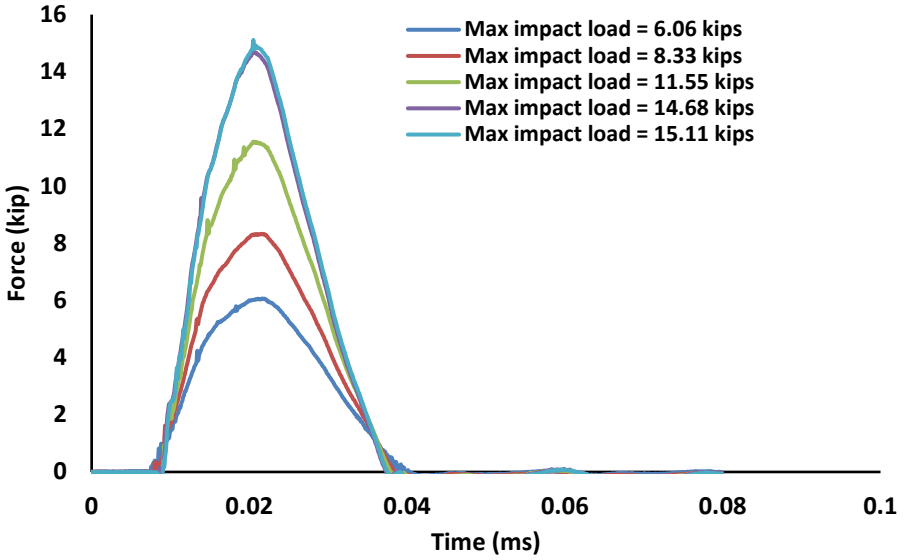

Figure 17. The impact load time histories for alternative calibration test pit (Geofoam Setup).

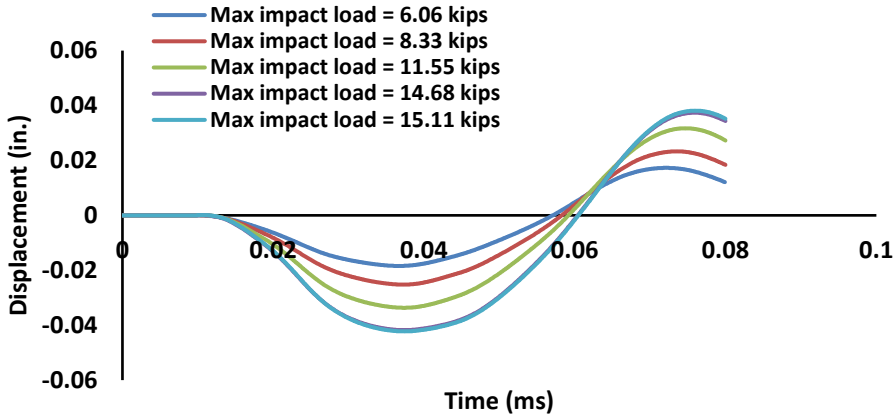

Figure 18. The corresponding displacement time histories recorded during the calibration tests (Geofoam Setup).

7.5 Results and Discussion

As explained before, the linear elastic constitutive models with fixed boundary conditions were used in the models. For each maximum impact load that was used in the calibration tests conducted on April 15, 2021, the recorded impact load time history was used in the model as an input to apply the dynamic load. The stress distribution and vertical displacements in the entire model 10 milliseconds after the weight drop, for the test conducted under the maximum impact load of 15.11 kip, are shown in Figure 19 and Figure 20, respectively.

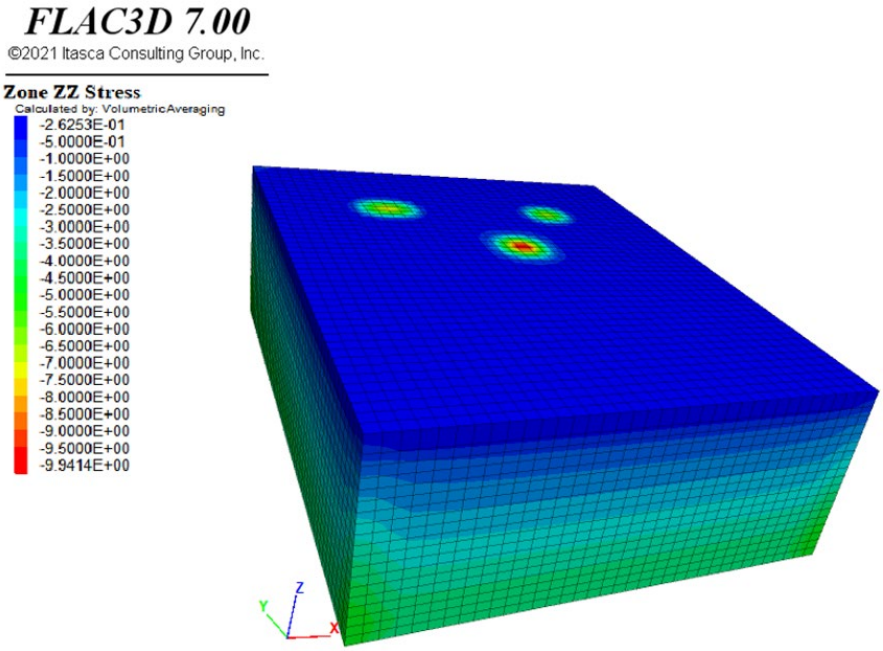

Figure 19. Stress distribution in the geofoam model (in psi), 10 milliseconds after the weight drop (for max impact load of 15.11 kip).

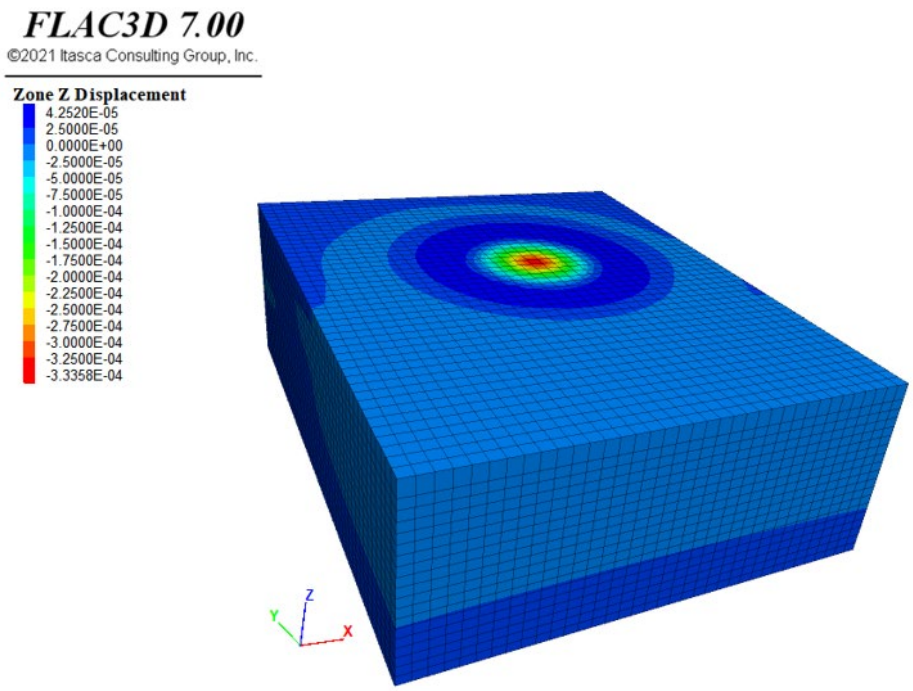

Figure 20. Vertical displacement of the model (in.), 10 milliseconds after the weight drop (for max impact load of 15.11 kip).

The displacements predicted by the model at the location of the sensors were recorded for the entire duration of the simulation, and the results were compared to the displacement histories recorded during the calibration tests conducted on the geofoam setup on April 15, 2021. Figure 21 to Figure 25 show the comparisons between the measured deflection time histories and the displacement time histories predicted by the model for five different maximum impact loads.

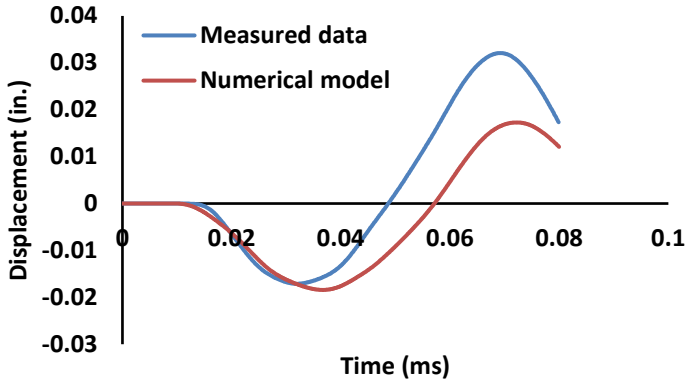

Figure 21. Predicted and measured displacements with the maximum impact load of 6.06 kip (Geofoam Setup).

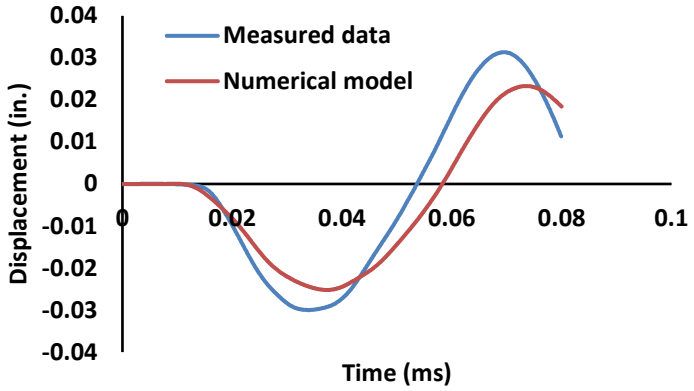

Figure 22. Predicted and recorded displacements with the maximum impact load of 8.33 kip (Geofoam Setup).

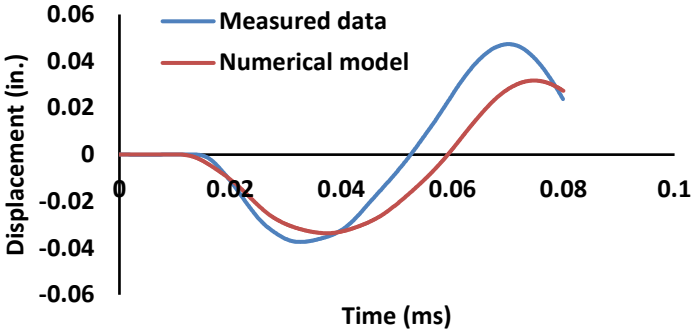

Figure 23. Predicted and recorded displacements with the maximum impact load of 11.55 kip (Geofoam Setup).

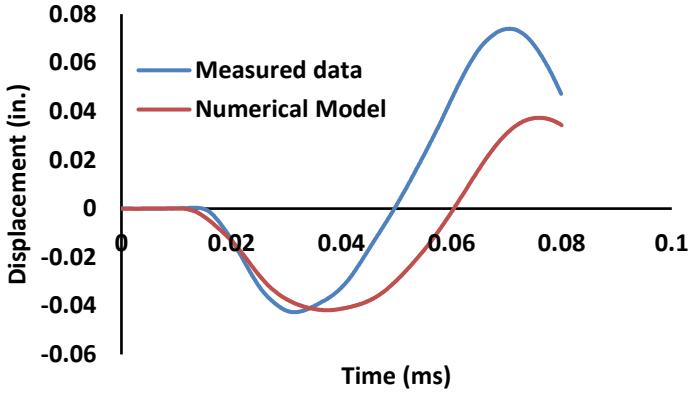

Figure 24. Predicted and recorded displacements with the maximum impact load of 14.68 kip (Geofoam Setup).

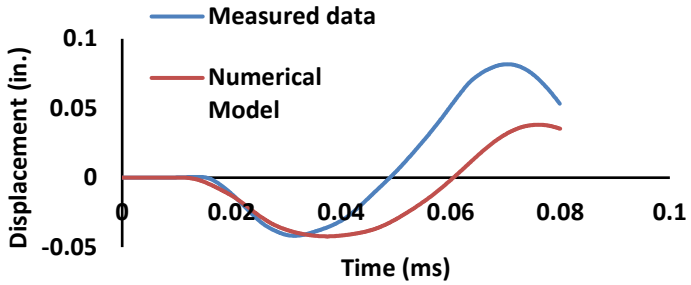

Figure 25. Predicted and recorded displacements with the maximum impact load of 15.11 kip (Geofoam Setup).

The results show reasonable agreement between the predicted and measured displacements, especially for the first half of the displacement time histories. In the rebound portion, i.e., the second half of the displacement time histories, some deviations are observed. These deviations are more pronounced for the two highest applied impact loads, i.e., 14.68 kip and 15.11 kip. It is also interesting to note that the measured displacement time histories show larger maximum rebound displacements than the original maximum displacements seen in the first half of the graphs. Theoretically, the maximum rebound displacement is expected to be less than the original maximum displacement due to the mechanical damping which is the case shown in our numerical models. These observed deviations between the predicted and measured displacement time histories as well as the higher rebound displacements in the measured data could be caused by a layer of air between the concrete slab and the sand layer, or between the sand layer and the geofoam. Further research is required, however, to better understand these deviations and to examine whether an air layer exists in the test pit. Meanwhile, as the maximum original displacements observed in the calibration tests and predicted by the model are in good agreement, it is believed that the model could be used to improve the alternative design. It should be mentioned that the maximum original displacements measured during the calibration tests conducted on the geofoam setup are twice that of the clay setup under similar maximum impact loads. The main purpose of this study is to modify the alternative design so that the maximum original displacements for the geofoam setup are similar to the displacements measured for clay setup, i.e., within the range required by [1]. Therefore, the results of the model seem to be acceptable to be used for the next stage of the project.

It is also worth noting that the effects of the weight of the truck on the predicted displacements of the geofoam setup were investigated. Figure 26, for example, shows the recorded displacement time history, and the predicted displacement time histories of the model with and without considering the weight of the truck for the maximum impact load of 14.68 kip. The results show that, unlike the clay setup, the predicted displacements changed significantly when the stresses caused by the weight of the truck were considered.

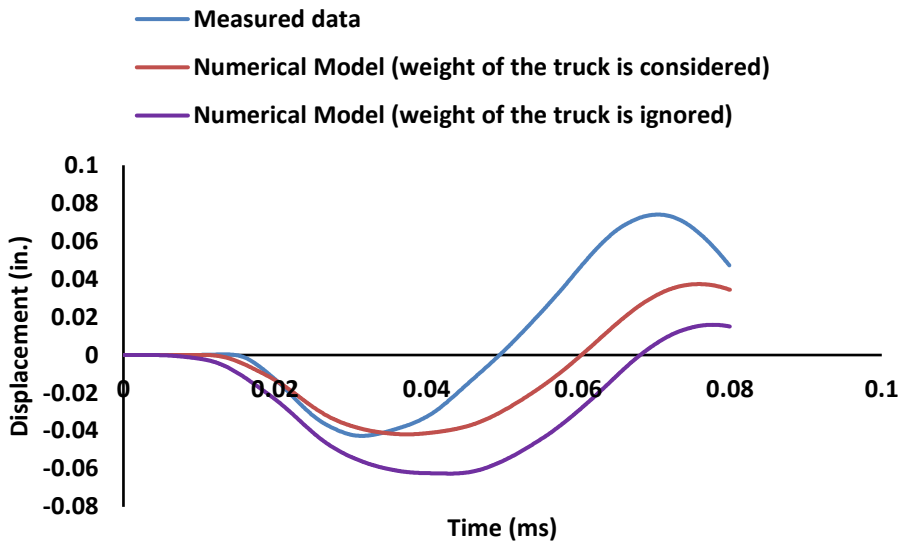

Figure 26. Predicted and recorded displacement time histories for maximum impact load of 14.68 kip with and without considering the weight of the truck (Geofoam Setup).

7.6 Conclusions-Task 3

The results show that although including the stresses caused by the weight of the truck did not affect the predicted displacements for the clay setup, they significantly changed the predicted results of the geofoam setup. The measured and predicted displacement histories for the geofoam setup are in reasonable agreement which indicates that the developed model can be used in the next steps of the project to modify the preliminary alternative design, i.e., the geofoam setup. In the next stage of the project, the developed models will be used to determine whether or not geofoam can be used instead of the clay layer in the calibration test pit. This will be done by using the developed models to modify the preliminary alternative test area design to achieve deflection amplitudes that are in the acceptable range suggested by AASHTO R32-11.

8. NUMERICAL MODELING- NEW GEOFOAM SETUP DESIGN (TASK 4)

In the previous sections, the ability of the developed numerical models to simulate the behavior of the FWD calibration test pit, both with a clay layer and a geofoam layer, was examined. The results showed that the model can in fact predict the behavior with reasonable accuracy. The final step of this study was to use the developed models to design a new geofoam setup where the displacements caused by the falling weights are in the range of maximum measured displacements of the original clay setup. According to AASHTO R32-11 [1], the deflections caused by a 16 kip load should be 0.012 (in.) or more. After discussions with the MDT Technical panel, it was decided that the new geofoam setup should be designed so that the maximum deflections are 10% to 15% more than those of the original clay setup.

The available data from the calibration tests conducted on the original clay setup and the alternative geofoam setup only include two common maximum impact loads, i.e., 11.55 kip, 15.11 kip. In order to design the new geofoam setup based on a larger set of applied loads, the expected displacements of the clay setup under two other loads, i.e., 8.33 kip and 14.68 kip, were estimated using Figure 27. As can be seen from Figure 27, the maximum applied load and the measured maximum displacement of the clay setup have a linear relationship expressed in Equation 6.

$$Y = 0.0016X - 0.0004. \quad (6)$$

Y and X in equation 6 represent displacement (in.) and force (kip), respectively. Equation 6 was, therefore, used to estimate the expected displacements of the clay setup under 8.33 kip and 14.68 kip maximum loads. These two loads were chosen because the displacement histories of the alternative geofoam setup under such loads were available from the previous calibration tests.

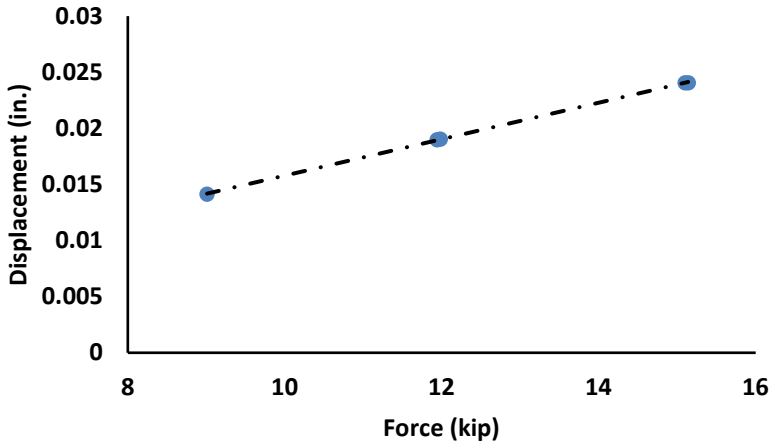

Figure 27. The linear relationship between values of maximum loads and corresponding displacements for the clay's setup.

The developed numerical models were then used to design new geofoam setups using four maximum impact loads, i.e., 8.33 (kip), 11.55 (kip), 14.68 (kip), and 15.11 (kip). The goal was to design the new setup with such geometry that the maximum displacements are in the acceptable ranges shown in Table 9, i.e., 110% to 115% of the clay setup's displacements under the same impact loads.

Table 9. Maximum impact loads and the corresponding measured/estimated displacements of the clay setup and the corresponding acceptable ranges used to design the new geofoam setup

Maximum Impact Load (kip)	Measured/Estimated Maximum Displacement of the Clay Setup (mils)	Range of Acceptable Displacements for the New Geofoam Setup (mils)	
		Min	Max
8.33	12.93	14.22	14.87
11.55	18.08	19.89	20.79
14.68	23.09	25.40	26.55
15.11	23.78	26.15	27.34

Three types of geofoam, i.e., EPS 19, EPS 29, and EPS 39, were used in the new geofoam designs. A set of sensitivity analysis simulations were also conducted to study the effects of different types of geometries on the behavior of the new geofoam designs.

8.1 Boundary Conditions, Material Constitutive Models, and Material Properties Used in the New Designs

Similar to the previous sections, free boundary conditions and fixed boundary conditions were used at the surface and the base, respectively. The other faces of the test pit in the model, i.e., North, East, South, and West, were fixed in X and Y directions and free to move in the Z direction. The unit weight, elastic modulus, Poisson's ratio, and structural damping's fitting constants used for the concrete slab and the sand layers in the new designs are the same as the previous models. Table 10 shows the material properties used in the new designs.

Table 10. Material Properties Used in the Model (Geofoam Setup)

Material	Unit Weight (pcf)	Elastic Modulus (psi)	Poisson's Ratio
Concrete	149.8	3. 5E6	0.15
Sand	120	4.9E3	0.4
Geofoam (EPS 19)	1.15	5.8E2	0.1
Geofoam (EPS 29)	1.80	1.09E3	0.1
Geofoam (EPS 39)	2.40	1.5E3	0.1

As in the models used in previous sections, hysteretic damping was used for all the models in the new designs. Unfortunately, required data for the damping fitting constants of different geofoam types were not available. Therefore, the same constants shown in Table 8 were used for all three types of geofoams used in the new designs. A set of brief sensitivity analysis simulations, however, showed that the effects of these constants are negligible in the range of the small displacements recorded in the calibration tests.

8.2 New Geofoam Design Using EPS 19

Five different geometries were designed using geofoam EPS19. As in the previous models, a 5 inches thick concrete slab is used in all the new designs. In order to better visualize the geometry of each design, three cross-sections along the X, Y, and, Z axes are shown for every design. For each design, the predicted displacement histories for each one of the four loads used in the models are shown. The displacement history of the clay setup under the same impact load along with the acceptable range of maximum displacements (presented in Table 9) are also shown on each displacement history plot.

8.2.1 EPS19-Design 1

The geometry of the EPS19-Design 1 is shown in Figure 28. The predicted displacement histories for four different maximum impact loads are shown in Figures 29 to 32.

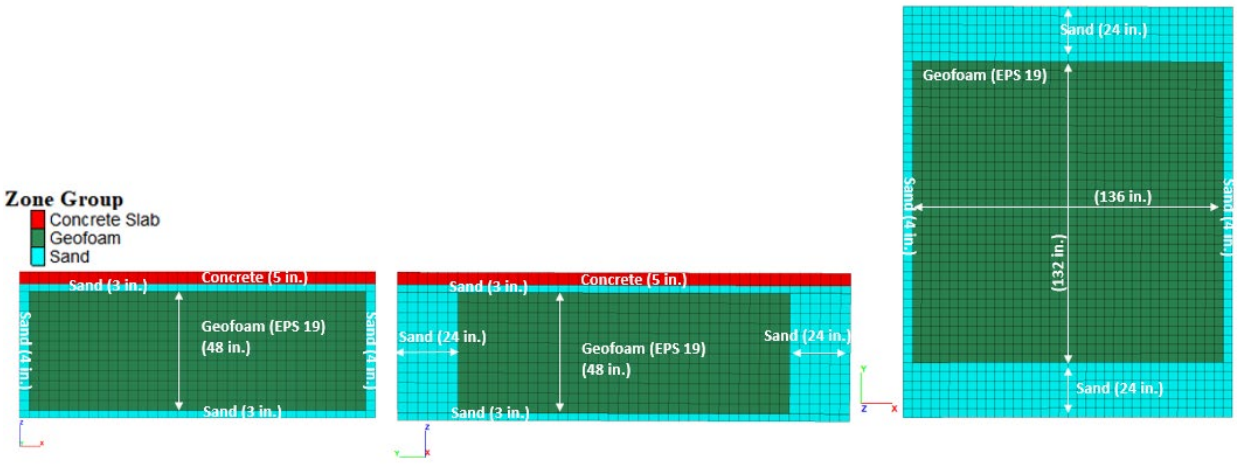

a) A cut along the Y axis b) A cut along the X axis c) A cut along the Z axis

Figure 28. The geometry of the test pit model (Geofoam-EPS 19-Design 1).

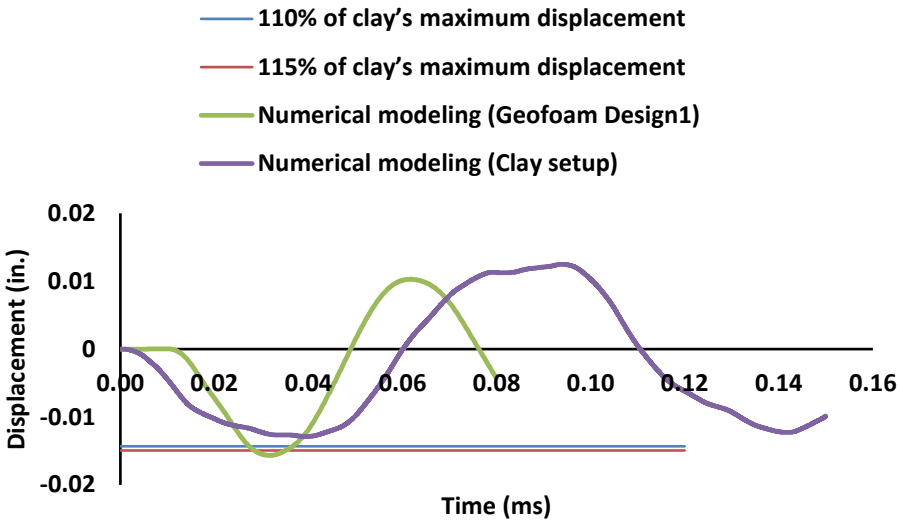

Figure 29. Predicted displacements of both setups with the maximum impact load of 8.33 kip (Geofoam-EPS19-Design 1).

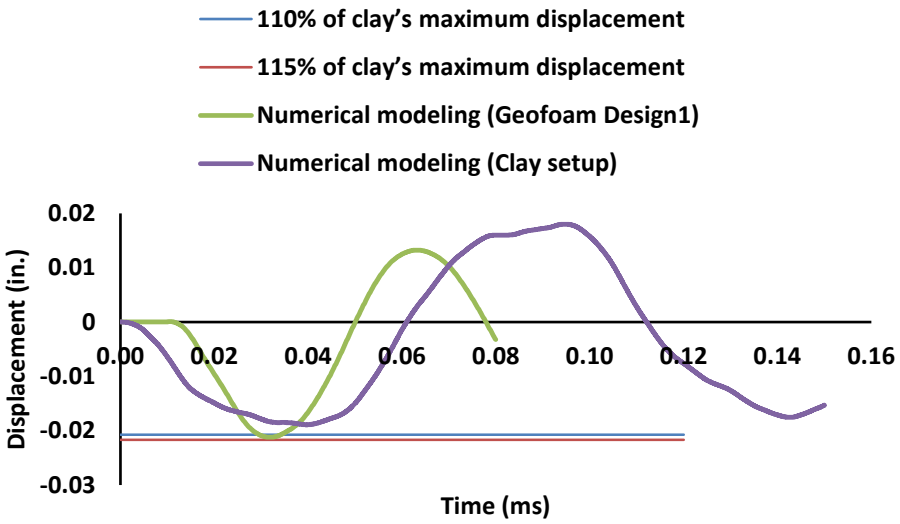

Figure 30. Predicted displacements of both setups with the maximum impact load of 11.55 kip (Geofoam-EPS19-Design 1).

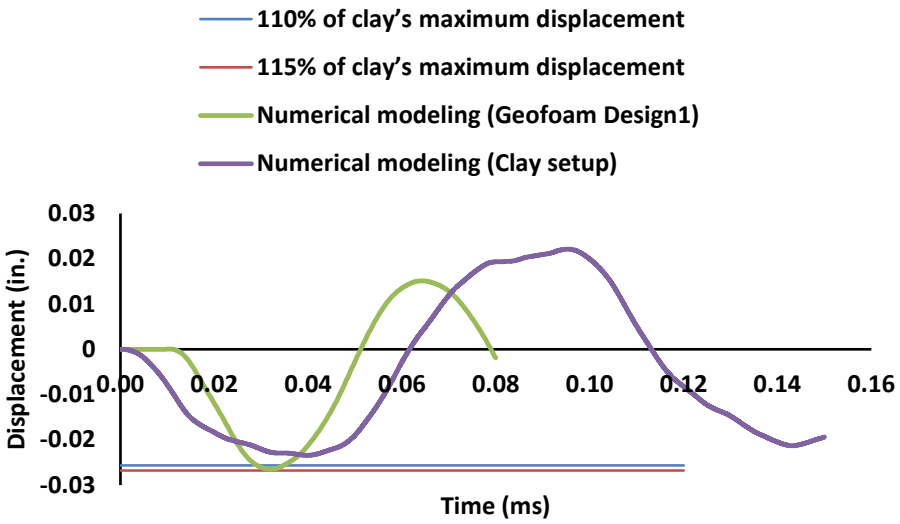

Figure 31. Predicted displacements of both setups with the maximum impact load of 14.68 kip (Geofoam-EPS19-Design 1).

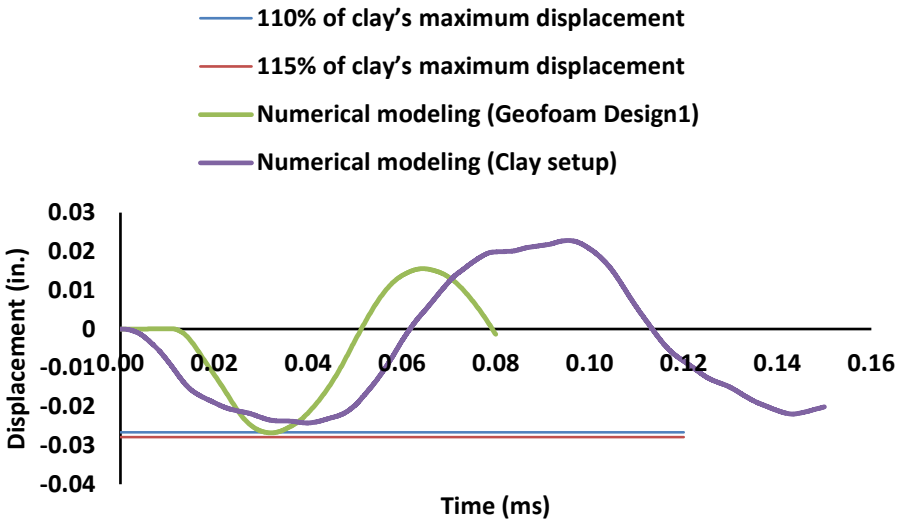

Figure 32. Predicted displacements of both setups with the maximum impact load of 15.11 kip (Geofoam-EPS19-Design 1).

8.2.2 EPS19-Design 2

The geometry of the EPS19-Design 2 is shown in Figure 33. The predicted displacement histories for four different maximum impact loads are shown in Figures 34 to 37.

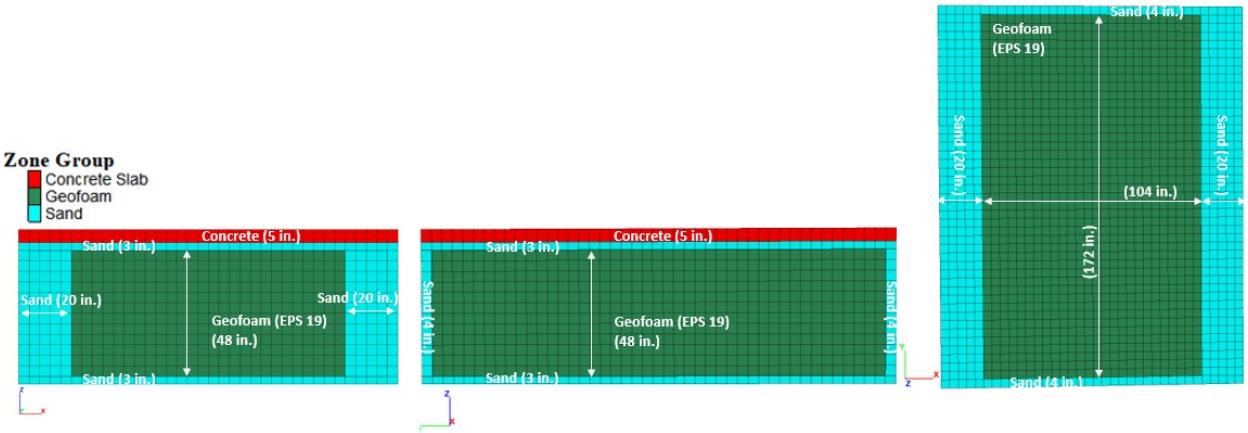

a) A cut along the Y axis b) A cut along the X axis c) A cut along the Z axis

Figure 33. The geometry of the test pit model (Geofoam-EPS 19-Design 2)

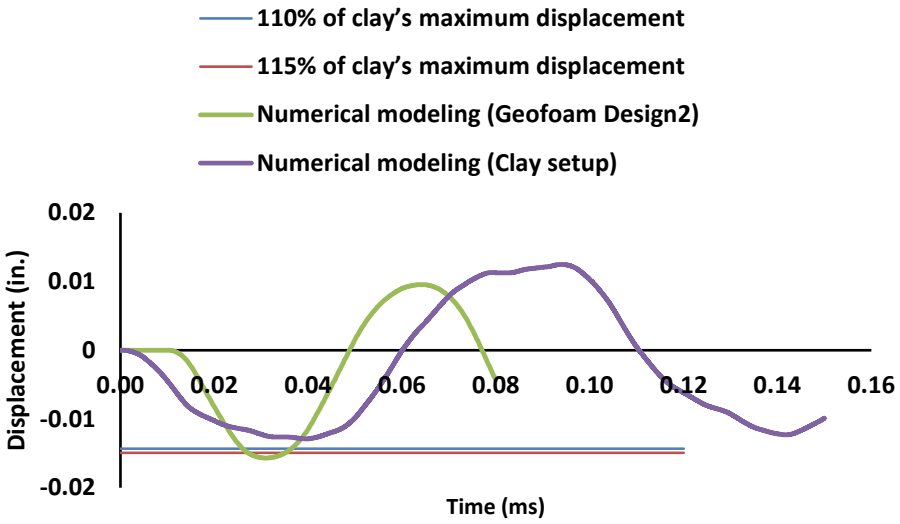

Figure 34. Predicted displacements of both setups with the maximum impact load of 8.33 kip (Geofoam-EPS19-Design 2).

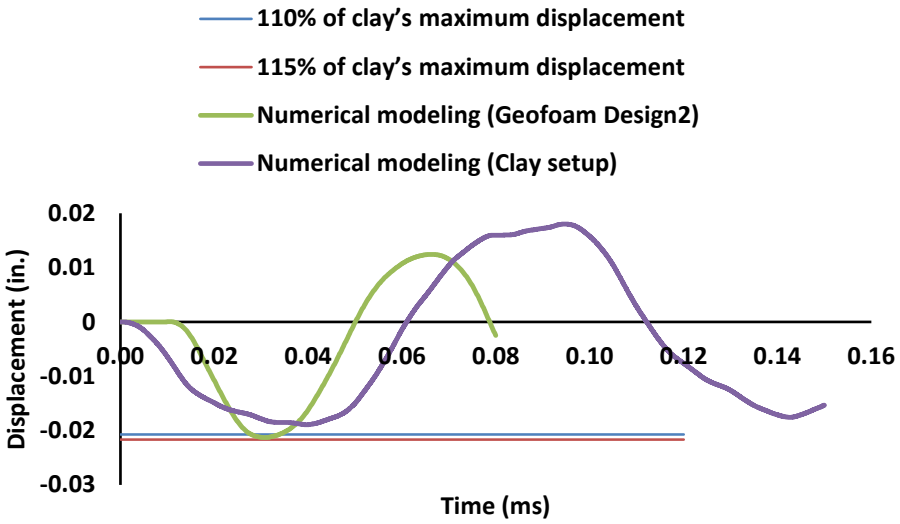

Figure 35. Predicted displacements of both setups with the maximum impact load of 11.55 kip (Geofoam-EPS19-Design 2).

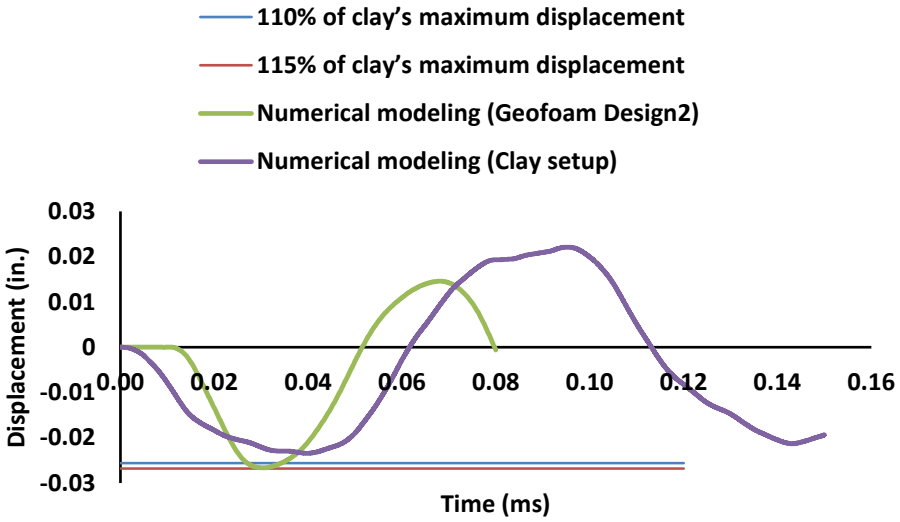

Figure 36. Predicted displacements of both setups with the maximum impact load of 14.68 kip (Geofoam-EPS19-Design 2).

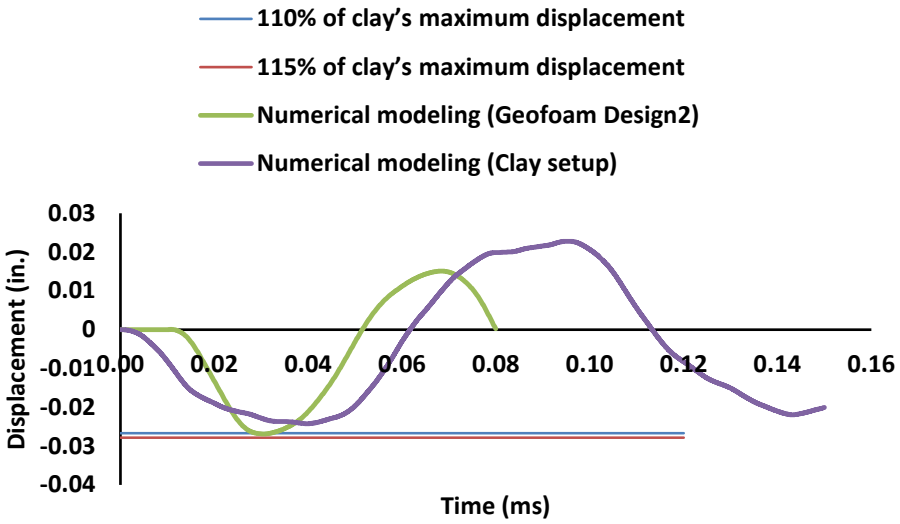

Figure 37. Predicted displacements of both setups with the maximum impact load of 15.11 kip (Geofoam-EPS19-Design 2).

8.2.3 EPS19-Design 3

The geometry of the EPS19-Design 3 is shown in Figure 38. The predicted displacement histories for four different maximum impact loads are shown in Figures 39 to 42.

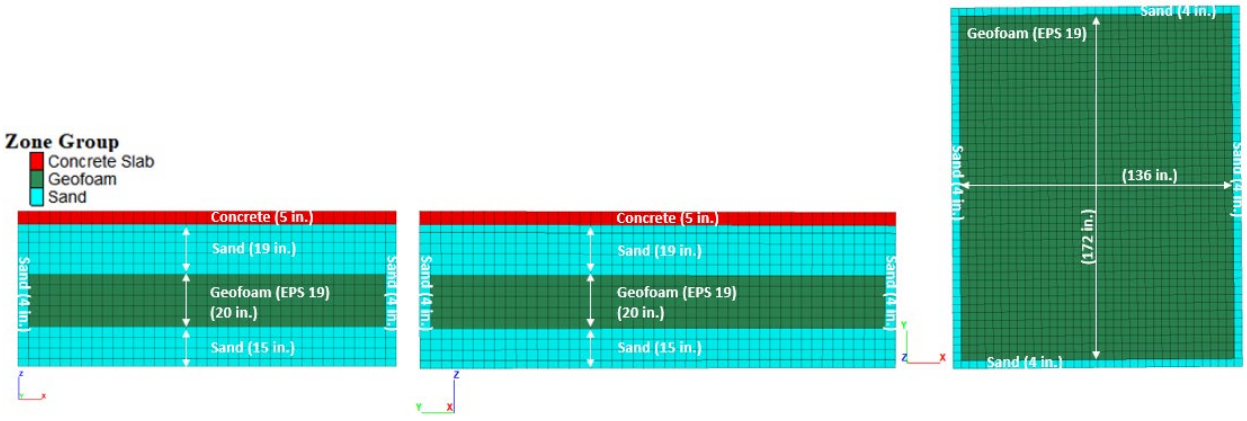

a) A cut along the Y axis b) A cut along the X axis c) A cut along the Z axis

Figure 38. The geometry of the test pit model (Geofoam-EPS 19-Design 3).

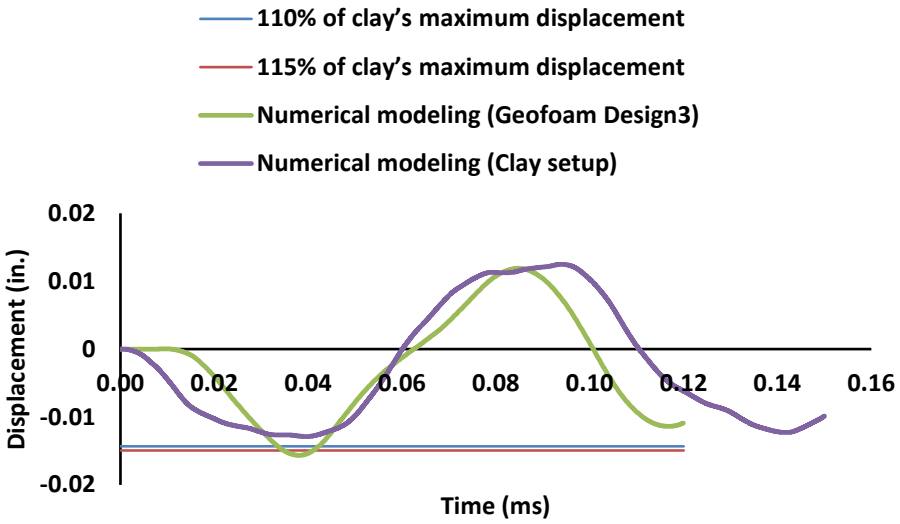

Figure 39. Predicted displacements of both setups with the maximum impact load of 8.33 kip (Geofoam-EPS19-Design 3).

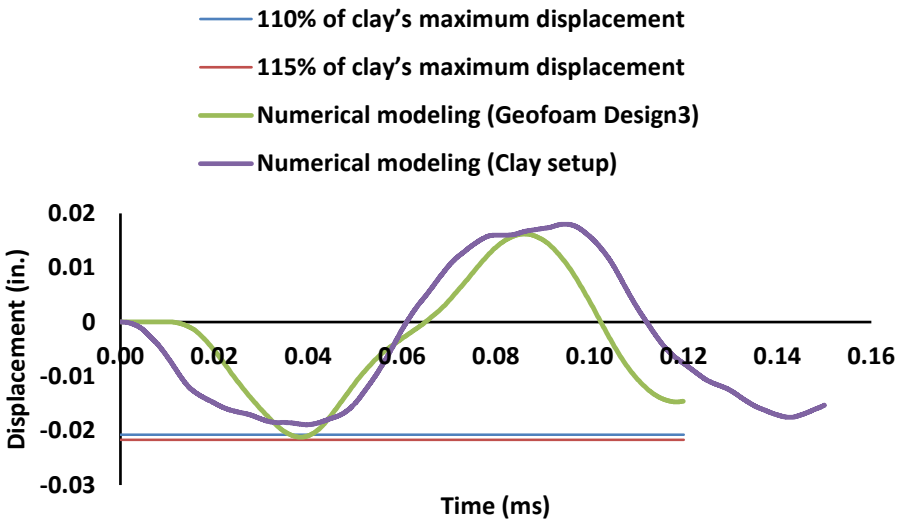

Figure 40. Predicted displacements of both setups with the maximum impact load of 11.55 kip (Geofoam-EPS19-Design 3).

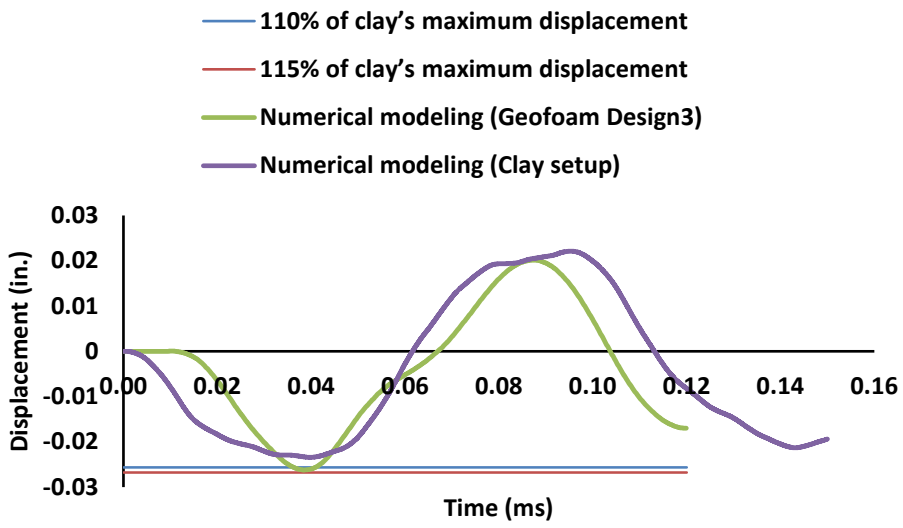

Figure 41. Predicted displacements of both setups with the maximum impact load of 14.68 kip (Geofoam-EPS19-Design 3).

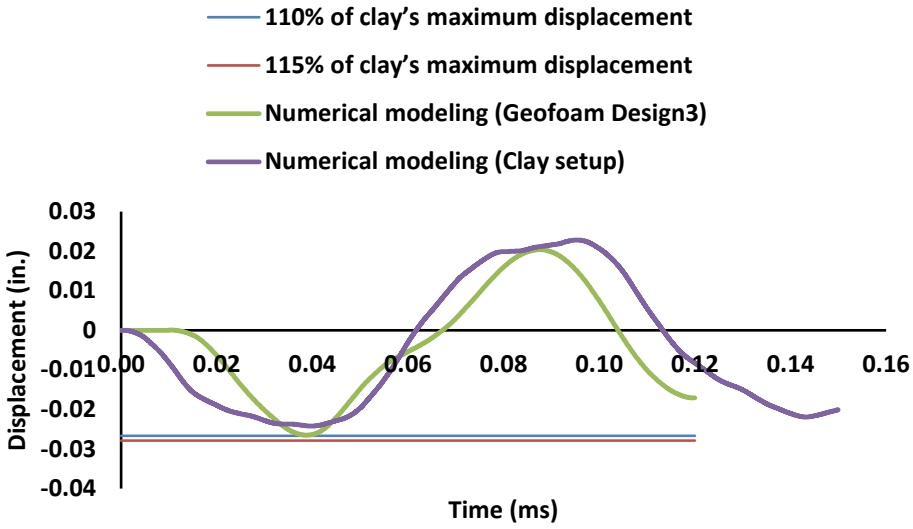

Figure 42. Predicted displacements of both setups with the maximum impact load of 15.11 kip (Geofoam-EPS19-Design 3).

8.2.4 EPS19-Design 4

The geometry of the EPS19-Design 4 is shown in Figure 43. The predicted displacement histories for four different maximum impact loads are shown in Figures 44 to 47.

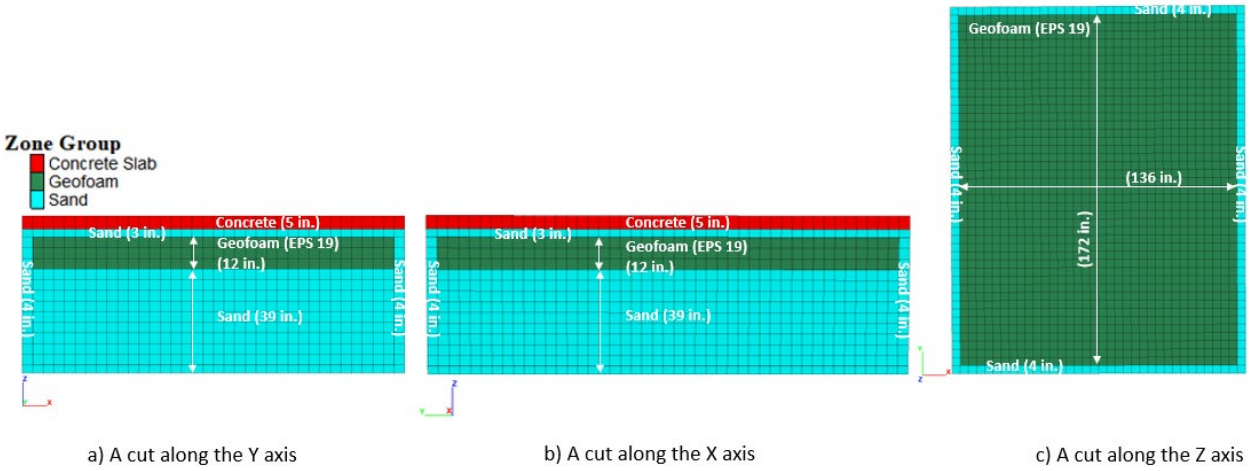

Figure 43. The geometry of the test pit model (Geofoam-EPS 19-Design 4).

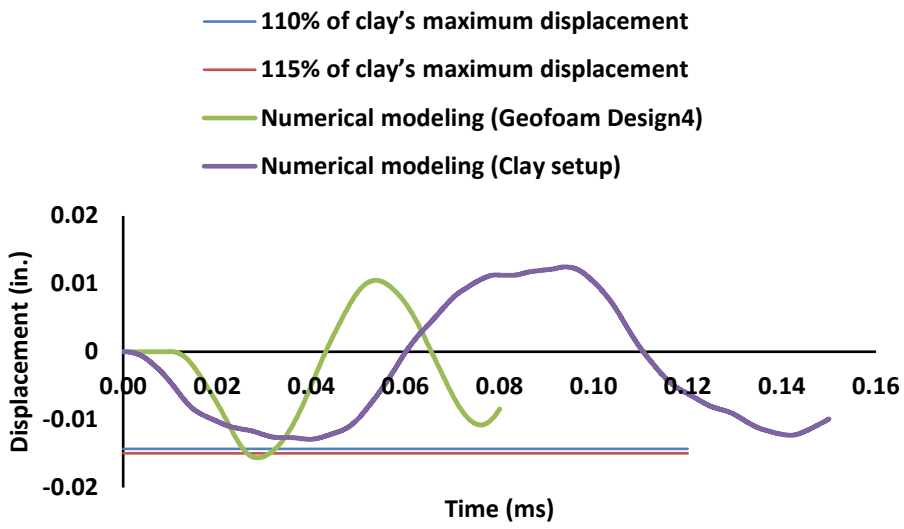

Figure 44. Predicted displacements of both setups with the maximum impact load of 8.33 kip (Geofoam-EPS19-Design 4).

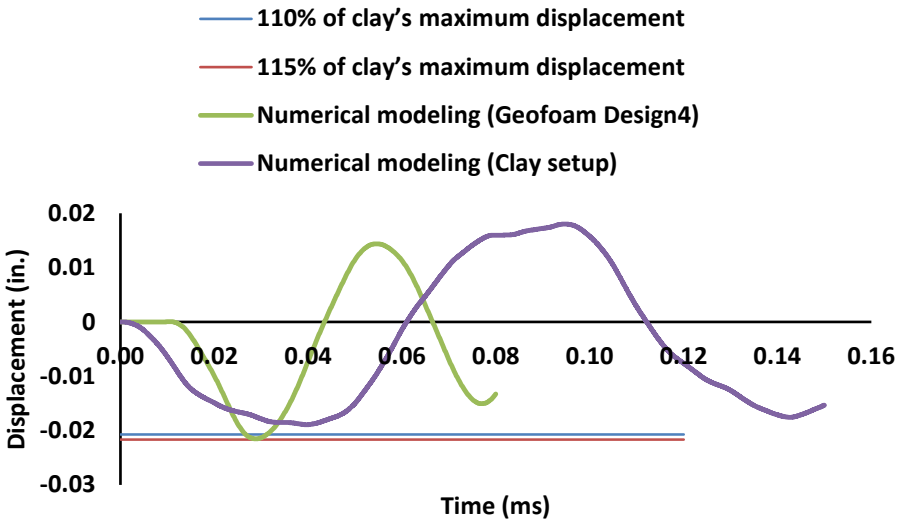

Figure 45. Predicted displacements of both setups with the maximum impact load of 11.55 kip (Geofoam-EPS19-Design 4).

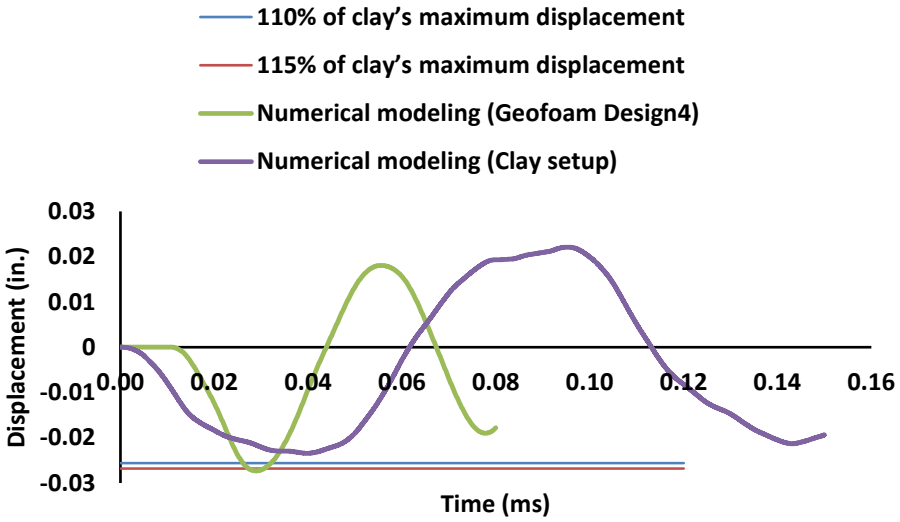

Figure 46. Predicted displacements of both setups with the maximum impact load of 14.68 kip (Geofoam-EPS19-Design 4).

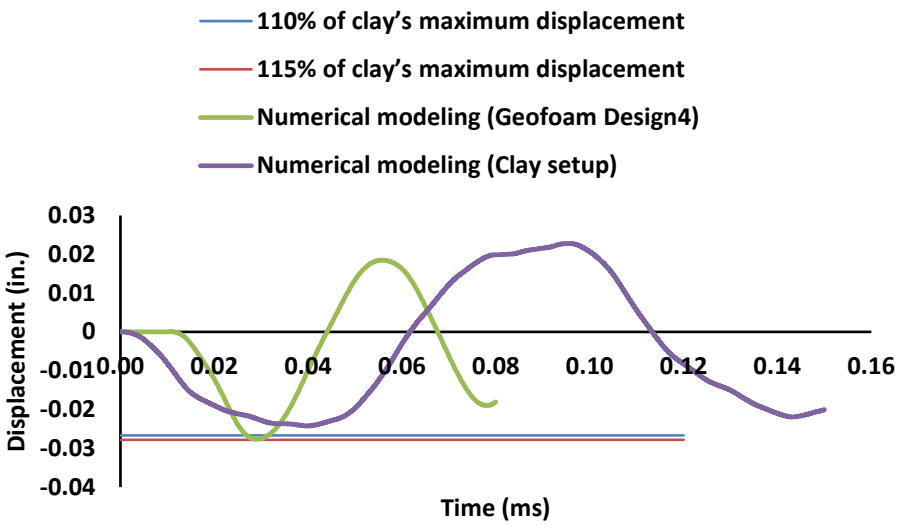

Figure 47. Predicted displacements of both setups with the maximum impact load of 15.11 kip (Geofoam-EPS19-Design 4).

8.2.5 EPS19-Design 5

The geometry of the EPS19-Design 5 is shown in Figure 48. The predicted displacement histories for four different maximum impact loads are shown in Figures 49 to 52.

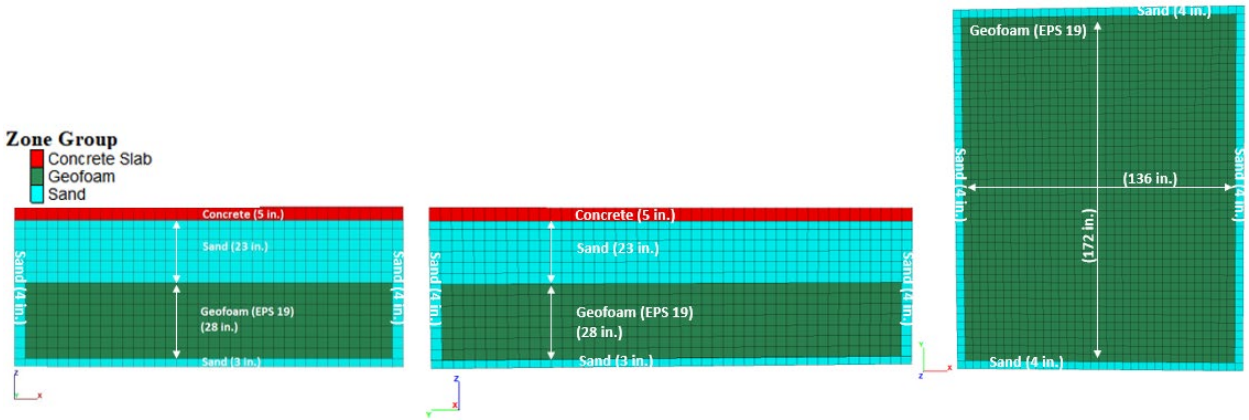

a) A cut along the Y axis b) A cut along the X axis c) A cut along the Z axis

Figure 48. The geometry of the test pit model (Geofoam-EPS 19-Design 5).

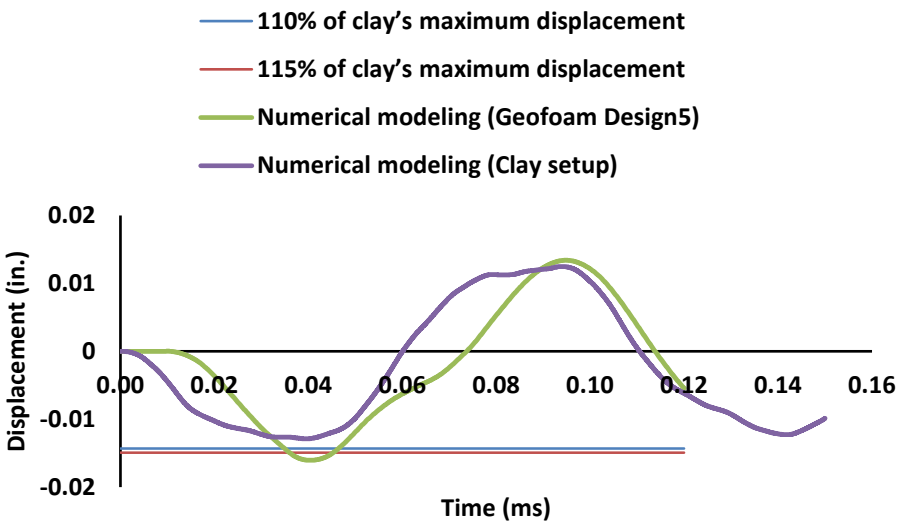

Figure 49. Predicted displacements of both setups with the maximum impact load of 8.33 kip (Geofoam-EPS19-Design 5).

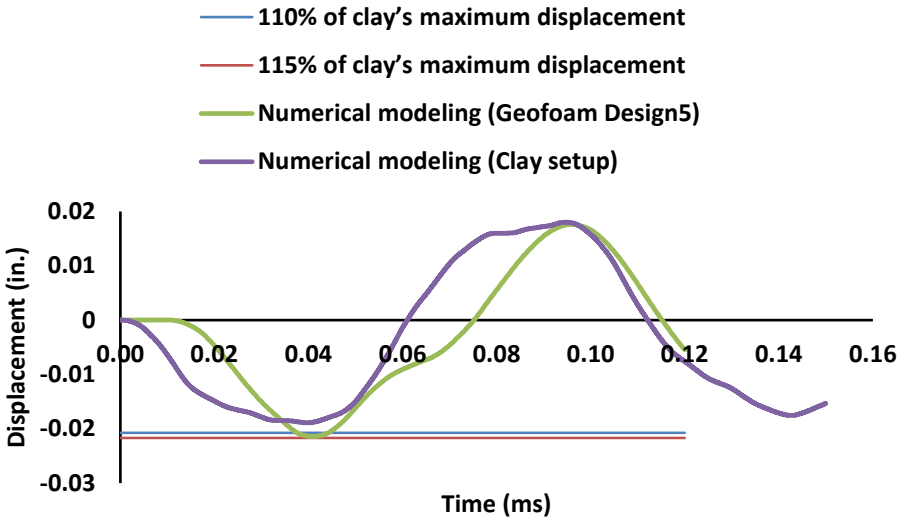

Figure 50. Predicted displacements of both setups with the maximum impact load of 11.55 kip (Geofoam-EPS19-Design 5).

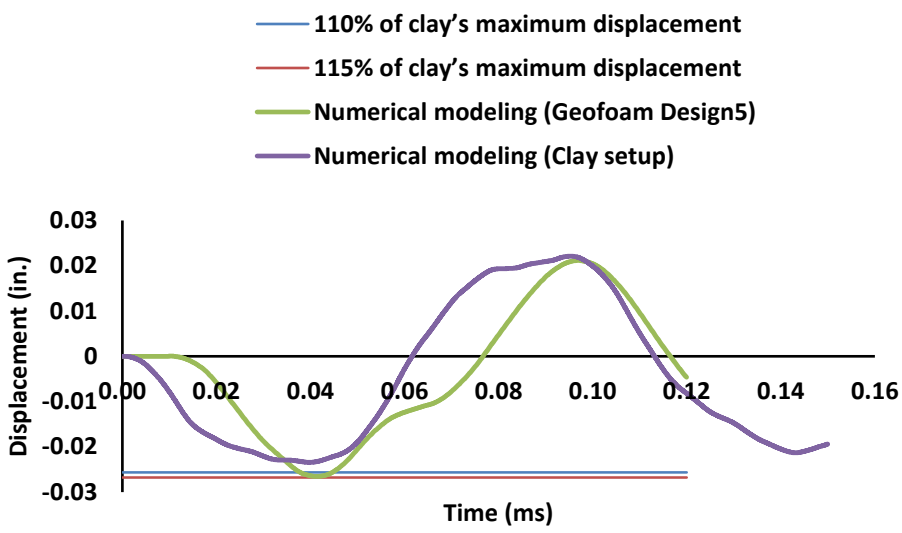

Figure 51. Predicted displacements of both setups with the maximum impact load of 14.68 kip (Geofoam-EPS19-Design 5).

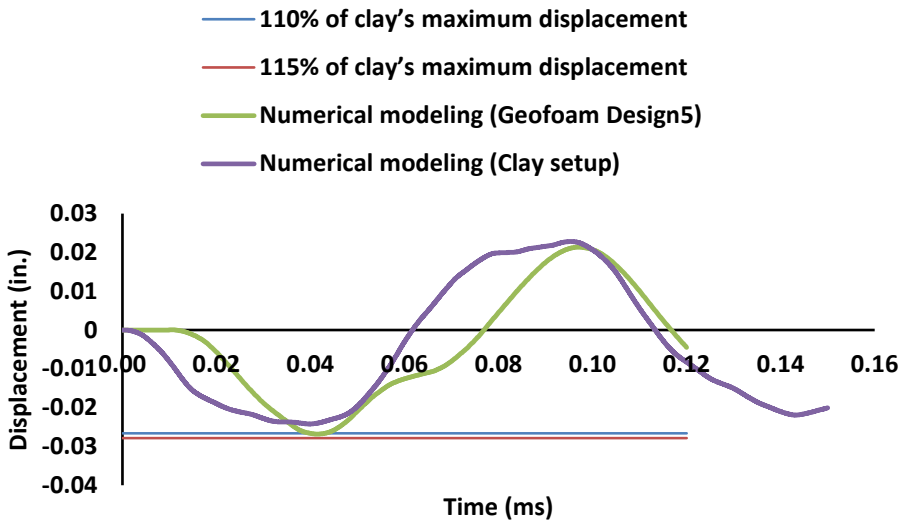

Figure 52. Predicted displacements of both setups with the maximum impact load of 15.11 kip (Geofoam-EPS19-Design 5).

8.3 Using EPS 29 Geofoam for the new Design

The second type of geofoam used is EPS 29 which has larger values for density and elastic modulus compared to EPS 19. There are four different designs provided for this type of geofoam.

8.3.1 EPS29-Design 1

The geometry of the EPS29-Design 1 is shown in Figure 53. The predicted displacement histories for four different maximum impact loads are shown in Figures 54 to 57.

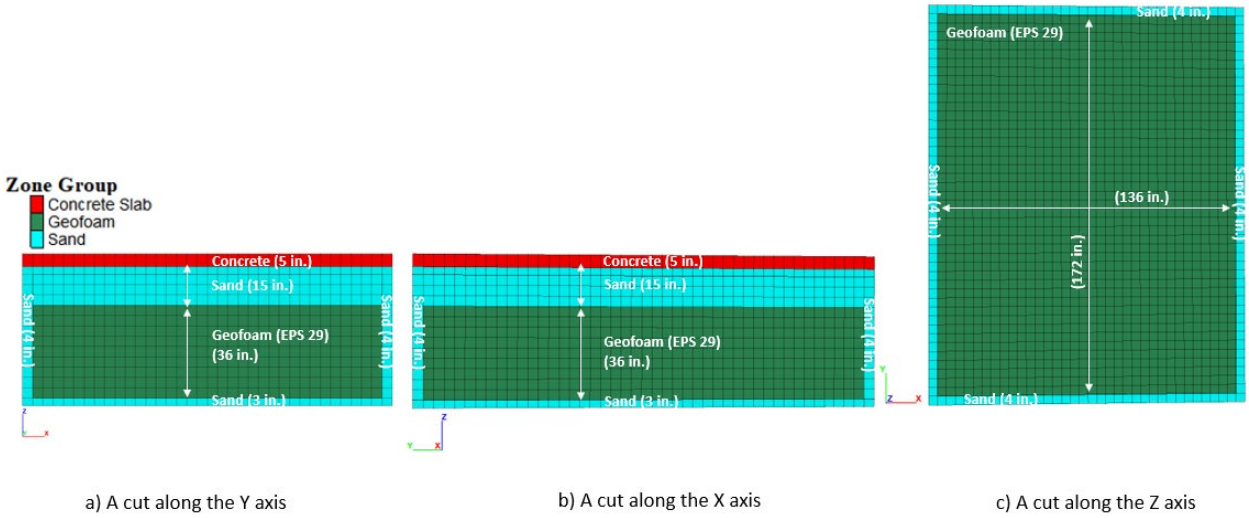

a) A cut along the Y axis b) A cut along the X axis c) A cut along the Z axis

Figure 53. The geometry of the test pit model (Geofoam-EPS 29-Design 1).

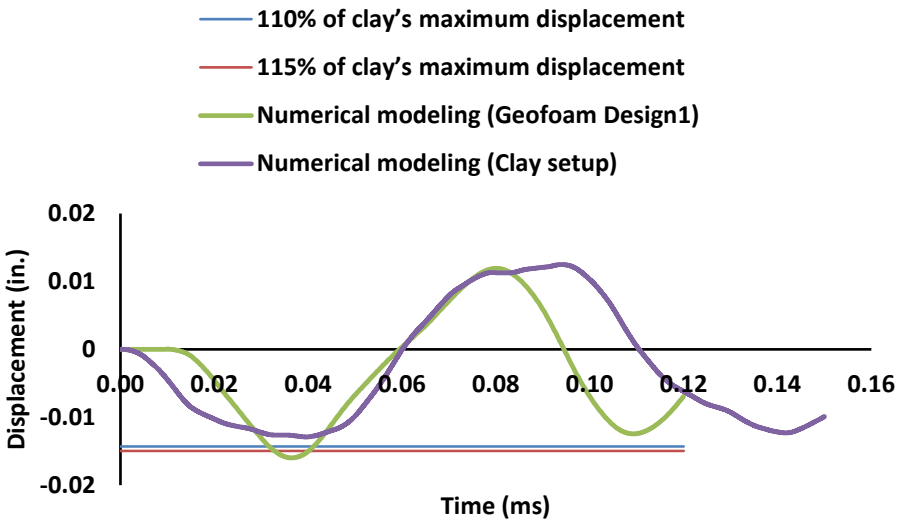

Figure 54. Predicted displacements of both setups with the maximum impact load of 8.33 kip (Geofoam-EPS29-Design 1).

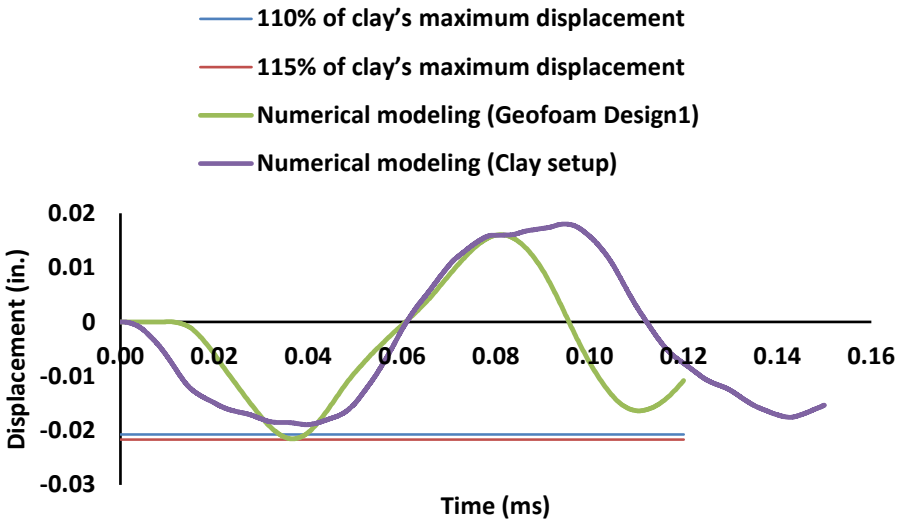

Figure 55. Predicted displacements of both setups with the maximum impact load of 11.55 kip (Geofoam-EPS29-Design 1).

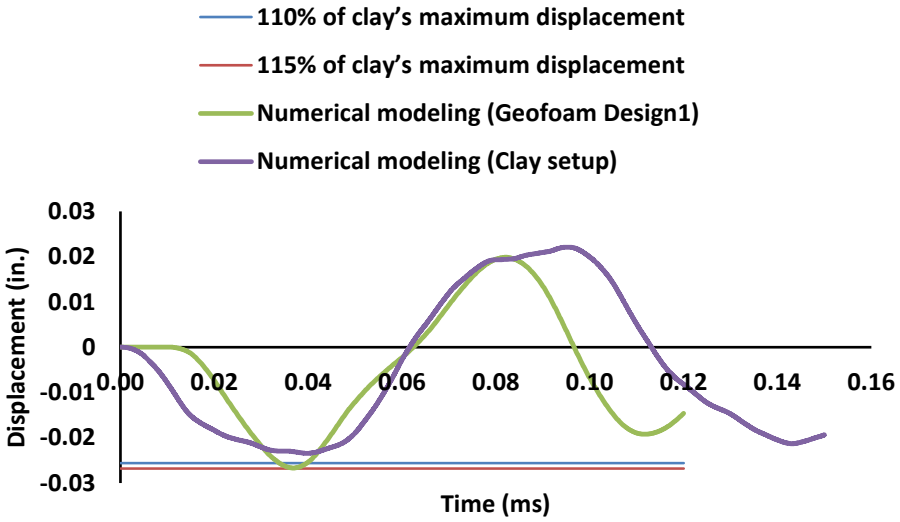

Figure 56. Predicted displacements of both setups with the maximum impact load of 14.68 kip (Geofoam-EPS29-Design 1).

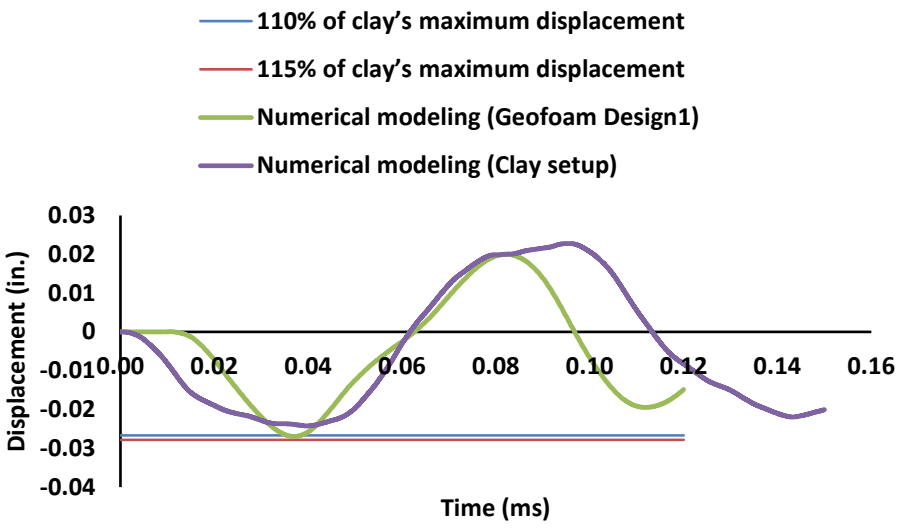

Figure 57. Predicted displacements of both setups with the maximum impact load of 15.11 kip (Geofoam-EPS29-Design 1).

8.3.2 EPS29-Design 2

The geometry of the EPS29-Design 2 is shown in Figure 58. The predicted displacement histories for four different maximum impact loads are shown in Figures 59 to 62.

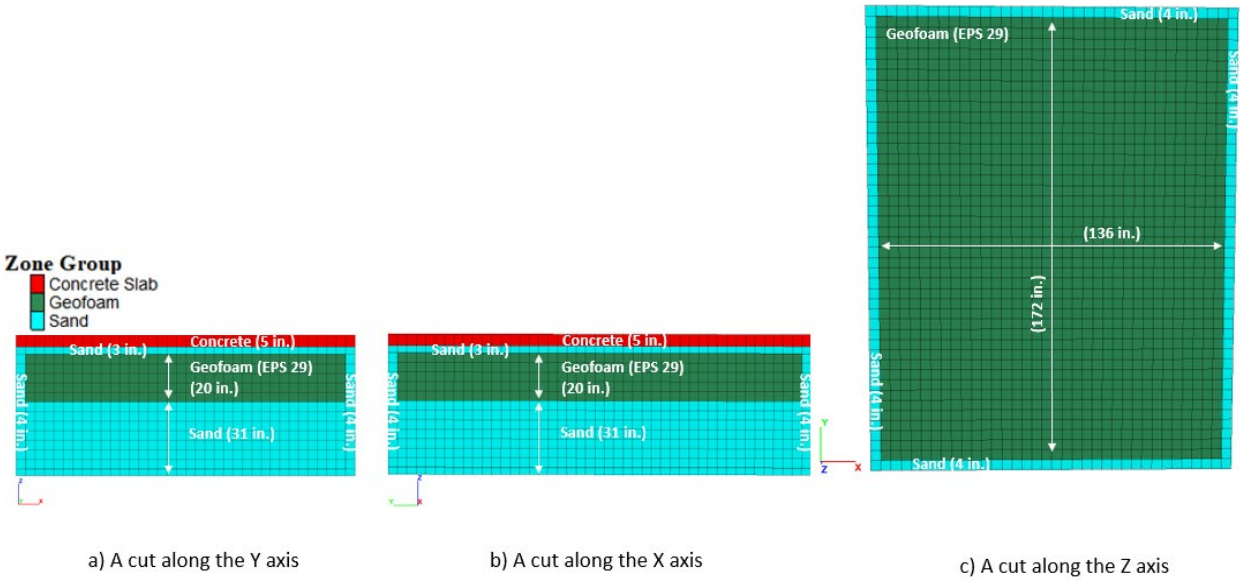

a) A cut along the Y axis b) A cut along the X axis c) A cut along the Z axis

Figure 58. The geometry of the test pit model (Geofoam-EPS 29-Design 2)

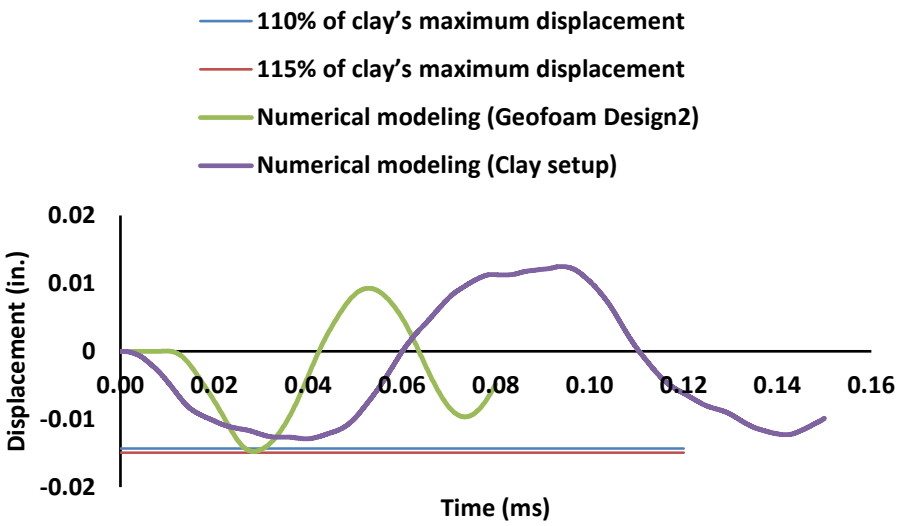

Figure 59. Predicted displacements of both setups with the maximum impact load of 8.33 kip (Geofoam-EPS29-Design 2).

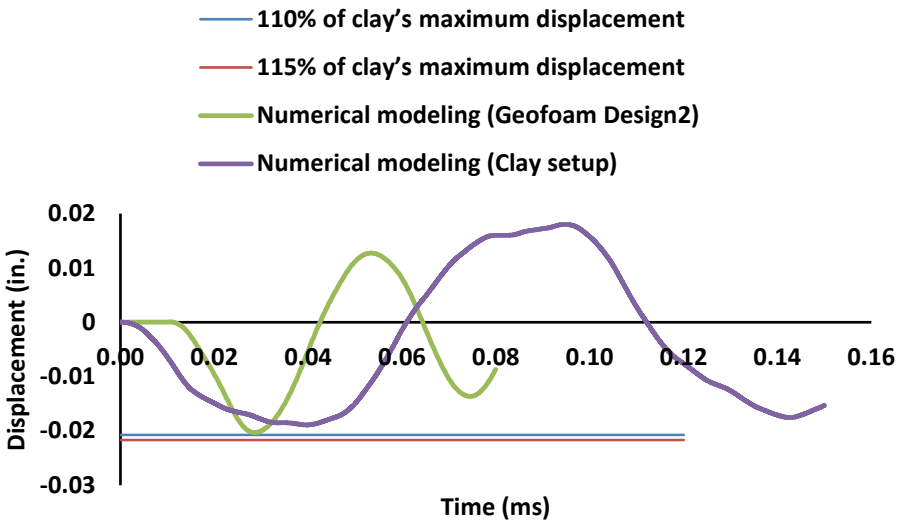

Figure 60. Predicted displacements of both setups with the maximum impact load of 11.55 kip (Geofoam Setup-EPS29-Design 2).

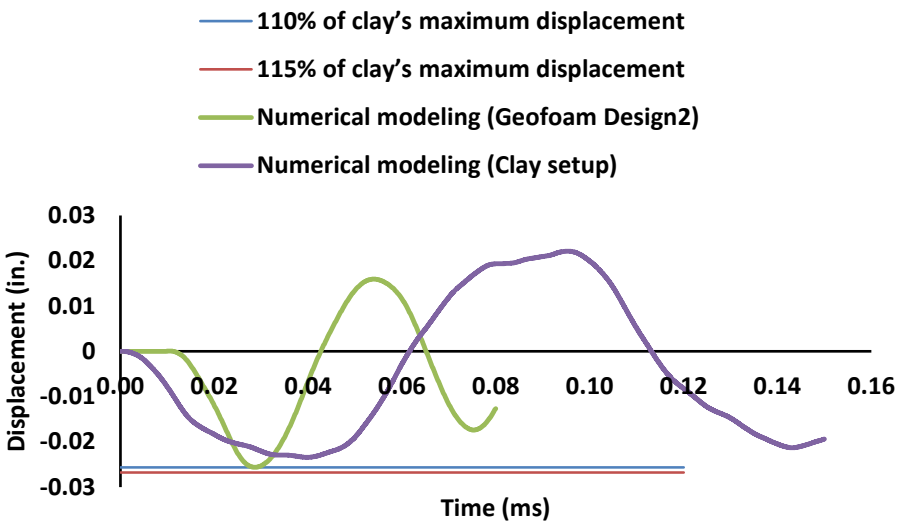

Figure 61. Predicted displacements of both setups with the maximum impact load of 14.68 kip (Geofoam Setup-EPS29-Design 2).

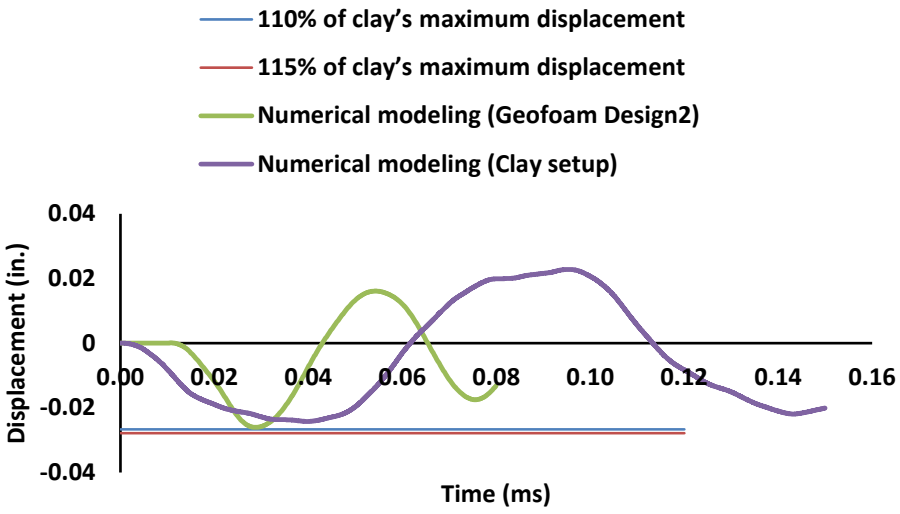

Figure 62. Predicted displacements of both setups with the maximum impact load of 15.11 kip (Geofoam Setup-EPS29-Design 2).

8.3.3 EPS29-Design 3

The geometry of the EPS29-Design 3 is shown in Figure 63. The predicted displacement histories for four different maximum impact loads are shown in Figures 64 to 67.

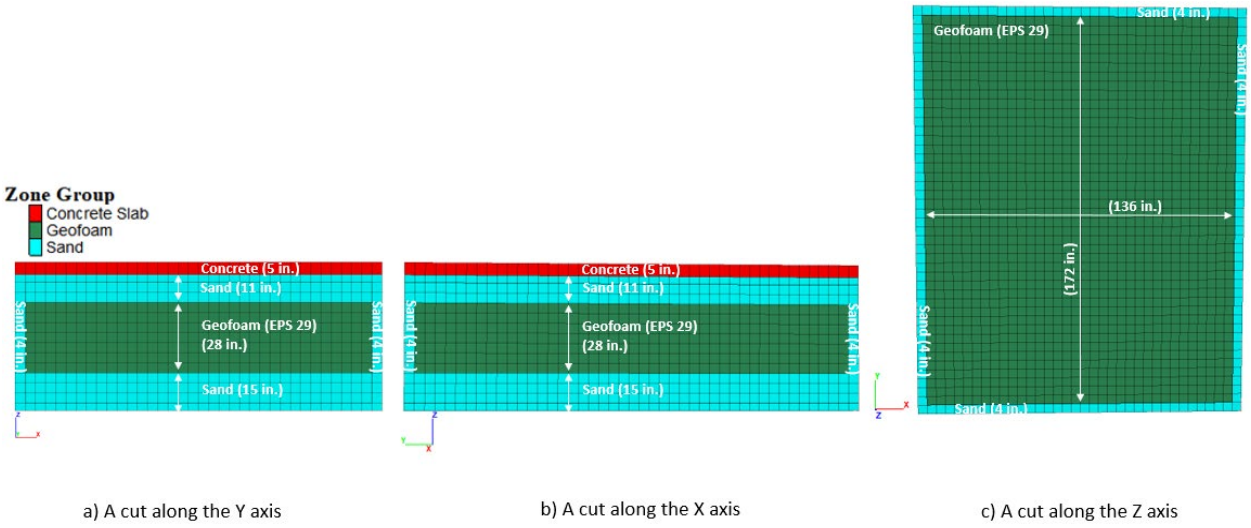

a) A cut along the Y axis b) A cut along the X axis c) A cut along the Z axis

Figure 63. The geometry of the test pit model (Geofoam-EPS 29-Design 3)

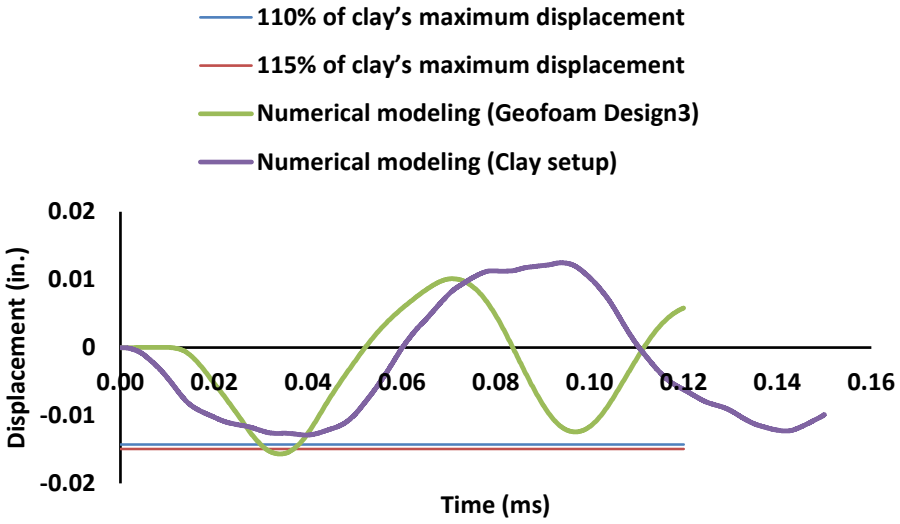

Figure 64. Predicted displacements of both setups with the maximum impact load of 8.33 kip (Geofoam-EPS29-Design 3).

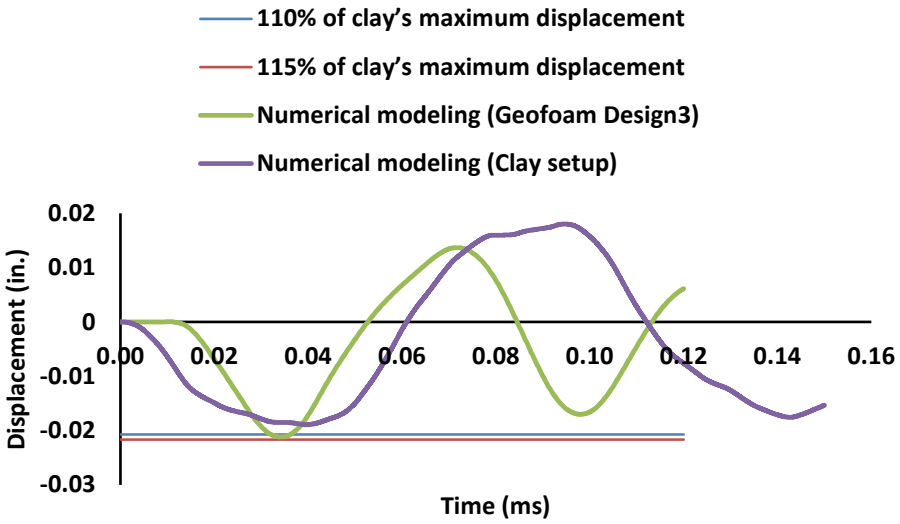

Figure 65. Predicted displacements of both setups with the maximum impact load of 11.55 kip (Geofoam-EPS29-Design 3).

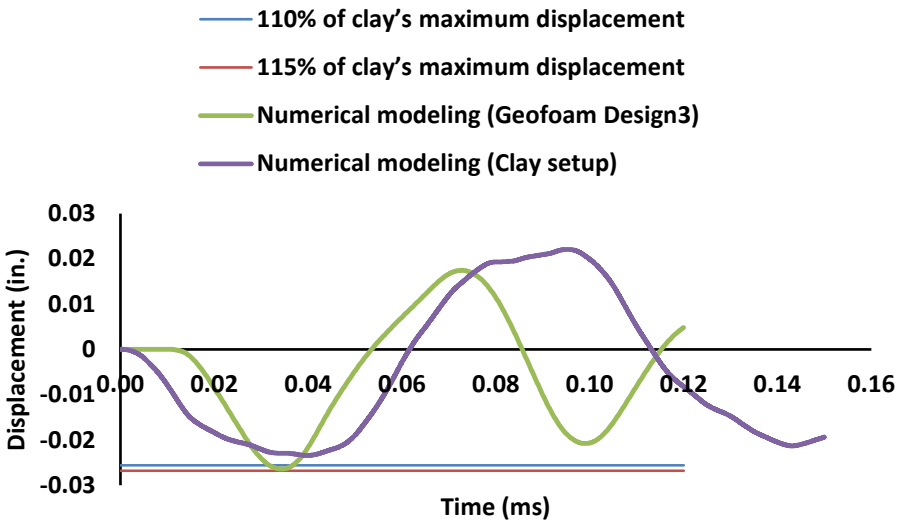

Figure 66. Predicted displacements of both setups with the maximum impact load of 14.68 kip (Geofoam-EPS29-Design 3).

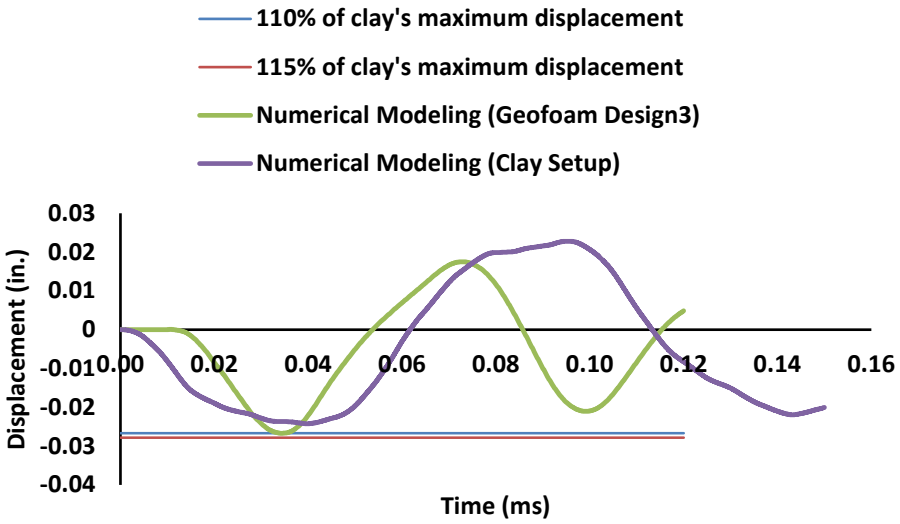

Figure 67. Predicted displacements of both setups with the maximum impact load of 15.11 kip (Geofoam-EPS29-Design 3).

8.3.4 EPS29-Design 4

The geometry of the EPS29-Design 4 is shown in Figure 68. The predicted displacement histories for four different maximum impact loads are shown in Figures 69 to Figure 72.

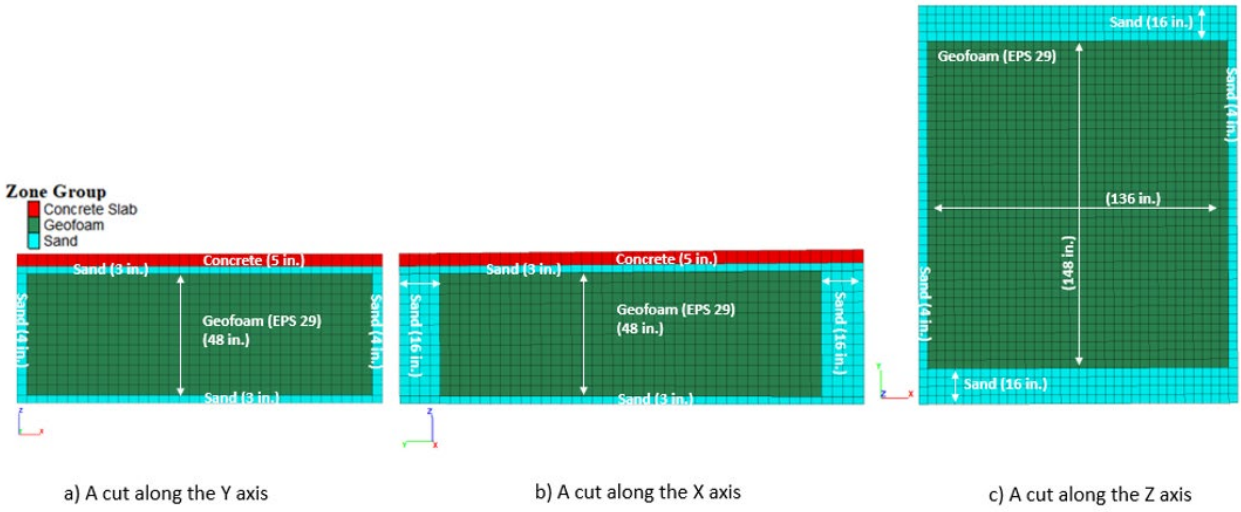

Figure 68. The geometry of the test pit model (Geofoam-EPS 29-Design 4)

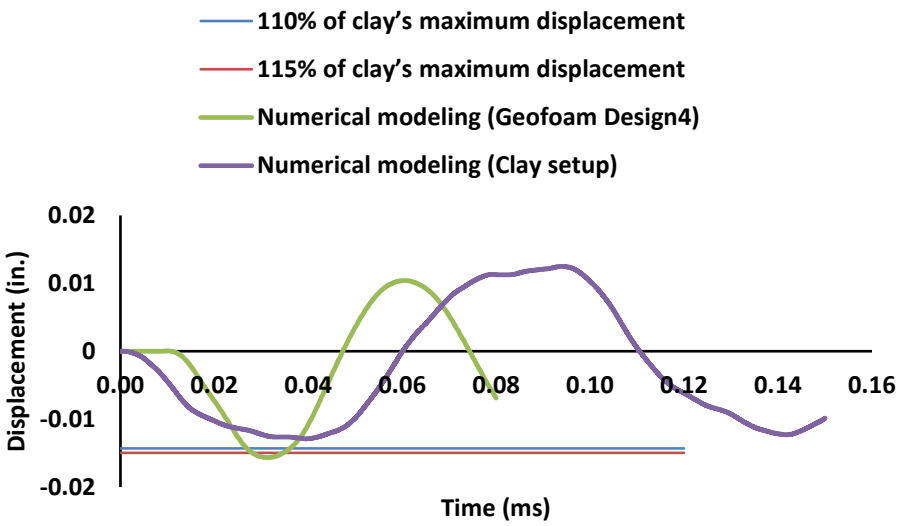

Figure 69. Predicted displacements of both setups with the maximum impact load of 8.33 kip (Geofoam-EPS29-Design 4).

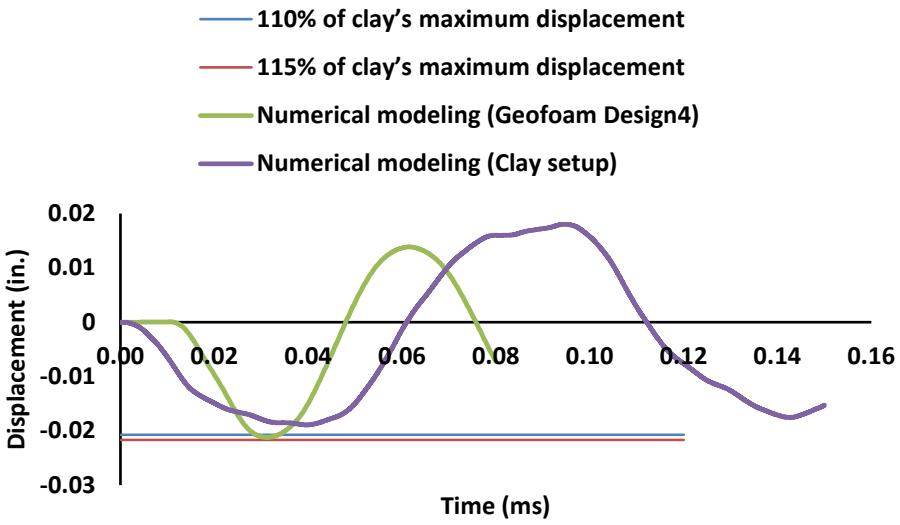

Figure 70. Predicted displacements of both setups with the maximum impact load of 11.55 kip (Geofoam-EPS29-Design 4).

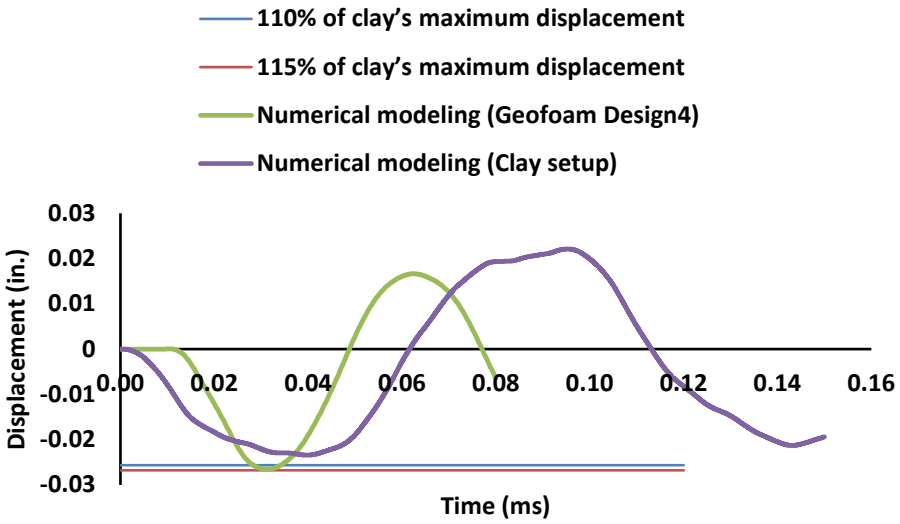

Figure 71. Predicted displacements of both setups with the maximum impact load of 14.68 kip (Geofoam-EPS29-Design 4).

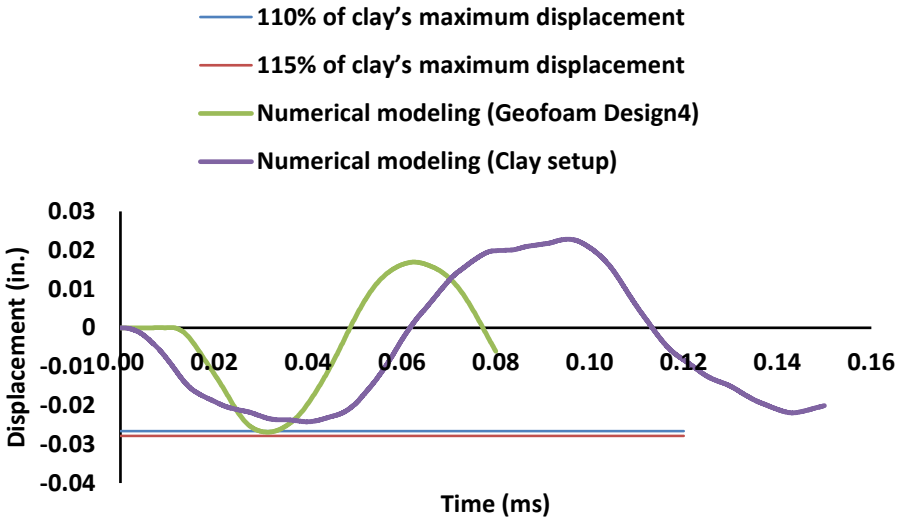

Figure 72. Predicted displacements of both setups with the maximum impact load of 15.11 kip (Geofoam-EPS29-Design 4).

8.4 Using EPS 39 Geofoam for the New Design

EPS 39 Geofoam is used in the next set of designs. As mentioned before, geofoam with a higher number of EPS provides higher values for density and young modulus.

8.4.1 EPS39-Design 1

The geometry of the EPS39-Design 1 is shown in Figure 73. The predicted displacement histories for four different maximum impact loads are shown in Figures 74 to 77.

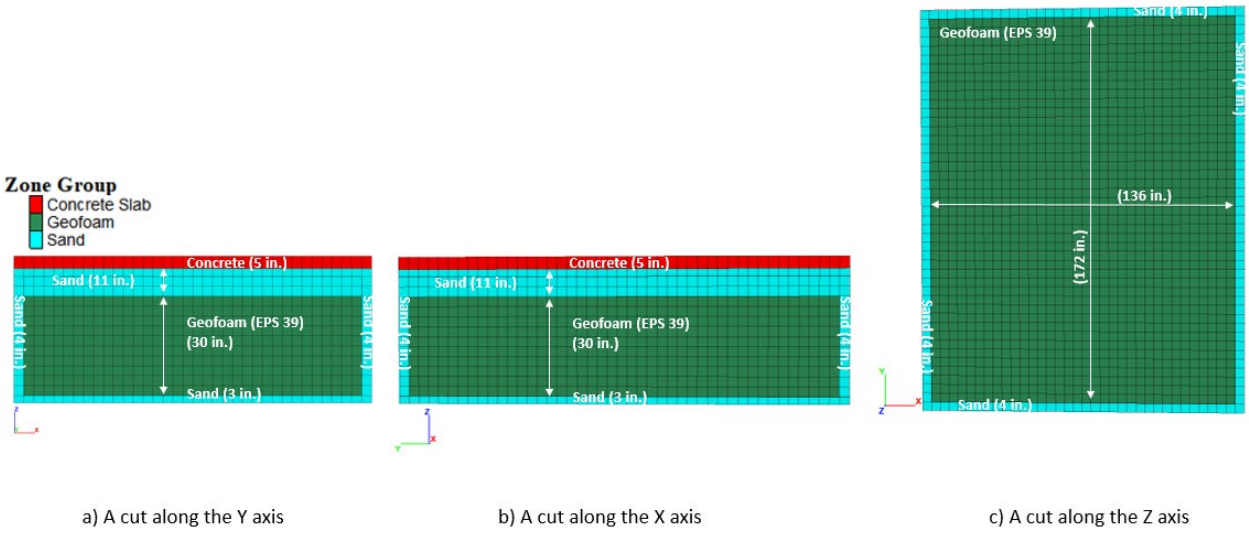

Figure 73. The geometry of the test pit model (EPS 39-Design 1).

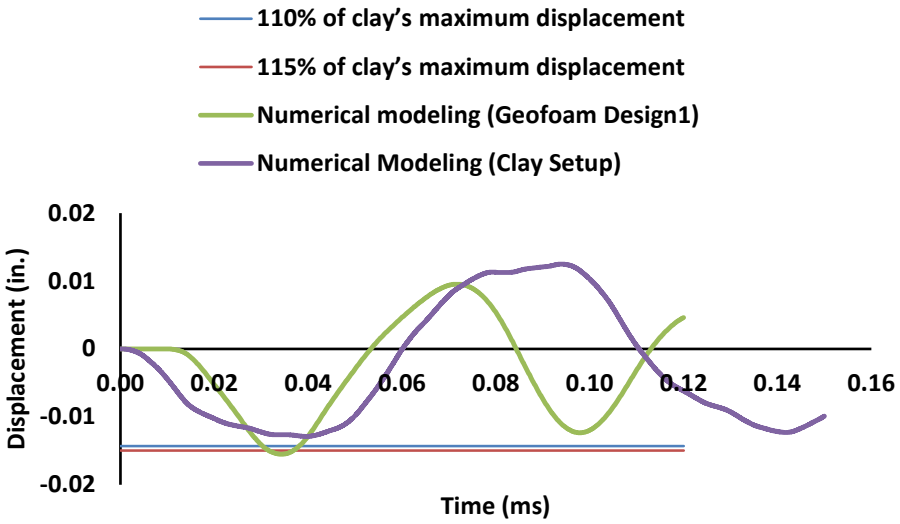

Figure 74. Predicted displacements of both setups with the maximum impact load of 8.33 kip (Geofoam-EPS39-Design 1).

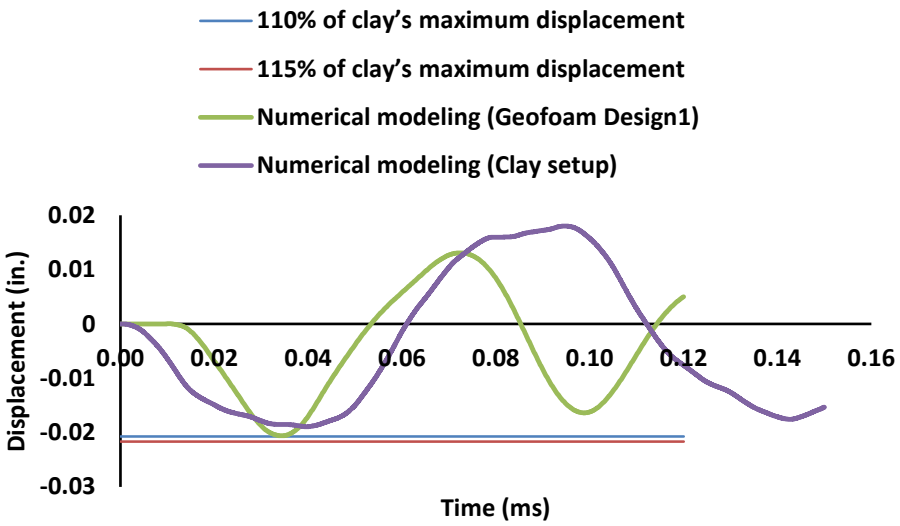

Figure 75. Predicted displacements of both setups with the maximum impact load of 11.55 kip (Geofoam-EPS39-Design 1).

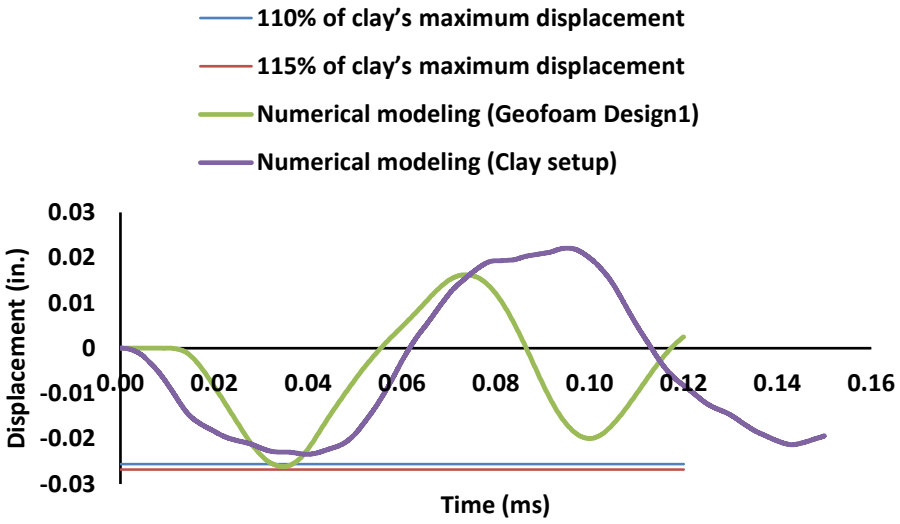

Figure 76. Predicted displacements of both setups with the maximum impact load of 14.68 kip (Geofoam-EPS39-Design 1).

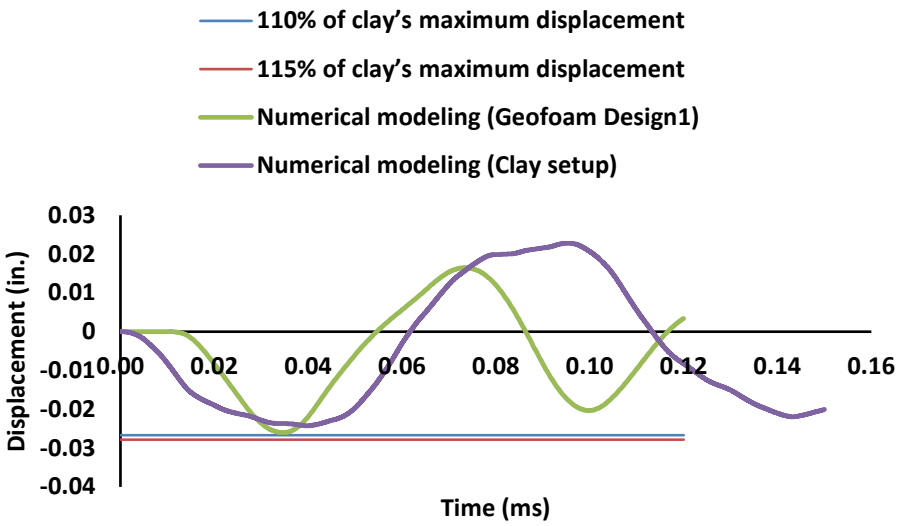

Figure 77. Predicted displacements of both setups with the maximum impact load of 15.11 kip (Geofoam-EPS39-Design 1).

8.4.2 EPS39-Design 2

The geometry of the EPS39-Design 2 is shown in Figure 78. The predicted displacement histories for four different maximum impact loads are shown in Figures 79 to 82.

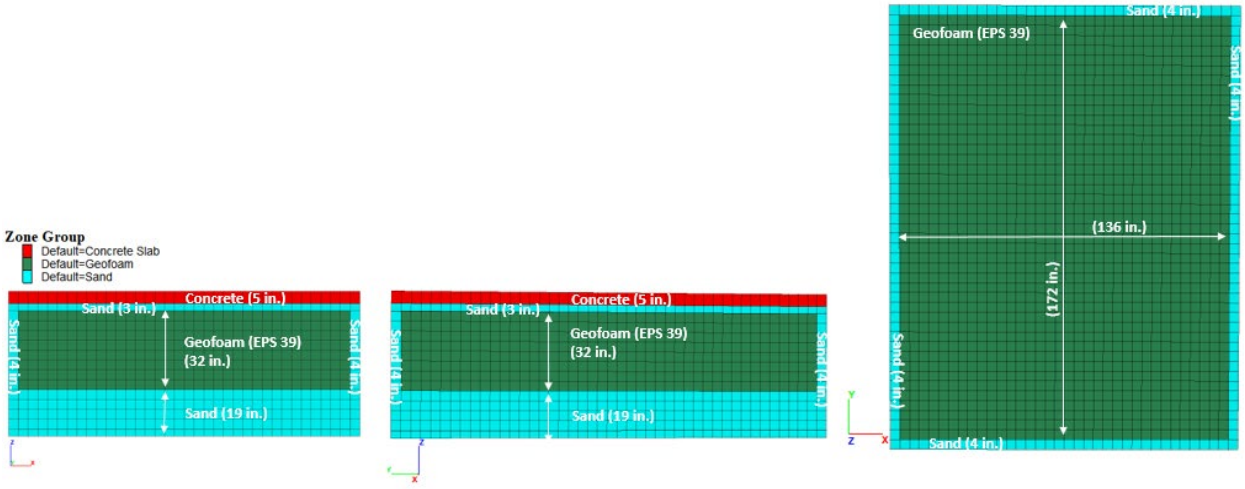

a) A cut along the Y axis b) A cut along the X axis c) A cut along the Z axis

Figure 78. The geometry of the test pit model (Geofoam-EPS 39-Design 2).

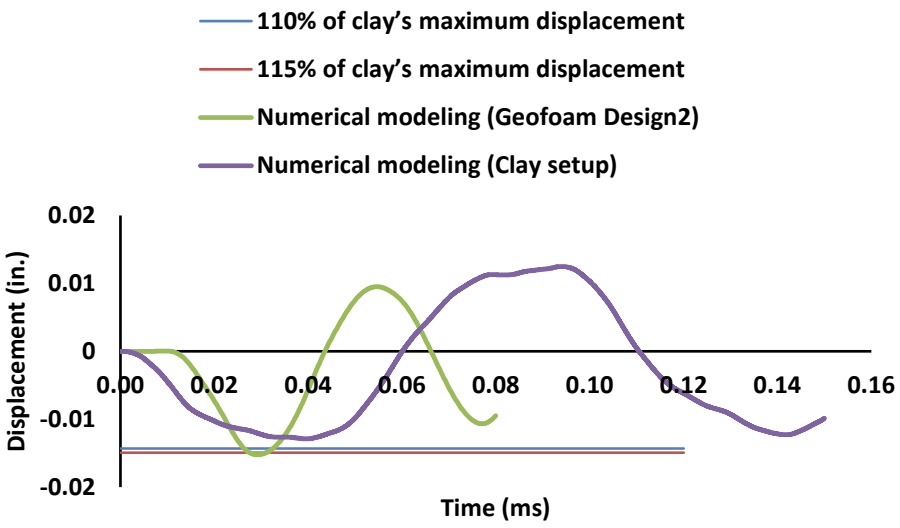

Figure 79. Predicted displacements of both setups with the maximum impact load of 8.33 kip (Geofoam-EPS39-Design 2).

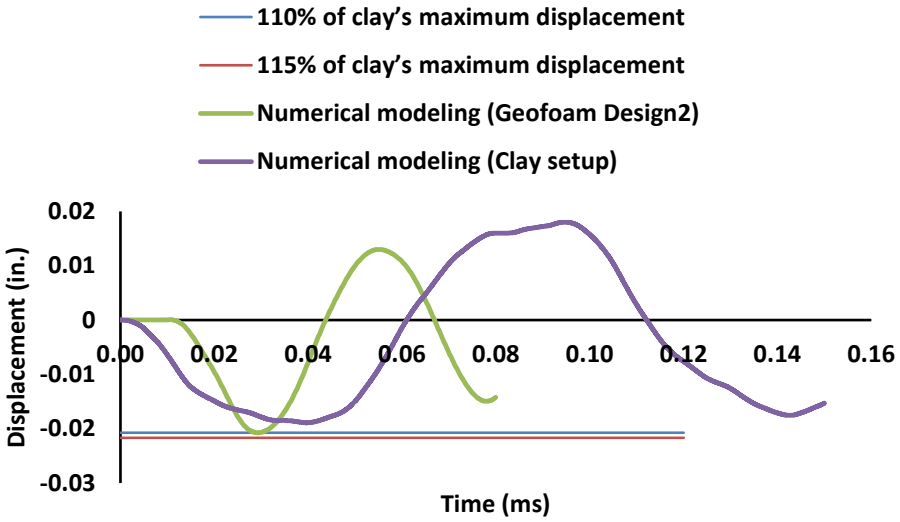

Figure 80. Predicted displacements of both setups with the maximum impact load of 11.55 kip (Geofoam-EPS39-Design 2).

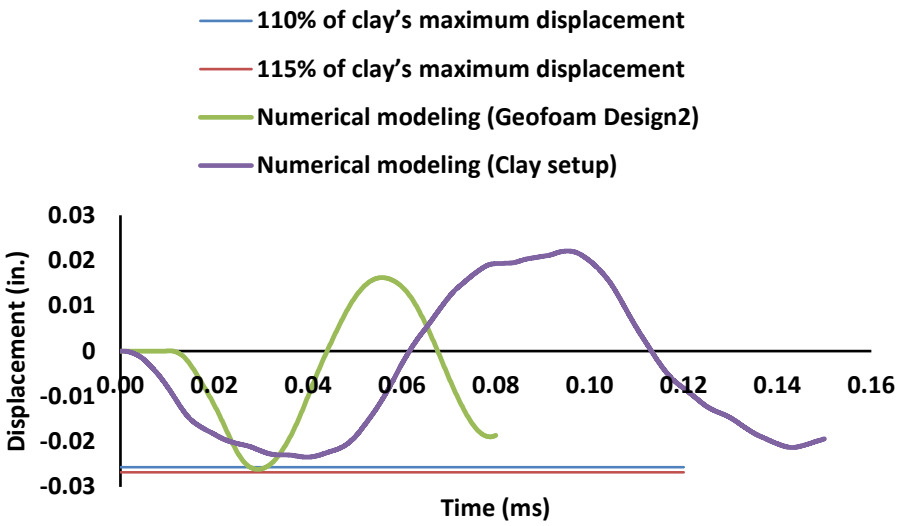

Figure 81. Predicted displacements of both setups with the maximum impact load of 14.68 kip (Geofoam-EPS39-Design 2).

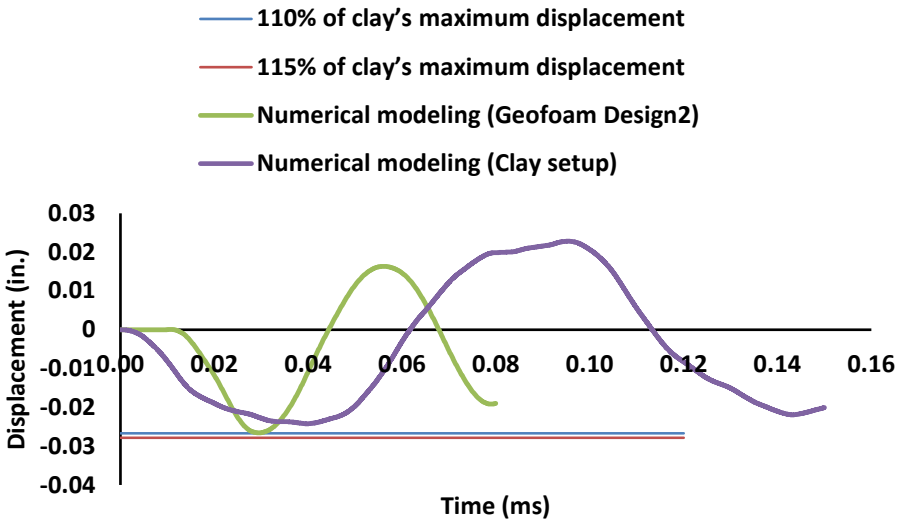

Figure 82. Predicted displacements of both setups with the maximum impact load of 15.11 kip (Geofoam-EPS39-Design 2).

8.4.3 EPS39-Design 3

The geometry of the EPS39-Design 3 is shown in Figure 83. The predicted displacement histories for four different maximum impact loads are shown in Figures 84 to 87.

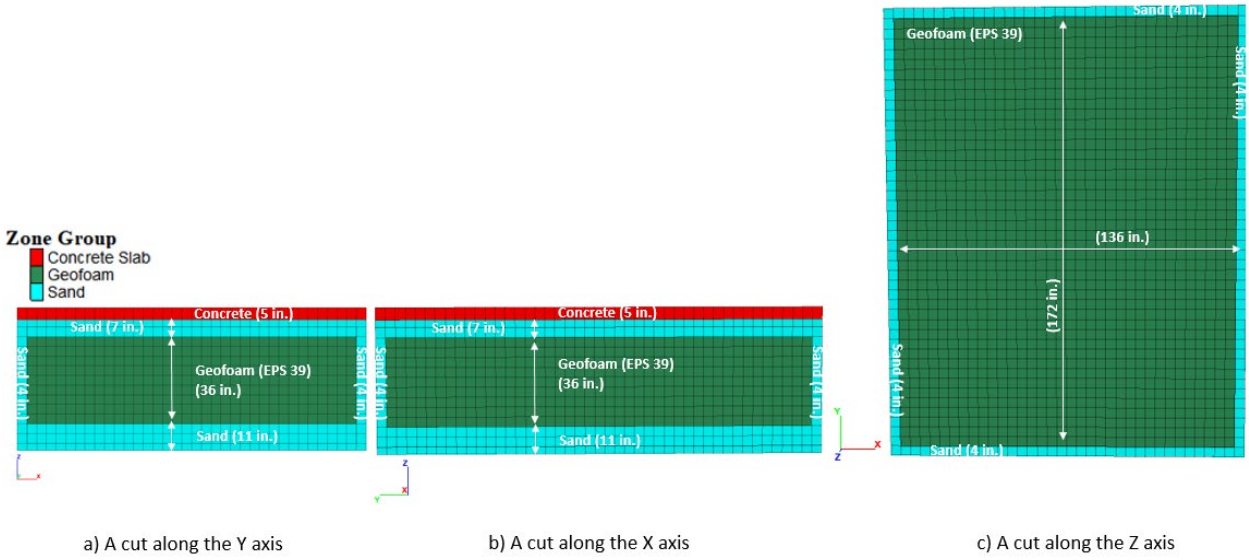

a) A cut along the Y axis b) A cut along the X axis c) A cut along the Z axis

Figure 83. The geometry of the test pit model (Geofoam-EPS 39-Design 3).

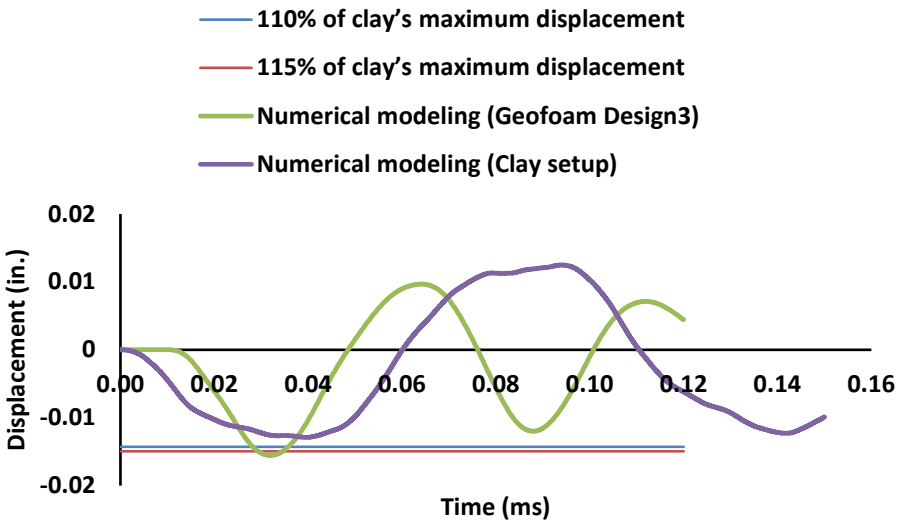

Figure 84. Predicted displacements of both setups with the maximum impact load of 8.33 kip (Geofoam-EPS39-Design 3).

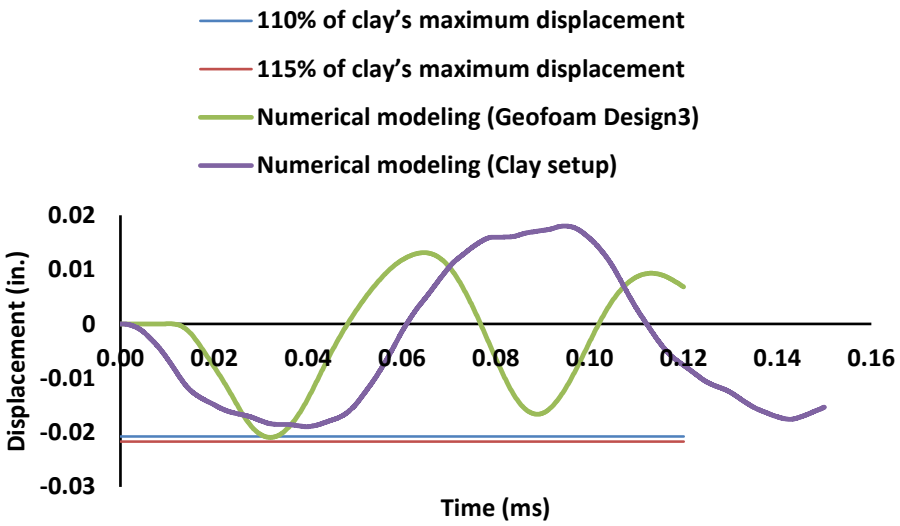

Figure 85. Predicted displacements of both setups with the maximum impact load of 11.55 kip (Geofoam-EPS39-Design 3).

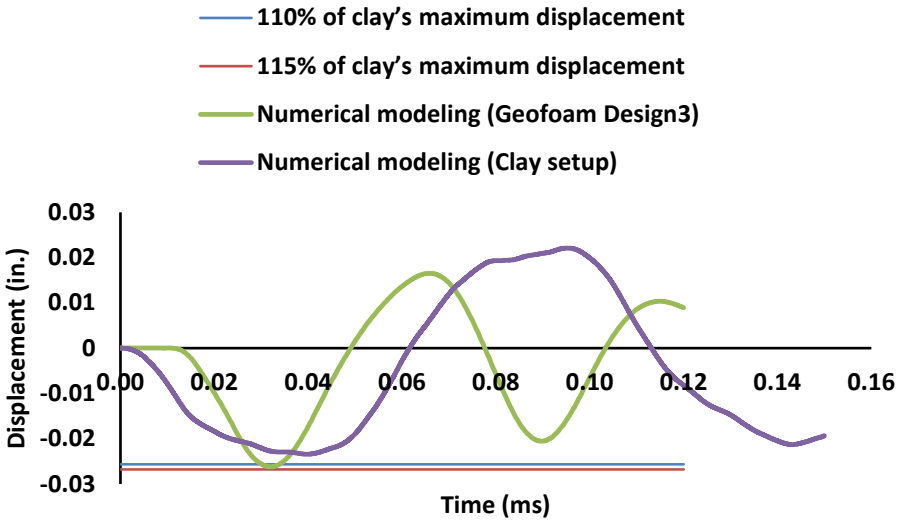

Figure 86. Predicted displacements of both setups with the maximum impact load of 14.68 kip (Geofoam-EPS39-Design 3).

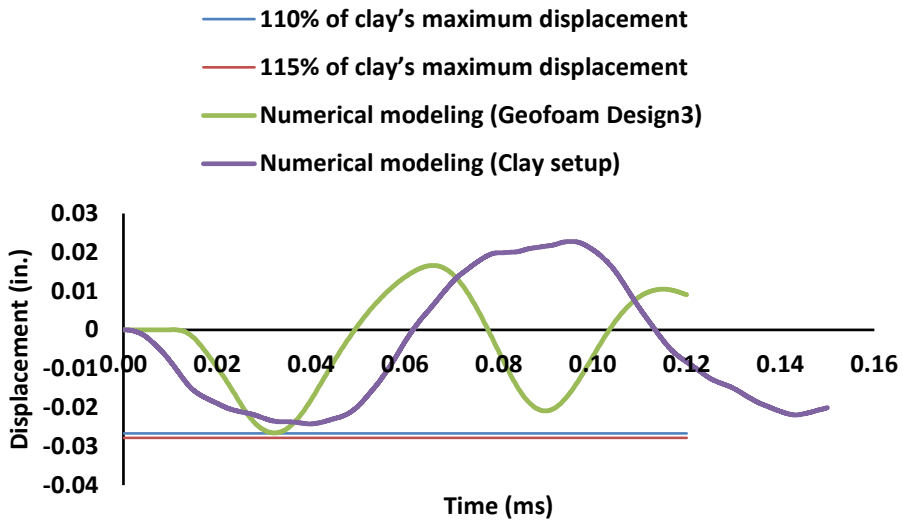

Figure 87. Predicted displacements of both setups with the maximum impact load of 15.11 kip (Geofoam-EPS39-Design 3).

After these geofoam setups were designed, the results were discussed with the MDT staff in a meeting. It was decided that, due to the problems that might arise during the construction of the newly designed setups, the thickness of the sand layers in X and Y directions should be kept at 4 (in.) in all the new designs (See Figure 83c for example). Therefore, the thickness of the sand layers in X and Y directions for all the designs in the next sections is 4 in.

8.5 Sensitivity Analysis

In order to evaluate the effects of different types of geofoam, their position, and thickness in the new designs, a set of sensitivity analysis simulations were conducted. These analyses will help to better understand how the behavior, i.e., displacement, damping, and noise, are affected by geofoam properties and location. In these analyses, geofoam EPS 19 with four thicknesses (16", 20", 24" and, 28) and EPS 29 with four thicknesses (20", 24", 28" and 32") were studied. In different scenarios, the position of the geofoam layer is changed (starting from the bottom to the top) while other variables are kept constant. Figure 88 shows an example of how geometry changes in each scenario. In this example, the position of the 16" thick geofoam EPS 19 layer is changed for each scenario. The cross-sections shown in Figure 88 are along the X-axis. It is also worth mentioning that if the 16" thick geofoam EPS 19 is located at any depth less than 19 (in.) from the bottom of the concrete slab (Figure 88d), the displacements exceed the acceptable range. The geometries shown in Figure 88, therefore, only show the possible positions of the 16" thick geofoam EPS 19 where the displacements are in the acceptable range.

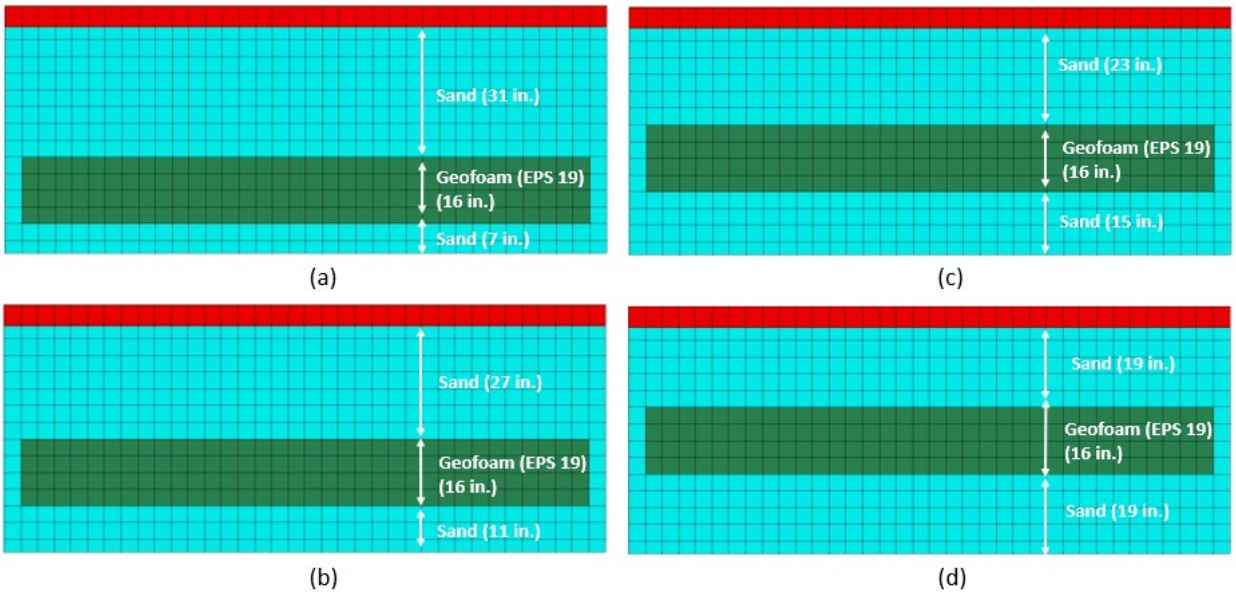

Figure 88. Different geometries in a sensitivity analysis with geofoam EPS 19 and the thickness of 16".

Figures 89 to 92 show the displacement histories predicted by the model for the four scenarios shown in Figure 88. Positions a, b, c, and d in Figures 89 to 92 refer to the position of the geofoam layers shown in Figures 88 a, b, c, and d, respectively. It is worth mentioning that two maximum impact loads, i.e., 11.55 kip and 14.68 kip, were used in these sensitivity analyses. Only the displacement time histories of the model that used an 11.55 kip load are presented here for example. The rest of the sensitivity analysis results are presented in Appendix C.

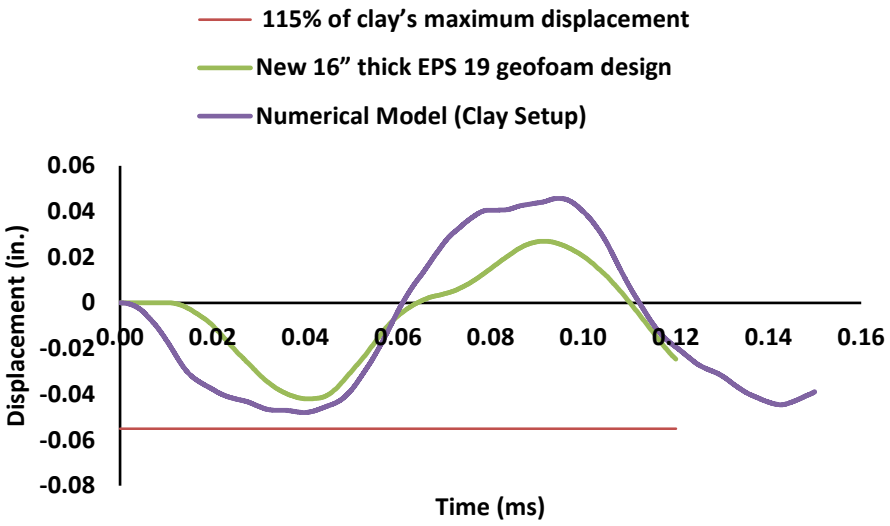

Figure 89. Sensitivity analysis of the alternative setup with the maximum impact load of 11.55 kip (EPS19-16"-position as in Figure 88 a).

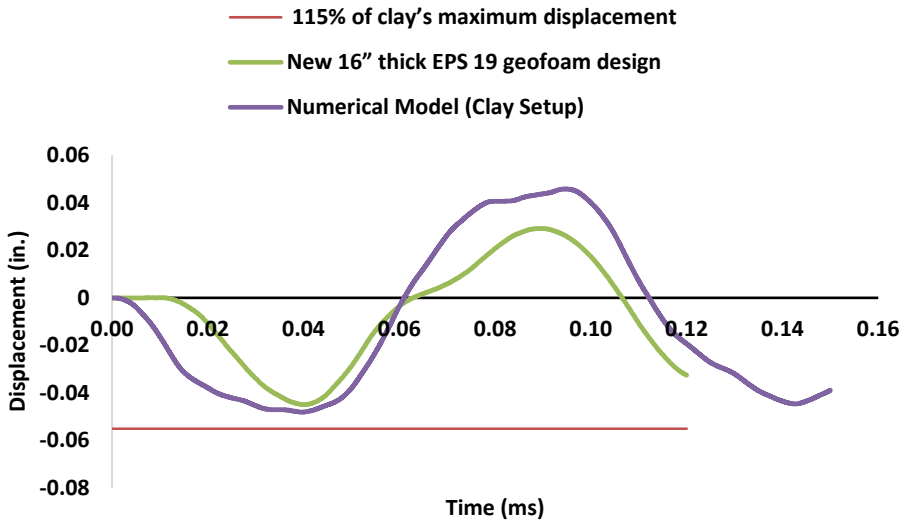

Figure 90. Sensitivity analysis of the alternative setup with the maximum impact load of 11.55 kip (EPS19-16"-position as in Figure 88 b).

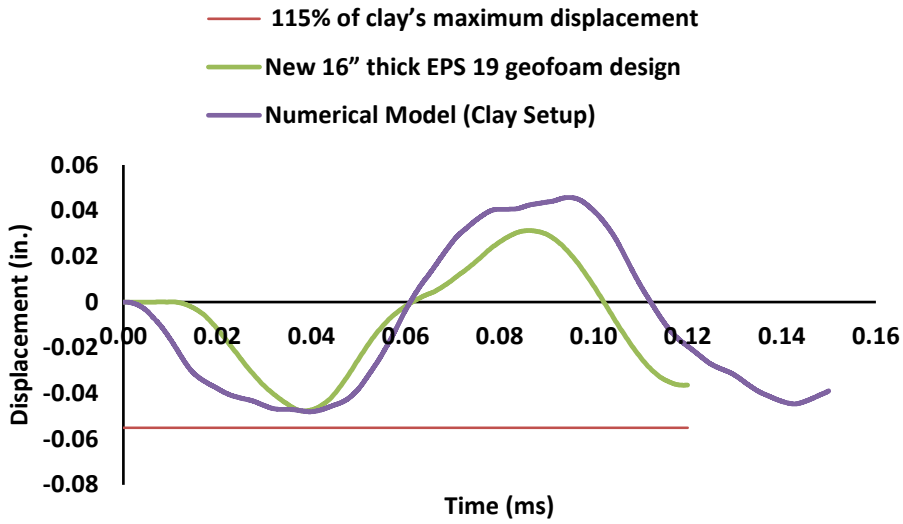

Figure 91. Sensitivity analysis of the alternative setup with the maximum impact load of 11.55 kip (EPS19-16"-position as in Figure 88 c).

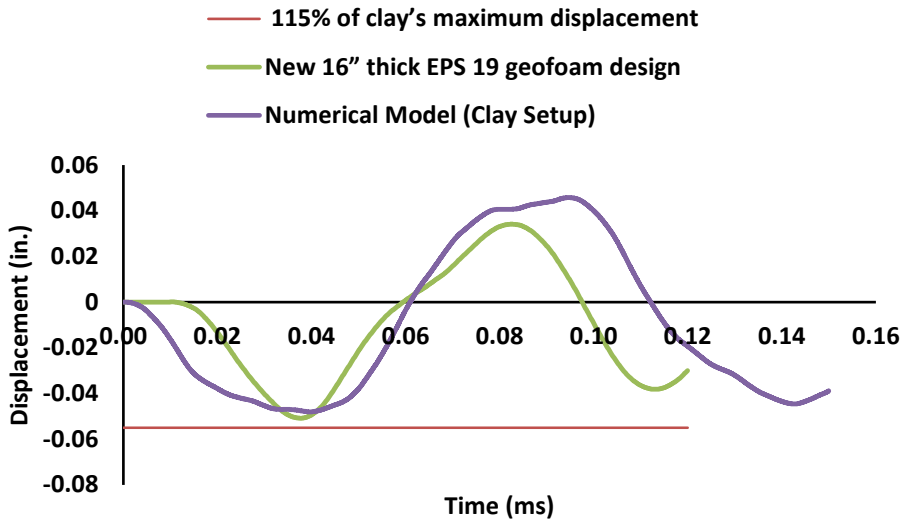

Figure 92. Sensitivity analysis of the alternative setup with the maximum impact load of 11.55 kip (EPS19-16"-position as in Figure 88 d).

The results of the sensitivity analyses show that thicker layers of geofoam are needed to achieve the desired displacements when using a denser geofoam. This is because although the denser geofoams have larger elastic moduli compared to the lighter ones, their moduli are still lower than that of sand. If a light geofoam layer is replaced by a dense geofoam layer with the same thickness, the maximum displacement is decreased to amounts lower than the acceptable range. Increasing the thickness of the denser geofoam, however, reduces the thickness of the sand layer (which has higher elastic modulus) in the test pit which in turn increases the maximum displacements.

The sensitivity analyses also revealed that as a given geofoam layer is located closer to the surface of the test pit, the maximum displacements are increased. This effect can be reduced by using denser geofoams or by reducing the thickness of the geofoam layer with the same density.

The sensitivity analyses further indicated that as a given geofoam layer is moved closer to the surface of the test pit, damping is decreased and the peak displacements in the predicted displacement time histories are reached in a shorter time period.

In an attempt to indirectly investigate the effects of the geofoam's density and location on the amount of noise observed in the calibration tests conducted on the alternative geofoam setup, the very first few milliseconds of the predicted displacement time histories were investigated. Based on the observed behavior of the test pit, this portion of the displacement time histories, i.e., the first 0.012 milliseconds, is assumed to correlate with the noise seen in the alternative geofoam setup from the time that the falling weight was released to the time that the falling weight hits the concrete slab. The noise was minimal in the original clay setup but was increased when the clay layer was replaced with a geofoam layer in the alternative setup. The noise makes it difficult to determine the exact time when the falling weight hits the concrete slab which in turn, makes it difficult to accurately determine the initial zero displacement point in the displacement time history. Accurate determination of this initial zero displacement point is very important in calibration tests because if this initial zero displacement point is erroneous, the displacement sensor's calibrations derived from these displacements will be incorrect. The first 0.012

milliseconds of the displacement time histories of the four scenarios depicted in Figure 88 are shown, for example, in Figures 93 to 96. The displacements of the alternative geofoam setup are also shown in these figures for comparison.

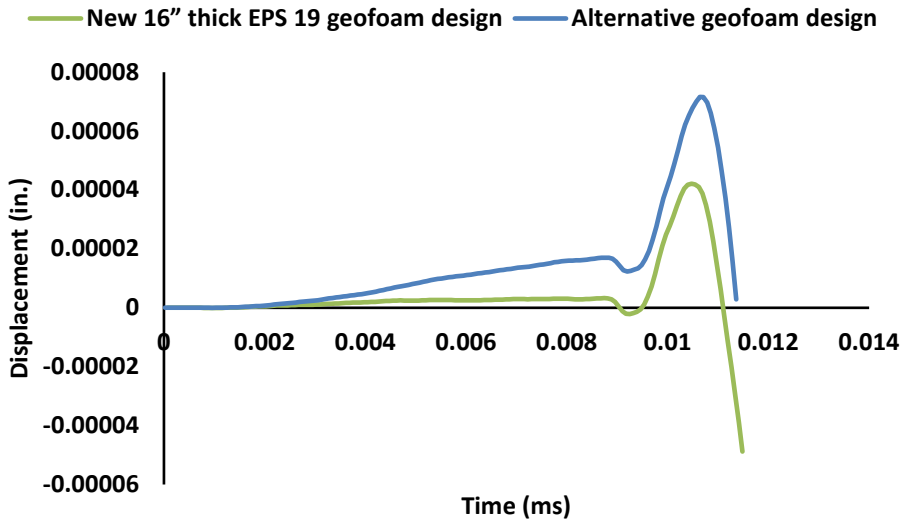

Figure 93. Sensitivity analysis for noise conditions before dropping the weight (EPS19-16”-position as in Figure 88 a).

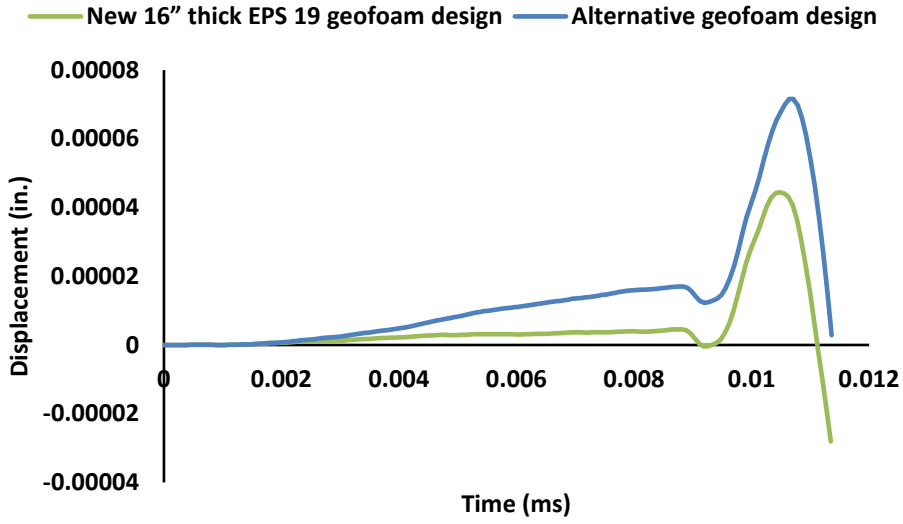

Figure 94. Sensitivity analysis for noise conditions before dropping the weight (EPS19-16”-position as in Figure 88 b).

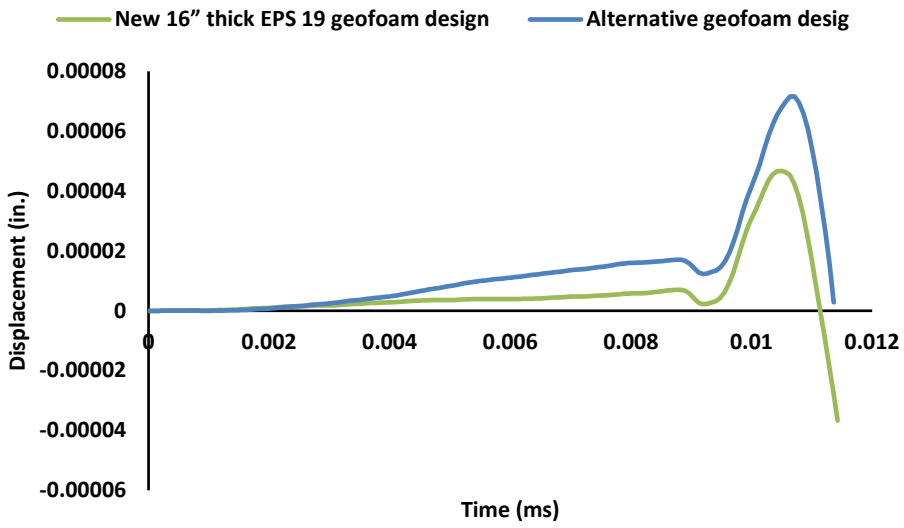

Figure 95. Sensitivity analysis for noise conditions before dropping the weight (EPS19-16"-position as in Figure 88 c).

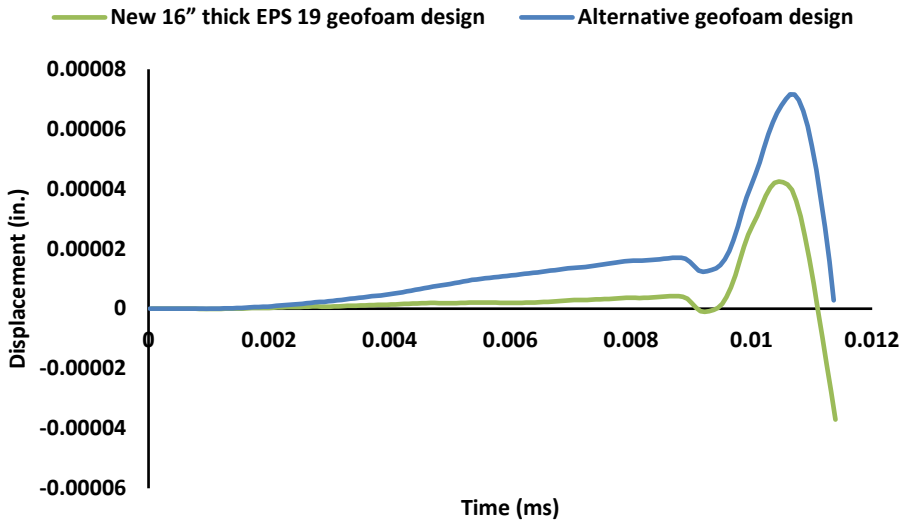

Figure 96. Sensitivity analysis for noise conditions before dropping the weight (EPS19-16"-position as in Figure 88 d).

This sensitivity analyses show that as a given geofoam layer is located closer to the bottom of the test pit, the predicted displacements before the falling weight hits the concrete (represented by the first few milliseconds of the displacement histories as shown in the figures) are generally decreased. This could be an indication that less noise can be expected when the geofoam layer is buried deeper in the test pit. The results also show that replacing a lighter geofoam layer with a denser geofoam layer of the same thickness and at the same location could decrease the expected noise in the data. There were, however, some exceptions to these general trends. For example, by

moving the 16” thick geofoam EPS 19 closer to the surface, the possibility of experiencing noise in the data generally increases except for when it is located 19 (in.) below the bottom of the concrete slab. At 19 (in.) below the bottom of the concrete slab, the possibility of experiencing noise in the data is actually lower than when it is located 23 (in.) below the bottom of the concrete slab. Another example of such a discrepancy was observed for the 24” thick geofoam EPS 19. By moving the 24” thick geofoam EPS 19 closer to the surface, the possibility of experiencing noise in the data generally increases except for when it is located 11 (in.) below the bottom of the concrete slab. At 11 (in.) below the bottom of the concrete slab, the possibility of experiencing noise in the data is actually lower than when it is located 15 (in.) below the bottom of the concrete slab. No attempt was made in this study to investigate the cause of these exceptions.

8.6 Selection of the Best Design

The results of previous sections show that multiple designs can be used to achieve the desired displacements. Based on the predicted deflections and after discussions with the MDT Technical Panel, it was decided to only consider the geofoam EPS19 and geofoam EPS29 for the selection of the best design. In this section, we propose a set of selection criteria that can be used to choose the best possible design. In addition to the maximum deflections, the proper design should produce proper damping and reduce the expected noise in the data. The cost of the construction of each designed test pit should also be considered in choosing the best possible design. If possible, the proper design should also reduce the possible deviation (variability) between the designed material properties and as-built material properties. In other words, it is a lot harder to control the properties (such as density, moisture content, and the elastic modulus) of granular material, i.e., sand layers, compared to those of a manufactured layer, i.e., geofoam layers. Therefore, the designs that use thicker sand layers in their geometries are less desirable.

To evaluate the designs based on these criteria, here we propose a decision matrix that allows the designs to be graded based on each individual criterion. Among the factors discussed above, meeting the maximum deflection requirements and reducing the possible noise are of the highest importance. The best score of 10, therefore, was chosen for each one of these two criteria and the designs were graded out of 10 based on how good their predicted behaviors are in regards to meeting the maximum deflection requirements and reducing the possible noise. For example, in all the designed setups, one that used a 16” thick geofoam EPS 19 with 23” of sand underneath it had deflections that were exactly 115% of the clay’s maximum displacements. This design was graded 10 out of 10 for the maximum deflection criterion. The second best designs according to the maximum deflection criterion with deflections of about 114% of the clay’s maximum displacements were assigned a grade of 9.75. In other words, for every 1% difference between the predicted maximum deflection and the target deflection (115% of the clay’s maximum displacements), 0.25 points were deducted from the maximum 10 points. The rest of the designs were then similarly assigned grades for the maximum displacement criterion and the noise criterion.

The proper damping and cost of construction are the next two most important factors, and therefore, the best score of 8 was chosen for each one of these two criteria. The damping was rated based on the closeness of the predicted behavior of the designed test pit to the observed behavior of the original clay setup. The construction cost of each design was calculated based on the itemized unit costs presented in Table 11.

Table 11. Unit costs used for calculating the construction cost of the designed test pits (Costs provided by MDT)

Item/activity	Cost per cubic yard
Geofoam	$75
Excavation	$30
Concrete materials and placement (12'x15'x5" slab)	$1000
Sand	$9

Lastly, the best score of 4 was chosen for the variability criterion because it was considered the least important factor. After grading the designs based on each criterion, the weighted score of each criterion for a design was calculated by multiplying the grade of each criterion by the best score assigned to that criterion. For example, if a design was assigned a grade of 9.5 out of 10 for the maximum deflection criterion, the weighted grade of that design for the maximum deflection criterion was calculated as $9.5 \times 10 = 95$. The overall score of each design based on all five criteria was then calculated by adding the five weighted grades of the five criteria for that design. The weighted grades and the overall scores of all the considered designs are shown in Table 12. In this table, the first number in the label in the first column indicates the type of geofoam (19 for EPS19; 29 for EPS29), the second number indicates the thickness of the geofoam (in the Z direction of the models), and the third number indicates the thickness of the sand layer underneath the geofoam. The top three highest ranks are shown in green.

Table 12. The decision matrix analysis for choosing the best geofoam design

New geofoam design (Geofoam type/Geofoam thickness in Z direction/Bottom sand layer thickness in Z direction)	Maximum Deflection	Noise	Damping	Variability	Cost	Score
Maximum Score	100	100	64	16	64	344
EPS19/16"/7"	40	100	56	4	64	264
EPS19 / 16" / 11"	45	90	54	4	64	257
EPS19 / 16" / 15"	70	80	50	4	64	268
EPS19 / 16" / 19"	90	100	46	4	64	304
EPS19 / 16" / 23"	100	75	44	4	64	287
EPS19 / 20" / 3"	45	72.5	54	7	60	238.5
EPS19 / 20" / 7"	60	65	60	7	60	252
EPS19 / 20" / 11"	87.5	72.5	54	7	60	281
EPS19 / 20" / 15"	100	50	52	7	60	269
EPS19 / 20" / 19"	45	40	50	7	60	202
EPS19 / 24" / 3"	70	72.5	52	10	56	260.5
EPS19 / 24" / 7"	97.5	75	62	10	56	300.5
EPS19 / 24" / 11"	77.5	50	58	10	56	251.5
EPS19 / 24" / 15"	45	50	54	10	56	215
EPS19 / 24" / 19"	30	72.5	50	10	56	218.5
EPS19 / 28" / 3"	100	95	60	13	52	320
EPS29 / 32" / 3"	85	100	50	16	48	299
EPS29 / 32" / 7"	100	45	48	16	48	257
EPS29 / 28" / 7"	70	75	48	13	52	258
EPS29 / 28" / 11"	95	47.5	46	13	52	253.5
EPS29 / 28" / 15"	100	45	38	13	52	248
EPS29 / 24" / 11"	45	87.5	40	10	56	238.5
EPS29 / 24" / 15"	70	85	38	10	56	259
EPS29 / 24" / 19"	95	75	36	10	56	272
EPS29 / 24" / 23"	100	60	32	10	56	258
EPS29 / 24" / 27"	97.5	55	30	10	56	248.5
EPS29 / 20" / 19"	40	95	38	7	60	240
EPS29 / 20" / 23"	50	80	36	7	60	233
EPS29 / 20" / 27"	87.5	75	32	7	60	261.5
EPS29 / 20" / 31"	95	70	28	7	60	260

As can be seen, the design with a 28” thick geofoam EPS 19 with 3” of sand at the bottom has gained the highest score. Figure 97 shows this design. Note that this design was introduced before in section 9.3.5 as the EPS19-Design 5.

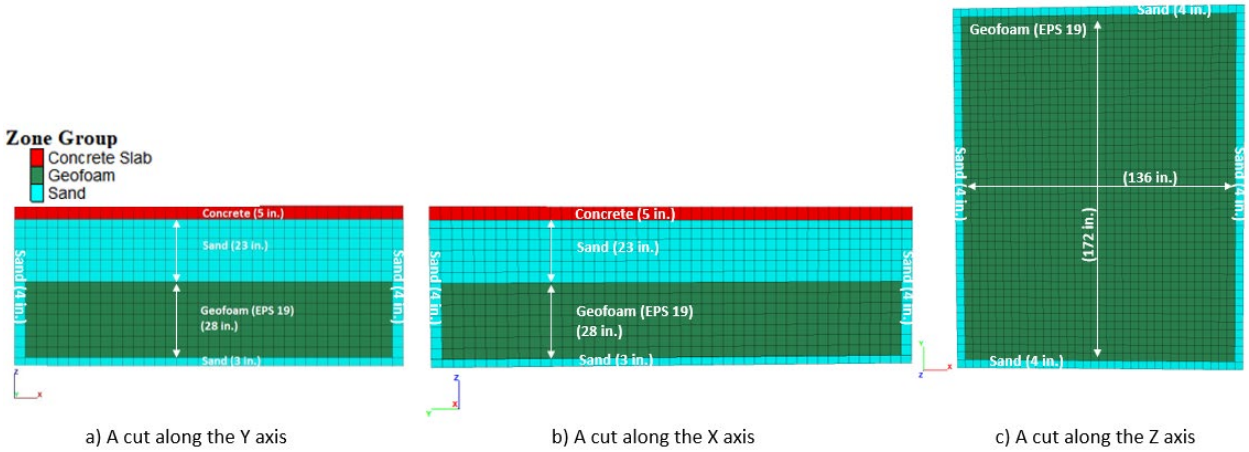

a) A cut along the Y axis b) A cut along the X axis c) A cut along the Z axis

Figure 97. The best geofoam design chosen based on the decision matrix analysis.

8.7 Conclusions-Task 4

The main goals of this study were two fold. The first goal was to use dynamic response analyses to investigate the possibility of using geofoam instead of the clay layer in the FWD calibration test pit. The second goal was to design a new geofoam setup that can meet the AASHTO R32-11 requirements if the results of the investigation revealed that geofoam can in fact be used in place of the clay layer. Based on the results of this investigation, it was determined that geofoam can be used instead of the clay layer in the FWD calibration test pit. In fact, 30 different setups were designed using two types of geofoam, i.e., EPS 19 and EPS 29, that met the AASHTO R32-11 requirements. These setups were designed based on the results of a set of sensitivity analyses that investigated the effects of different types of geofoam and their locations in the test pit on the behavior of the test pit under the applied impact loads. The results of these analyses showed that thicker layers of geofoam are needed to achieve the desired displacements when using a denser geofoam. Consequently, while the thickness of the geofoam layer can change from 16 in. to 24 in. (the required thickness depends on the location of the geofoam layer in the setup) when using an EPS 19 geofoam, the acceptable range for the thickness of an EPS 29 geofoam is from 20 in. to 32 in. The sensitivity analyses further indicated that as a given geofoam layer is located closer to the surface of the test pit, the maximum displacements are generally increased, damping is decreased, the peak displacements are reached in a shorter time period, and the possibility of experiencing noise in the data is also increased. For example, if the 16” thick geofoam EPS 19 is located at any depth less than 19 (in.) from the bottom of the concrete slab, the displacements would exceed the acceptable range. There were, however, few exceptions to these general trends. For example, by moving the 16” thick geofoam EPS 19 closer to the surface, the possibility of experiencing noise in the data generally increases except for when it is located 19 (in.) below the bottom of the concrete slab. At 19 (in.) below the bottom of the concrete slab, the possibility of experiencing noise in the data is actually lower than when it is located 23 (in.) below the bottom of the concrete slab. Due to these exceptions, a decision matrix analyses approach was proposed to rank these designs from best to worst based on five criteria, i.e., AASHTO’s maximum deflection requirements, reducing the noise observed in the alternative geofoam setup, proper damping, construction cost, and variability. Based on this decision matrix analysis it was determined that the best choice would be to use a 28” thick geofoam EPS 19 with 3” of sand at the bottom of the test pit.

9. SUMMARY AND RECOMMENDATIONS

The FWD calibration facility operated by the Montana Department of Transportation (MDT) has used a 12 ft wide, 15 ft long, and 5 in thick concrete slab overlying a 6-in thick sandy base and a 4-ft thick clay subgrade. The measured deflections during calibration tests conducted by MDT on this clay test pit met the deflection requirements for a few years, after which the test area needed to be replaced. Because rebuilding the test area is both costly and time-consuming, the MDT was interested in a new design that could operate over longer periods. MDT designed an alternative to the clay setup, using geofoam instead of the clay layer as the soft subgrade (alternative geofoam setup). The alternative geofoam test pit was designed based on static analyses. The designed test area was constructed, and several FWD calibration tests were conducted. The new setup did not meet all the deflection requirements. Also, some deflections (noise) upon initiation of the falling weight (before the weight actually hits the plate) were detected by the accelerometers during the calibration tests conducted on the geofoam test pit. In this study, a three-dimensional explicit finite volume dynamic model was developed to investigate the possibility of using geofoam instead of the clay layer as the soft subgrade in the calibration test pit. The model was validated using the results of previous FWD calibration tests. The model was then used to design new geofoam calibration test pits where the displacement requirements are met and minimum noise is expected. A total of 30 different setups were designed using two types of geofoam, i.e., EPS 19 and EPS 29, that met the AASHTO R32-11 requirements. Among those, the three best designs were (1) a 28” thick geofoam EPS 19 with 3” of sand at the bottom (Figure 98a), (2) 16” thick geofoam EPS 19 with 19” of sand at the bottom (Figure 98b), and (3) a 24” thick geofoam EPS 19 with 7” of sand at the bottom (Figure 98c).

Figure 98. The three best geofoam designs.

In all three designs, the sand layer should have a unit weight of 120 (pcf), an elastic modulus of 4900 (psi), and a Poisson's ratio of 0.4. These properties can be achieved by using loose to medium dense SP-poorly graded sand [30]. The elastic modulus and Poisson's ratio of the sand to be used in the test pits can be determined using different laboratory tests. The most common tests used to determine these parameters are the resilient modulus test, consolidated undrained (CU) triaxial compression test, and low strain ultrasonic test. According to Maher and Bennert [31], however, the low strain ultrasonic test is the best method for measuring the Poisson's ratio of the soil. The EPS 19 geofoam should be used which has a unit weight of 1.15 (pcf), an elastic modulus of 580 (psi), and a Poisson's ratio of 0.1. The concrete layer should have a unit weight of 149.8 (pcf), an elastic modulus of 3500000 (psi), and a Poisson's ratio of 0.15.

Due to the inherent variability of soil parameters, it might be proven very hard to acquire a soil with the exact suggested unit weight, elastic modulus, and Poisson's ratio. A set of sensitivity analyses were therefore conducted to provide a range of acceptable values for each one of these soil properties. The results of these analyses are shown in Figures 99 to 104.

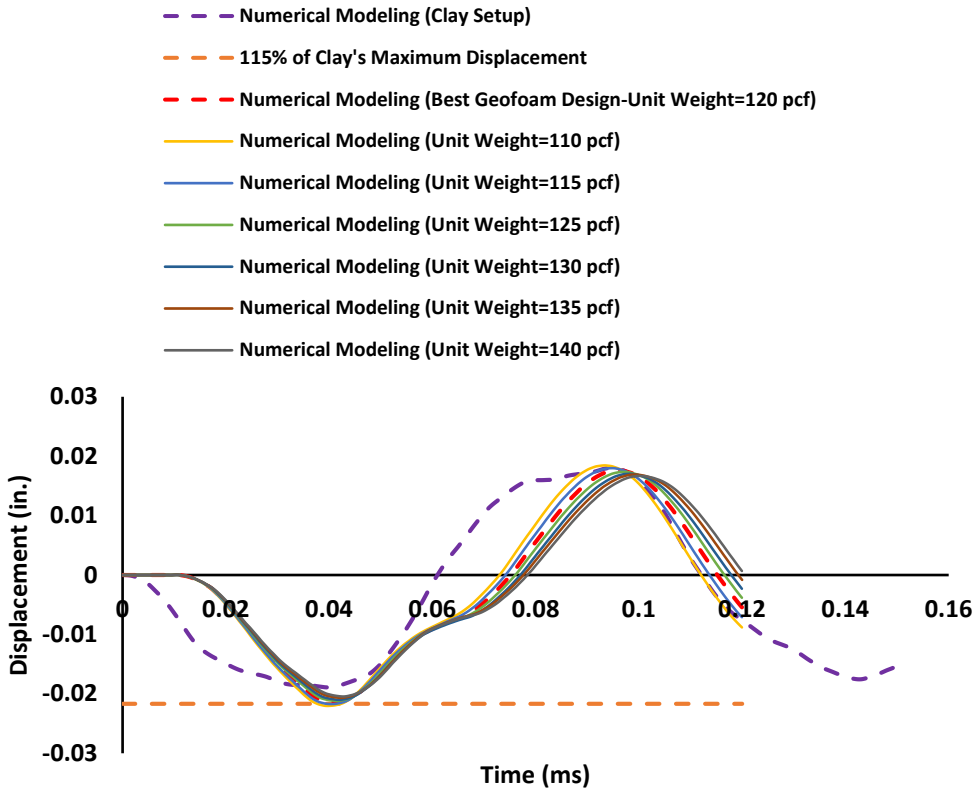

Figure 99. Effect of the unit weight of the sand layer on the behavior of the best geofoam design (the maximum impact load of 11.55 kip).

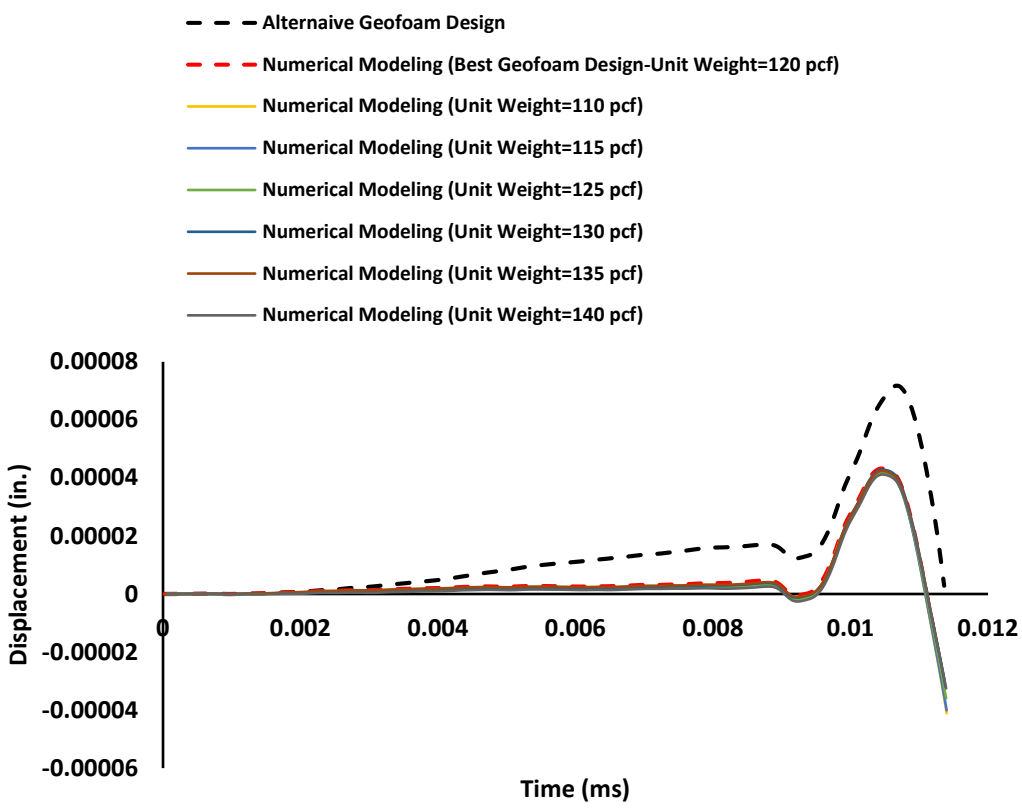

Figure 100. Effect of the unit weight of the sand layer on the predicted noise before dropping the weight of the best geofoam design (the maximum impact load of 11.55 kip).

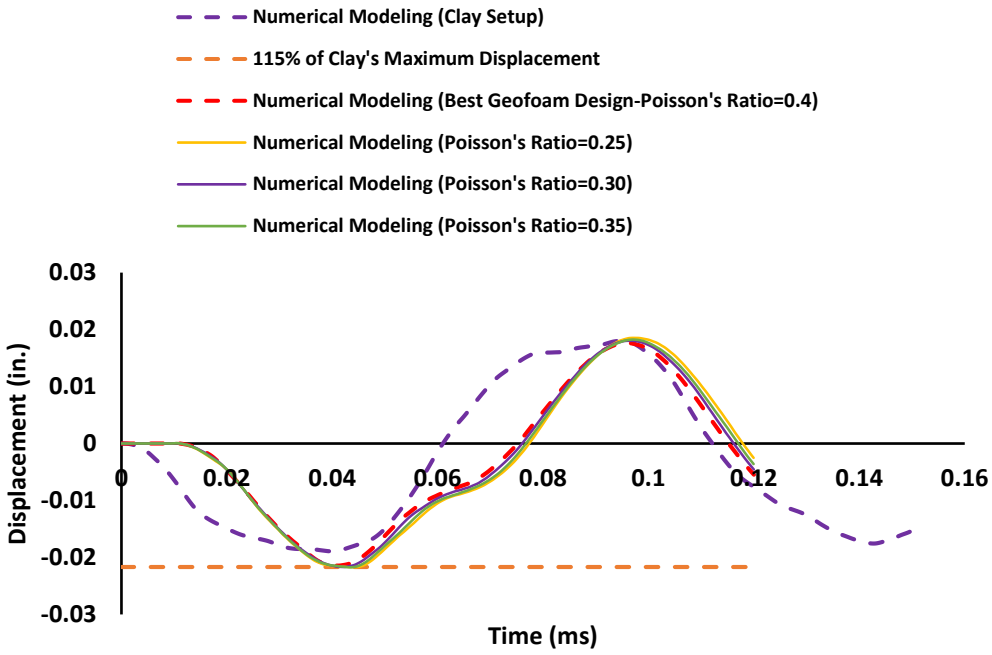

Figure 101. Effect of the Poisson's ratio of the sand layer on the behavior of the best geofoam design (the maximum impact load of 11.55 kip).

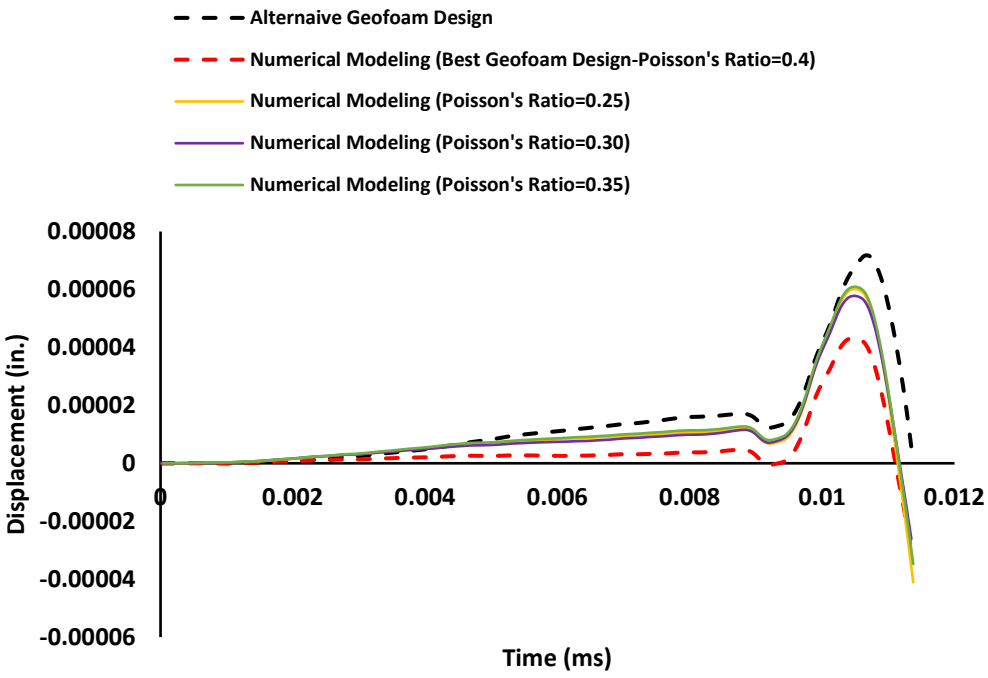

Figure 102. Effect of the Poisson's ratio of the sand layer on the predicted noise before dropping the weight of the best geofoam design (the maximum impact load of 11.55 kip).

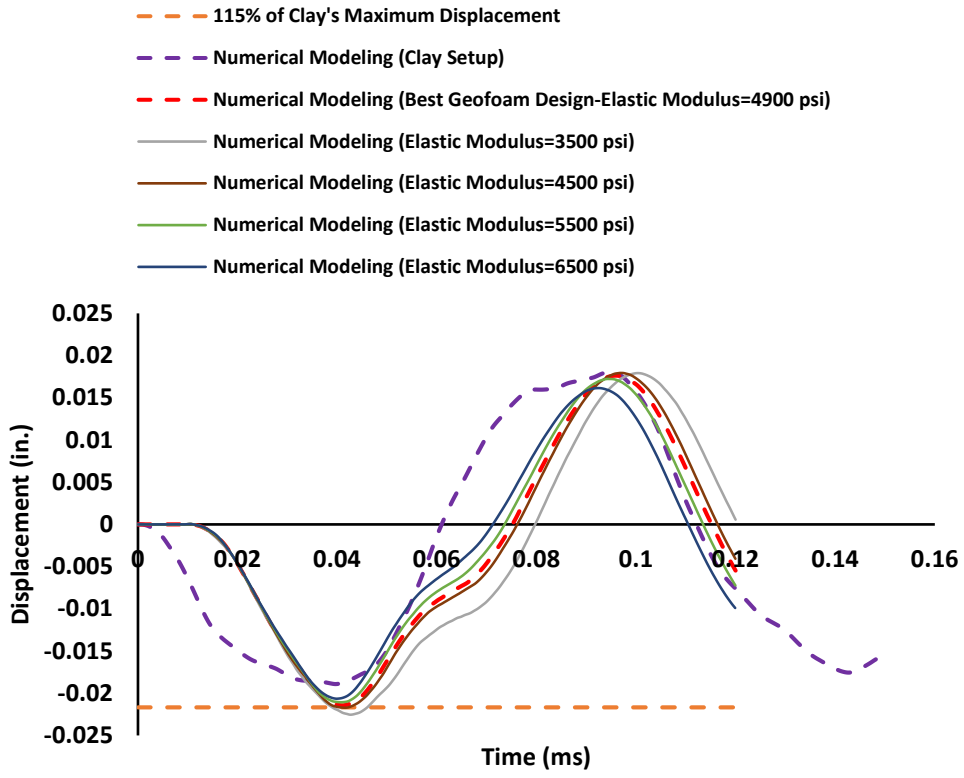

Figure 103. Effect of the Elastic Modulus of the sand layer on the behavior of the best geofoam design (the maximum impact load of 11.55 kip).

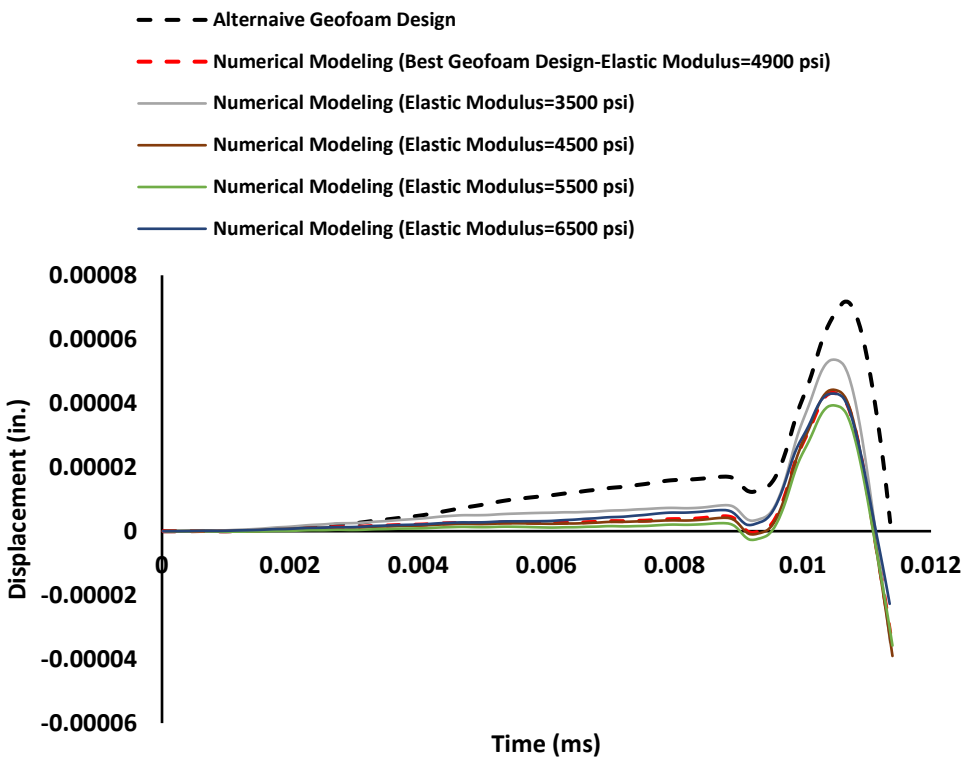

Figure 104. Effect of the Elastic Modulus of the sand layer on the predicted noise before dropping the weight of the best geofoam design (the maximum impact load of 11.55 kip).

As the aforementioned sensitivity analyses only investigated the effect of each individual property of the sand layer on the behavior of the best design, another model was developed using the parameters with the least favorable outcomes, i.e., unit weight of 140 (pcf), Poisson's ratio of 0.25, and Elastic Modulus of 6500 psi. This investigation was conducted to make sure that the behavior of a test pit that is constructed using a sand layer with all the least favorable properties is still acceptable. Figures 105 and 106 show the displacement time history and the predicted noise before dropping the weight for such a test pit, respectively.

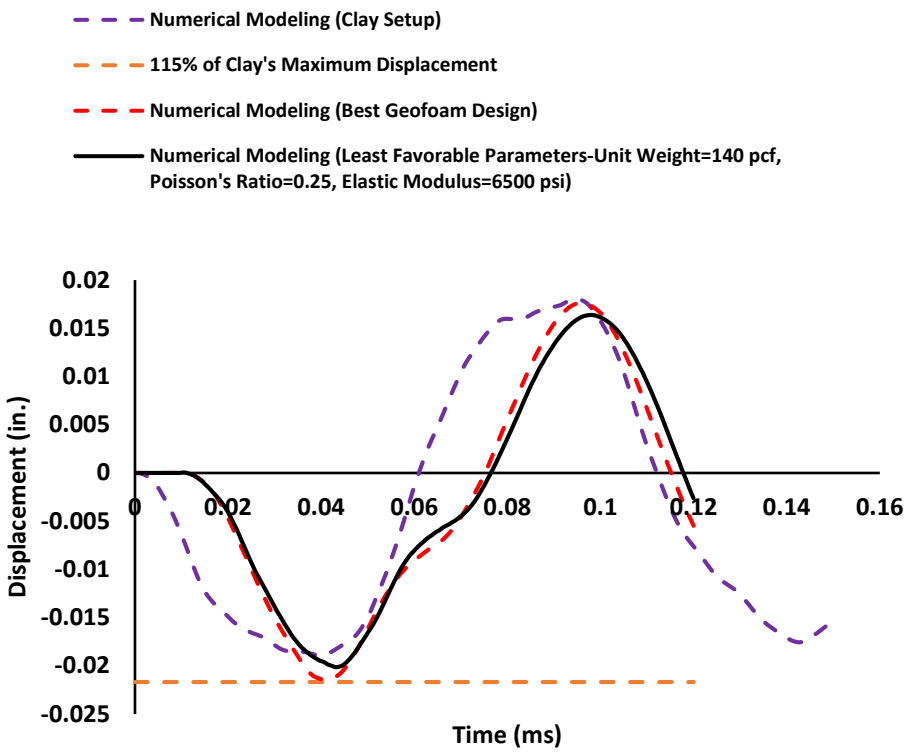

Figure 105. The behavior of the best geofoam design when a sand layer with all the least favorable properties is used (the maximum impact load of 11.55 kip).

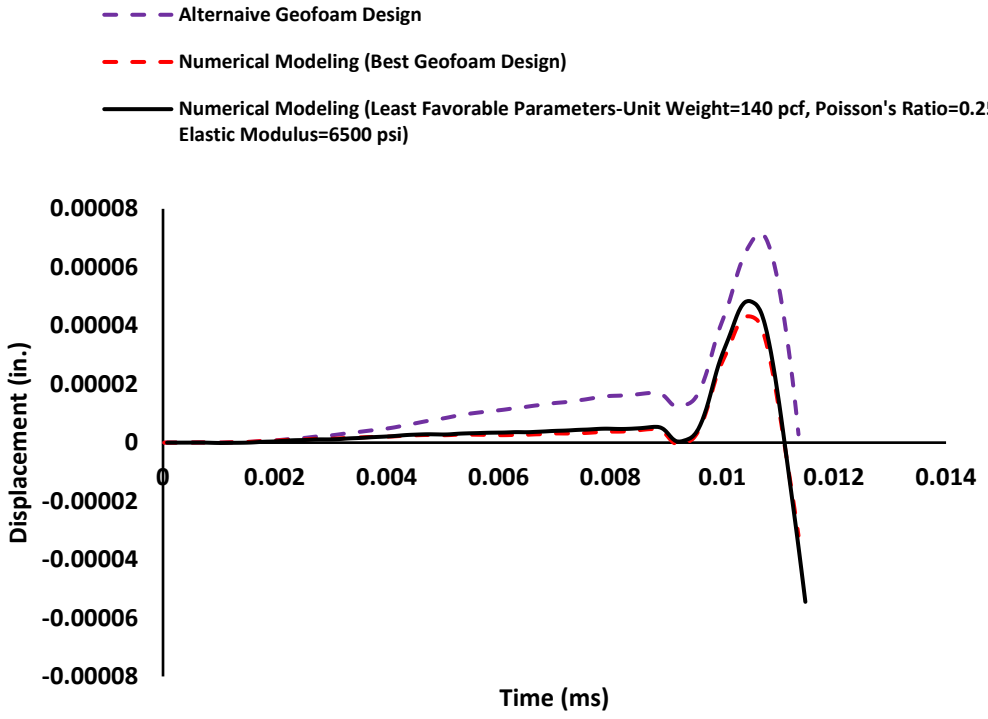

Figure 106. The predicted noise before dropping the weight of the best geofoam design when a sand layer with all the least favorable properties is used (the maximum impact load of 11.55 kip).

As can be seen in figures 105 and 106, the results of this model showed that the behavior of a test pit that is constructed using a sand layer with all the least favorable properties is satisfactory. Based on these sensitivity analyses, using a sand layer with a unit weight between 110 (pcf) and 140 (pcf), an elastic modulus between 3500 (psi) and 6500 (psi), and a Poisson's ratio between 0.25 and 0.4, is acceptable.

Although the results of this study suggested a slightly better performance of the design with 28" thick geofoam EPS 19 and 3" of sand at the bottom, we recommend that the MDT implement the third best design, i.e., 24" thick geofoam EPS 19 with 7" of sand at the bottom (Figure 98c). This is because the current geofoam setup at MDT includes two 24" thick geofoam layers. By choosing the third design, the MDT can easily modify their existing test pit without the need to purchase new geofoam layer(s). It is also worth noting that the difference between the decision matrix analyses score of the third best design and the best design is 19.5 points (out of 344) which is about 5%. The difference between the score of the third best design and the second best design is 3.5 points (out of 344) which is about 1%.

10. REFERENCES

[1] AASHTO-R32-11. Calibrating the Load Cell and Deflection Sensors for a Falling Weight Deflectometer 2011.

[2] Irwin LH, Orr DP, Atkins D. FHWA-HRT-07-040, FWD Calibration Center and Operational Improvements: Redevelopment of the Calibration Protocol and Equipment. 2011.

[3] Irwin L, Yang W, Stubstad R. Deflection Reading Accuracy and Layer Thickness Accuracy in Backcalculation of Pavement Layer Moduli. Nondestruct. Test. Pavements Backcalc. Modul., ASTM International; 2008, p. 229-229–16. https://doi.org/10.1520/stp19810s.

[4] Kuo CM, Chou FJ. Development of 3-D finite element model for flexible pavements. J Chinese Inst Eng Trans Chinese Inst Eng A/Chung-Kuo K Ch'eng Hsuch K'an 2004;27:707–17. https://doi.org/10.1080/02533839.2004.9670918.

[5] Lytton R. Backcalculation of Pavement Layer Properties. Nondestruct. Test. Pavements Backcalc. Modul., ASTM International; 2008, p. 7-7–32. https://doi.org/10.1520/stp19797s.

[6] Chatti K, Kim TK. Simple dynamic backcalculation procedure for falling weight deflectometer testing of rigid pavements. Transp. Res. Rec., 2001, p. 30–8. https://doi.org/10.3141/1764-04.

[7] Khazanovich L, Booshehrian A. Dynamic viscoelastic analysis of falling weight deflectometer deflections for rigid and flexible pavements. Transp Res Rec 2015;2525:31–9. https://doi.org/10.3141/2525-04.

[8] Donovan P, Tutumluer E. Falling weight deflectometer testing to determine relative damage in asphalt pavement unbound aggregate layers. Transp Res Rec 2009:12–23. https://doi.org/10.3141/2104-02.

[9] Balzarini D, Chatti K, Zaabar I, Butt AA, Harvey JT. Mechanistic-Based Parametric Model for Predicting Rolling Resistance of Concrete Pavements. Transp Res Rec 2019;2673:341–50. https://doi.org/10.1177/0361198119847611.

[10] Meier RW, Rix GJ. Backcalculation of flexible pavement moduli using artificial neural networks. Transp Res Rec 1994:75–82.

[11] Meier R, Rix G. Backcalculation of flexible pavement moduli from dynamic deflection basins using artificial neural networks. Transp Res Rec J Transp Res Board 1995;1473:72–81.

[12] Khazanovich L. Dynamic Analysis of FWD Test Results for Rigid Pavements. Nondestruct. Test. Pavements Backcalc. Modul. Third Vol., 100 Barr Harbor Drive, PO Box C700, West Conshohocken, PA 19428-2959: ASTM International; 1999, p. 398-398–15. https://doi.org/10.1520/STP14780S.

[13] Kuo CM, Lin CC, Huang CH, Lai YC. Issues in simulating falling weight deflectometer test on concrete pavements. KSCE J Civ Eng 2016;20:702–8. https://doi.org/10.1007/s12205-015-0299-y.

[14] Foinquinos R, Roesset JM, Stokoe KH. Response of pavement systems to dynamic loads imposed by nondestructive tests. Transp Res Rec 1995:57–67.

[15] Mallela J, George KP. Three-dimensional dynamic response model for rigid pavements. Transp Res Rec 1448, TRB, Natl Res Counc Washington, DC 1994:92–9.

[16] Shoukry SN, William GW, Martinelli DR. Assessment of the performance of rigid pavement back-calculation through finite element modeling. In: Chase SB, editor. Nondestruct. Eval. Bridg. Highw. III, vol. 3587, SPIE; 1999, p. 146–56. https://doi.org/10.1117/12.339920.

[17] William GW. Backcalculation of pavement layers moduli using 3D nonlinear explicit finite element analysis. West Virginia University, 1999.

[18] Park K-C, Chang Y-C. An Analytical Study of Flexible Pavement Design Using Resilient Modulus Model of Expanded Polystyrene (EPS). J Korean Geosynth Soc 2015;14:35–44. https://doi.org/10.12814/jkgss.2015.14.2.035.

[19] Loizos A, Scarpas A. Verification of falling weight deflectometer backanalysis using a dynamic finite elements simulation. Int J Pavement Eng 2005;6:115–23. https://doi.org/10.1080/10298430500141030.

[20] Itasca. Dynamic Analysis. FLAC3D Version 6 User's Guid., Itasca Consulting Group Inc., Minneapolis, Minnesota, 1 USA; 2012.

[21] Wegel RL, Walther H. Internal dissipation in solids for small cyclic strains. J Appl Phys 1935;6:141–57. https://doi.org/10.1063/1.1745306.

[22] Gemant A, Jackson W. XCIII. The measurement of internal friction in some solid dielectric materials. London, Edinburgh, Dublin Philos Mag J Sci 1937;23:960–83. https://doi.org/10.1080/14786443708561868.

[23] Tiwari B, Ajmera B, Villegas D. Dynamic Properties of Lightweight Cellular Concrete for Geotechnical Applications. J Mater Civ Eng 2018;30:04017271. https://doi.org/10.1061/(asce)mt.1943-5533.0002155.

[24] Kishida T. Comparison and Correction of Modulus Reduction Models for Clays and Silts. J Geotech Geoenvironmental Eng 2017;143:04016110. https://doi.org/10.1061/(asce)gt.1943-5606.0001627.

[25] Pallav K, Raghukanth STG, Singh KD. Estimation of Seismic Site Coefficient and Seismic Microzonation of Imphal City, India, Using the Probabilistic Approach. Acta Geophys 2015;63:1339–67. https://doi.org/10.1515/acgeo-2015-0045.

[26] EPRI-TR-102293. Electric Power Research Institute: Guidelines for determining design basis ground motions. 1993.

[27] Athanasopoulos GA, Pelekis PC, Xenaki VC. Dynamic properties of EPS geofoam: An experimental investigation. Geosynth Int 1999;6:171–94. https://doi.org/10.1680/gein.6.0149.

[28] Rydén N. Surface Wave Testing of Pavements. University of Kansas, 2004.

[29] Itasca I. FLAC3D. V5 user manual 2012.

[30] Obrzud R l F, Truty A. The hardening soil model - a practical guidebook-Z Soil.PC 100701 report. 2018.

[31] Maher A, Bennert T. Evaluation of Poisson ' s Ratio for Use in the Mechanistic Empirical Pavement Design Guide. Dep Transp State New Jersey 2008;FHWA-NJ:60.

11. APPENDIX A - FLAC3D SCRIPT (ORIGINAL TEST PIT-CLAY SET UP)

The code used for modeling the behavior of MDT's FWD calibration test pit is presented here.

```
project new
model config dynamic
model dynamic active off

fish define MatMechPrprtes
;;Units: Length:in,  Density:snail/in3,   Force:lb, Stress:psi, Gravity: 386.04 in/s2
densityConcrete=2.245e-4
densityBaseSand=1.8e-4
densityClay=1.5e-4
densityLevelingSand=1.8e-4

FrictionConcrete=46
FrictionBaseSand=35
FrictionClay=29
FrictionLevelingSand=35

CohesionConcrete=337
CohesionBaseSand=0
CohesionClay=7
CohesionLevelingSand=0

Poison=0.1
PoisonConcrete=0.15
PoisonBaseSand=0.4
PoisonClay=0.2
PoisonLevelingSand=0.4

YoungConcrete=3.5e6
YoungBaseSand=4900
YoungClay=870
YoungLevelingSand=4900

end
@MatMechPrprtes

fish automatic-create on
model title 'MDT-FWD Calibration site'
;;  Generating the geometry (dimensions in inches)
zone create brick point 0 0 0 0 point 1 144 0 0 point 2 0 180 0 point 3 0 0 1 size 12 15 1 group 'Leveling Sand';
zone create brick point 0 0 0 1 point 1 144 0 1 point 2 0 180 1 point 3 0 0 49 size 12 15 6 group 'Clay Subgrade';
zone create brick point 0 0 0 49 point 1 144 0 49 point 2 0 180 49 point 3 0 0 55 size 12 15 1 group 'Sand Base';
zone create brick point 0 0 0 55 point 1 144 0 55 point 2 0 180 55 point 3 0 0 60 size 12 15 5 group 'Concrete Slab';
zone attach by-face tolerance-absolute 0.05

zone cmodel assign elastic
zone property young = 1e40 poiss = 0.1
zone property density @densityConcrete range group 'Concrete Slab'
zone property density @densityBaseSand range group 'Sand Base'
zone property density @densityClay range group 'Clay Subgrade'
zone property density @densityLevelingSand range group 'Leveling Sand'

model gravity 0 0 -386.04
zone initialize-stresses

zone gridpoint fix velocity-x range position-x 0.0
zone gridpoint fix velocity-y range position-x 0.0
```

```
47. zone gridpoint fix velocity-x range position-x 144
48. zone gridpoint fix velocity-y range position-x 144
49. zone gridpoint fix velocity-x range position-y 0.0
50. zone gridpoint fix velocity-y range position-y 0.0
51. zone gridpoint fix velocity-x range position-y 180
52. zone gridpoint fix velocity-y range position-y 180
53. zone gridpoint fix velocity-x range position-z 0
54. zone gridpoint fix velocity-y range position-z 0
55. zone gridpoint fix velocity-z range position-z 0

56. model largestrain off

57. zone cmodel assign elastic
58. zone property density @densityConcrete range group 'Concrete Slab'
59. zone property density @densityBaseSand range group 'Sand Base'
60. zone property density @densityClay range group 'Clay Subgrade'
61. zone property density @densityLevelingSand range group 'Leveling Sand'
62. zone property young @YoungConcrete poiss @PoisonConcrete range group 'Concrete Slab'
63. zone property young @YoungBaseSand poiss @PoisonBaseSand range group 'Sand Base'
64. zone property young @YoungClay poiss @PoisonClay range group 'Clay Subgrade
65. zone property young @YoungLevelingSand poiss @PoisonLevelingSand range group 'Leveling Sand'

66. model save 'FWD-Clay-1-InitialCondition'

67. model config dynamic
68. model restore 'FWD-Clay-1-InitialCondition'

69. plot create  'Geometry initial'
70. plot item create zone
71. plot item create structure-shell
72. plot item create axes
73. plot view projection perspective magnification 1 ...
74. center (72,90,27.5) eye (220.13,-193.34,86.485) roll 356.772 ...
75. clip-front -1e+10 clip-back 1e+10

76. plot create  'Zones ZZ-Stress'
77. plot item create zone active on contour stress quantity zz ...
78. method average ramp rainbow reversed on
79. plot item create axes
80. plot view projection perspective magnification 1 ...
81. center (72,90,27.5) eye (220.13,-193.34,86.485) roll 356.772 ...
82. clip-front -1e+10 clip-back 1e+10

83. plot create  'Zones Z-Displacement'
84. plot item create zone active on contour displacement component z log off ...
85. method average ramp rainbow reversed on
86. plot item create axes
87. plot view projection perspective magnification 1 ...
88. center (72,90,27.5) eye (220.13,-193.34,86.485) roll 356.772 ...
89. clip-front -1e+10 clip-back 1e+10

90. table '5' import 'SHISTPSINORM'

91. plot create  'Input Stress History'
92. Plot item create chart-table active on ...
93. table '5' name "Stress History" ...
94. axis-x label "Time (Sec)" exponent  show on value 1 auto on ...
95. axis-y label "Stress (psi)" exponent  show on value 2 auto on

96. model largestrain off
97. model dynamic active on
```

```
model history name='time' dynamic time-total
zone history name='szzCenter' stress-zz position (78 104 60)
zone history name='DispCenter' displacement-z position (78 104 60)
zone history name='DispSensor' displacement-z position (72 144 60)

zone dynamic damping hysteretic sigmoidal-3 1.05      -0.5   -1.15 range group 'Sand Base'
zone dynamic damping hysteretic sigmoidal-3 1.05      -0.5   -1.15 range group 'Leveling Sand'
zone dynamic damping hysteretic sigmoidal-3 1.07      -0.6   -0.63 range group 'Clay Subgrade'
zone dynamic damping hysteretic sigmoidal-3 1.07      -0.55  -0.4 range group 'Concrete Slab'

zone face apply stress-zz -133.51 table '5' time dynamic range position-x 72 84 position-y 96 108 position-z 60

plot create  'Stress center History'
plot item create chart-history active on ...
history 'szzCenter' name "szzCenter ZZ Stress at (72,96,55)" style line reversed-x off reversed-y off ...
style-line width 2 style solid color 'cyan' ...
alias "" ...
vs step reversed off ...
begin 0 end 0 skip 0 ...
axis-x log off minimum auto maximum auto inside on ...
label "Step" exponent  show on value 4 auto on ...
axis-y log off minimum auto maximum auto inside on ...
label "Y-Axis" exponent  show on value -1 auto on

plot create  'Displacement center History'
plot item create chart-history active on ...
history 'DispCenter' name "DispCenter Z Displacement at (72,90,55)" style line reversed-x off reversed-y off ...
style-line width 2 style solid color 'cyan' ...
alias "" ...
vs step reversed off ...
begin 0 end 0 skip 0 ...
axis-x log off minimum auto maximum auto inside on ...
label "Step" exponent  show on value 4 auto on ...
axis-y log off minimum auto maximum auto inside on ...
label "Y-Axis" exponent  show on value -37 auto on

plot create  'Displacement Sensor vs Step'
plot item create chart-history active on ...
history 'DispSensor' name "Displacement Sensor vs Step" style line reversed-x off reversed-y off ...
style-line width 2 style solid color 'cyan' ...
alias "" ...
vs step reversed off ...
begin 0 end 0 skip 0 ...
axis-x log off minimum auto maximum auto inside on ...
label "Step" exponent  show on value 4 auto on ...
axis-y log off minimum auto maximum auto inside on ...
label "Y-Axis" exponent  show on value -37 auto on

model solve dynamic time-total 0.008
model save 'FWD-Clay-2-8msecDynamic'

model solve dynamic time-total 0.010
model save 'FWD-Clay-2-10msecDynamic'

model solve dynamic time-total 0.012
model save 'FWD-Clay-2-12msecDynamic'

model solve dynamic time-total 0.018
model save 'FWD-Clay-2-18msecDynamic'

model solve dynamic time-total 0.020
model save 'FWD-Clay-2-20msecDynamic'
```

```
model solve dynamic time-total 0.022
model save 'FWD-Clay-2-22msecDynamic'

model solve dynamic time-total 0.025
model save 'FWD-Clay-2-25msecDynamic'

model solve dynamic time-total 0.030
model save 'FWD-Clay-2-30msecDynamic'

model solve dynamic time-total 0.060
model save 'FWD-Clay-2-60msecDynamic'

model solve dynamic time-total 0.15

history export 'szzCenter' vs 'time' table 'szzCenter.VS.DynamicTime'

plot create  'Stress center vs Dynamic time'
plot item create chart-table active on ...
table 'szzCenter.VS.DynamicTime' name "szzCenter.VS.DynamicTime" style line reversed-x off reversed-y off ...
style-line width 2 style solid color 'cyan' ...
alias "" ...
axis-x log off minimum auto maximum auto inside on ...
label "Dynamic Time (Seconds)" exponent  show on value -2 auto on ...
axis-y log off minimum auto maximum auto inside on ...
label "ZZ-Stress at center (psi)" exponent  show on value 0 auto on

history export 'DispCenter' vs 'time' table 'DispCenter.VS.DynamicTime'

plot create  'Stress center vs Dynamic time'
plot item create chart-table active on ...
table 'DispCenter.VS.DynamicTime' name "DispCenter.VS.DynamicTime" style line reversed-x off reversed-y off ...
style-line width 2 style solid color 'cyan' ...
alias "" ...
axis-x log off minimum auto maximum auto inside on ...
label "Dynamic Time (Seconds)" exponent  show on value -2 auto on ...
axis-y log off minimum auto maximum auto inside on ...
label "Center ZZ-Stress at center (psi)" exponent  show on value 0 auto on

history export 'DispSensor' vs 'time' table 'DispSensor.VS.DynamicTime'

plot create  'Sensor Displacement History'
plot item create chart-table active on ...
table 'DispSensor.VS.DynamicTime' name "Displacement at  Z Displacement at Sensor location" style line reversed-x
    off reversed-y off ...
style-line width 2 style solid color 'cyan' ...
alias "" ...
axis-x log off minimum auto maximum auto inside on ...
label "Dynamic Time (Seconds)" exponent  show on value 4 auto on ...
axis-y log off minimum auto maximum auto inside on ...
label "Z Displacement at Sensor location" exponent  show on value -37 auto on


zone face list apply conditions

table list
zone list stress range  position-x 72 84 position-y 98 110 position-z 60

model save 'FWD-Clay-2-0.15secDynamic-end'

table 'DispSensor.VS.DynamicTime' export 'Deflection' csv
```

12. APPENDIX B - FLAC3D SCRIPT (ALTERNATIVE TEST PIT-GEOFOAM SETUP)

```
project new
model config dynamic
model dynamic active off

fish define MatMechPrprtes

;;Units: Length:in, Density:snail/in3, Force:lb, Stress:psi, Gravity: 386.04 in/s2
densityConcrete=0.2245e-3
densitySand=0.18e-3
densityGeofoam=0.1867e-5

PoisonConcrete=0.15
PoisonSand=0.4
PoisonGeofoam=0.1

YoungConcrete=3.5e6
YoungSand=4900
YoungGeofoam=655

end
@MatMechPrprtes

fish automatic-create on
model title 'MDT-FWD Calibration site'
;; Generating the geometry (dimensions in inches)
zone create brick point 0 0 0 0 point 1 144 0 0 point 2 0 180 0 point 3 0 0 3 size 36 45 1 group 'Sand'; Bottom of Geofoam
zone create brick point 0 0 0 3 point 1 4 0 3 point 2 0 180 3 point 3 0 0 51 size 1 45 16 group 'Sand'; Vertical Left
zone create brick point 0 140 0 3 point 1 144 0 3 point 2 140 180 3 point 3 140 0 51 size 1 45 16 group 'Sand'; Vertical right
zone create brick point 0 0 0 51 point 1 144 0 51 point 2 0 180 51 point 3 0 0 54 size 36 45 1 group 'Sand'; on top of Geofoam
zone create brick point 0 4 4 3 point 1 140 4 3 point 2 4 176 3 point 3 4 4 51 size 34 43 16 group 'Geofoam';
zone create brick point 0 4 0 3 point 1 140 0 3 point 2 4 4 3 point 3 4 0 51 size 34 1 16 group 'Sand'; in front of Geofoam
zone create brick point 0 4 176 3 point 1 140 176 3 point 2 4 180 3 point 3 4 176 51 size 34 1 16 group 'Sand'; behind the Geofoam
zone create brick point 0 0 0 54 point 1 144 0 54 point 2 0 180 54 point 3 0 0 59 size 36 45 1 group 'Concrete Slab';
zone attach by-face tolerance-absolute 0.05

zone cmodel assign elastic
zone property young = 1e40 poiss = 0.1
zone property density @densityConcrete range group 'Concrete Slab'
zone property density @densitySand range group 'Sand'
zone property density @densityGeofoam range group 'Geofoam'
zone property density @densitySand range group 'Sand'

model gravity 0 0 -386.04
zone initialize-stresses

zone gridpoint fix velocity-x range position-x 0.0
zone gridpoint fix velocity-y range position-x 0.0
zone gridpoint fix velocity-x range position-x 144
zone gridpoint fix velocity-y range position-x 144
zone gridpoint fix velocity-x range position-y 0.0
zone gridpoint fix velocity-y range position-y 0.0
```

```
zone gridpoint fix velocity-x range position-y 180
zone gridpoint fix velocity-y range position-y 180
zone gridpoint fix velocity-x range position-z 0
zone gridpoint fix velocity-y range position-z 0
zone gridpoint fix velocity-z range position-z 0

model largestrain off

zone cmodel assign elastic
zone property density @densityConcrete range group 'Concrete Slab'
zone property density @densitySand range group 'Sand'
zone property density @densityGeofoam range group 'Geofoam'
zone property density @densitySand range group 'Sand'
zone property young @YoungConcrete poiss @PoisonConcrete range group 'Concrete Slab'
zone property young @YoungSand poiss @PoisonSand range group 'Sand'
zone property young @YoungGeofoam poiss @PoisonGeofoam range group 'Geofoam'
zone property young @YoungSand poiss @PoisonSand range group 'Sand'

model save 'FWD-GeoFoam-1-InitialCondition'

model config dynamic
model restore 'FWD-GeoFoam-1-InitialCondition'

plot create  'Geometry initial'
plot item create zone
plot item create structure-shell
plot item create axes
plot view projection perspective magnification 1 ...
center (72,90,27.5) eye (220.13,-193.34,86.485) roll 356.772 ...
 clip-front -1e+10 clip-back 1e+10

plot create  'Zones ZZ-Stress'
plot item create zone active on contour stress quantity zz ...
method average ramp rainbow reversed on
plot item create axes
plot view projection perspective magnification 1 ...
center (72,90,27.5) eye (220.13,-193.34,86.485) roll 356.772 ...
clip-front -1e+10 clip-back 1e+10

plot create  'Zones Z-Displacement'
plot item create zone active on contour displacement component z log off ...
method average ramp rainbow reversed on
plot item create axes
plot view projection perspective magnification 1 ...
center (72,90,27.5) eye (220.13,-193.34,86.485) roll 356.772 ...
clip-front -1e+10 clip-back 1e+10

table '5' import '15'

plot create  'Input Stress History'
Plot item create chart-table active on ...
table '5' name "Stress History" ...
axis-x label "Time (Sec)" exponent  show on value 1 auto on ...
axis-y label "Stress (psi)" exponent  show on value 2 auto on

model largestrain off

zone face apply stress-zz -15.27 range position-x 32 48 position-y 132 144 position-z 59
zone face apply stress-zz -15.27 range position-x 96 108 position-y 132 144 position-z 59
zone face apply stress-zz -10.41 range position-x 72 84 position-y 96 108 position-z 59

model solve
```

```
model save 'FWD-Clay-After applying weights'
zone gridpoint initialize displacement 0 0 0

model dynamic active on

model history name='time' dynamic time-total
zone history name='szzCenter' stress-zz position (78 104 59)
zone history name='DispCenter' displacement-z position (78 104 59)
zone history name='DispSensor' displacement-z position (72 148 59)

zone dynamic damping hysteretic sigmoidal-3 1.07 -0.55 -0.4 range group 'Concrete Slab'
zone dynamic damping hysteretic sigmoidal-3 1.05 -0.5 -1.15 range group 'Sand'
zone dynamic damping hysteretic sigmoidal-3 1.1 -0.6 -1.5 range group 'Geofoam'

zone face apply stress-zz -6.944 table '5' time dynamic range position-x 72 84 position-y 100 112 position-z 59 ; ;
;position (72 96 55) ;

zone history name='stresscorner1' displacement-z position (72 96 59)
zone history name='stresscorner2' displacement-z position (72 108 59)
zone history name='stresscorner3' displacement-z position (84 96 59)
zone history name='stresscorner4' displacement-z position (84 108 59)
plot create  'Stress center History'
plot item create chart-history active on ...
history 'szzCenter' name "szzCenter ZZ Stress at (72,96,55)" style line reversed-x off reversed-y off ...
style-line width 2 style solid color 'cyan' ...
alias "" ...
vs step reversed off ...
begin 0 end 0 skip 0 ...
axis-x log off minimum auto maximum auto inside on ...
 label "Step" exponent  show on value 4 auto on ...
 axis-y log off minimum auto maximum auto inside on ...
  label "Y-Axis" exponent  show on value -1 auto on

plot create  'Displacement center History'
plot item create chart-history active on ...
history 'DispCenter' name "DispCenter Z Displacement at (72,90,55)" style line reversed-x off reversed-y off ...
style-line width 2 style solid color 'cyan' ...
 alias "" ...
 vs step reversed off ...
 begin 0 end 0 skip 0 ...
  axis-x log off minimum auto maximum auto inside on ...
  label "Step" exponent  show on value 4 auto on ...
  axis-y log off minimum auto maximum auto inside on ...
  label "Y-Axis" exponent  show on value -37 auto on

plot create  'Displacement Sensor vs Step'
plot item create chart-history active on ...
 history 'DispSensor' name "Displacement Sensor vs Step" style line reversed-x off reversed-y off ...
style-line width 2 style solid color 'cyan' ...
alias "" ...
vs step reversed off ...
begin 0 end 0 skip 0 ...
axis-x log off minimum auto maximum auto inside on ...
label "Step" exponent  show on value 4 auto on ...
axis-y log off minimum auto maximum auto inside on ...
label "Y-Axis" exponent  show on value -37 auto on

model solve dynamic time-total 0.008 ;fish-call -1 shell_load
model save 'FWD-GeoFoam-2-8msecDynamic'

model solve dynamic time-total 0.010 ;fish-call -1 shell_load
model save 'FWD-GeoFoam-2-10msecDynamic'
```

```
model solve dynamic time-total 0.012 ;fish-call -1 shell_load
model save 'FWD-GeoFoam-2-12msecDynamic'

model solve dynamic time-total 0.018 ;fish-call -1 shell_load
model save 'FWD-GeoFoam-2-18msecDynamic'
model solve dynamic time-total 0.020 ;fish-call -1 shell_load
model save 'FWD-GeoFoam-2-20msecDynamic'

model solve dynamic time-total 0.022 ;fish-call -1 shell_load
model save 'FWD-GeoFoam-2-22msecDynamic'

model solve dynamic time-total 0.025 ;fish-call -1 shell_load
model save 'FWD-GeoFoam-2-25msecDynamic'

model solve dynamic time-total 0.030 ;fish-call -1 shell_load
model save 'FWD-GeoFoam-2-30msecDynamic'

model solve dynamic time-total 0.060 ;fish-call -1 shell_load;
model save 'FWD-GeoFoam-2-60msecDynamic'

model solve dynamic time-total 0.08 ;fish-call -1 shell_load;

history export 'szzCenter' vs 'time' table 'szzCenter.VS.DynamicTime'

plot create  'Stress center vs Dynamic time'
plot item create chart-table active on ...
table 'szzCenter.VS.DynamicTime' name "szzCenter.VS.DynamicTime" style line reversed-x off reversed-y off ...
style-line width 2 style solid color 'cyan' ...
 alias "" ...
 axis-x log off minimum auto maximum auto inside on ...
 label "Dynamic Time (Seconds)" exponent  show on value -2 auto on ...
 axis-y log off minimum auto maximum auto inside on ...
 label "ZZ-Stress at center (psi)" exponent  show on value 0 auto on

history export 'DispCenter' vs 'time' table 'DispCenter.VS.DynamicTime'

plot create  'Stress center vs Dynamic time'
plot item create chart-table active on ...
table 'DispCenter.VS.DynamicTime' name "DispCenter.VS.DynamicTime" style line reversed-x off reversed-y off ...
style-line width 2 style solid color 'cyan' ...
alias "" ...
axis-x log off minimum auto maximum auto inside on ...
 label "Dynamic Time (Seconds)" exponent  show on value -2 auto on ...
 axis-y log off minimum auto maximum auto inside on ...
 label "Center ZZ-Stress at center (psi)" exponent  show on value 0 auto on

 history export 'DispSensor' vs 'time' table 'DispSensor.VS.DynamicTime'

 plot create  'Sensor Displacement History'
 plot item create chart-table active on ...
 table 'DispSensor.VS.DynamicTime' name "Displacement at  Z Displacement at Sensor location" style line reversed-x
    off reversed-y off ...
 style-line width 2 style solid color 'cyan' ...
 alias "" ...
 axis-x log off minimum auto maximum auto inside on ...
 label "Dynamic Time (Seconds)" exponent  show on value 4 auto on ...
 axis-y log off minimum auto maximum auto inside on ...
 label "Z Displacement at Sensor location" exponent  show on value -37 auto on

zone face list apply conditions
table list
```

192. zone list stress range position-x 72 84 position-y 98 110 position-z 60

193. model save 'FWD-GeoFoam-2-80msecDynamic-end'

194. table 'DispSensor.VS.DynamicTime' export 'Deflection' csv

13. Appendix C (Results of the Sensitivity Analysis)

Results of the sensitivity analysis section that were not included in the report are presented in this appendix. Two figures are provided for each scenario: the first one represents a cross-section along the X-axis of the test pit design, and the second figure shows the predicted displacement time histories for the two maximum impact loads of 11.55 kip and 14.68 kip. The second figure for each scenario also includes the first 0.012 milliseconds of the displacement time history of that scenario along with the first 0.012 milliseconds of the displacement time history of the alternative geofoam setup under the same impact load. This portion of the displacement time histories, i.e., the first 0.012 milliseconds, are assumed to correlate with the noise seen in the alternative geofoam setup from the point when the falling weight was released to the point that the falling weight hits the concrete slab.

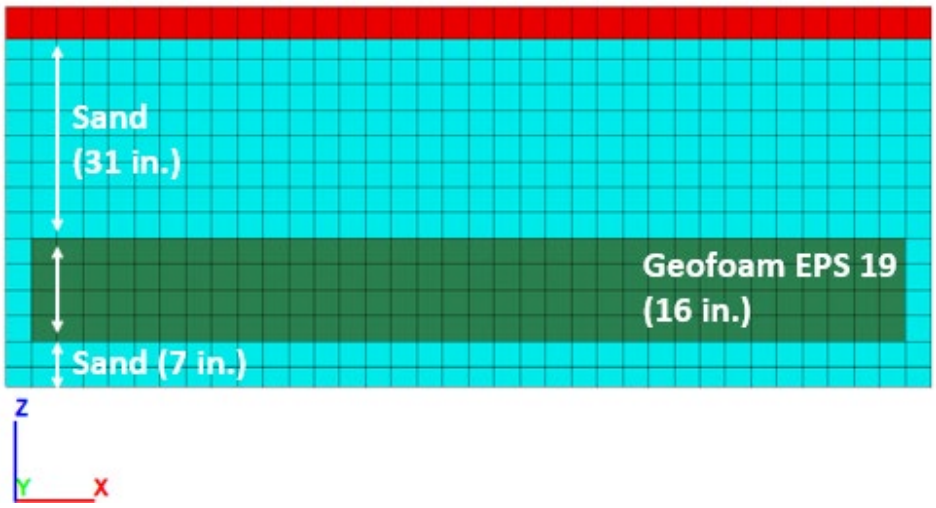

Figure C1. A cross-section in X direction for scenario 1-Geofoam EPS 19 (16 in. thick in Z direction).

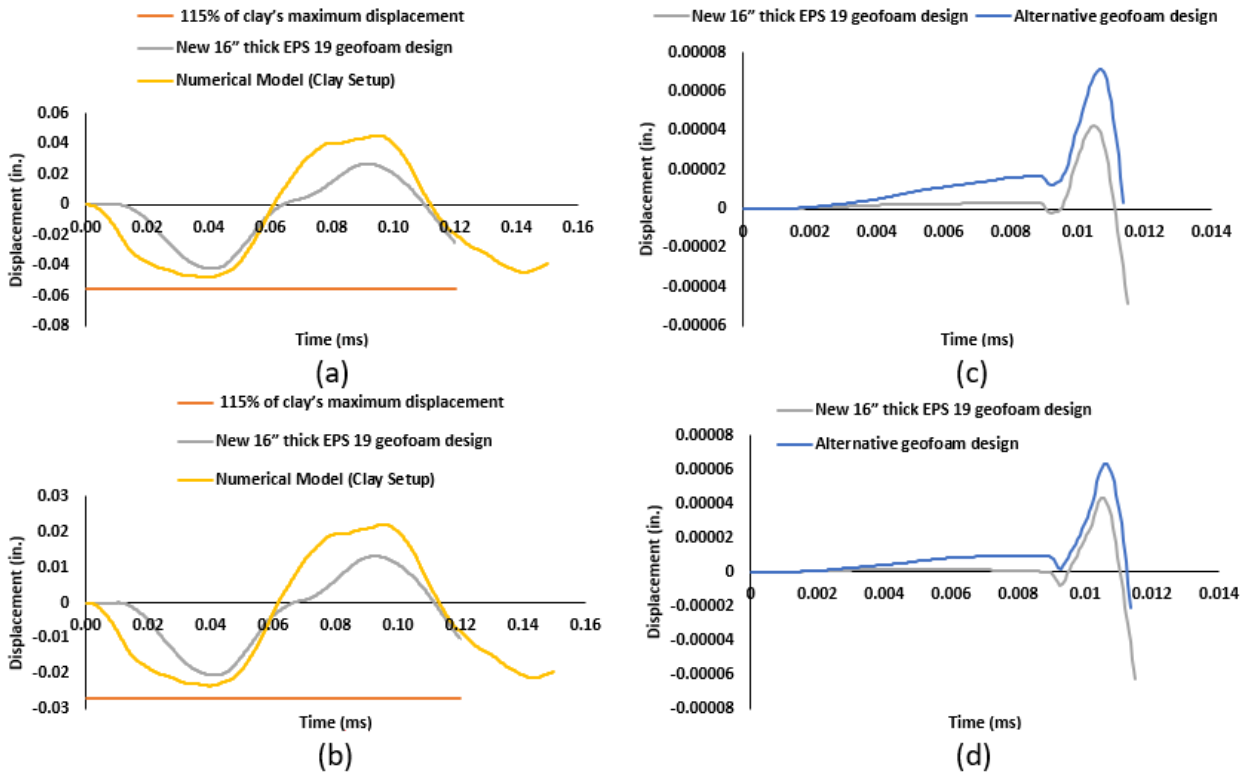

Figure C2. Scenario 1-a) Compares the predicted displacement time history of the new design with the clay setup under 11.55 kip load, b) Compares the predicted displacement time history of the new design with the clay setup under 14.68 kip load, c) Compares the first 0.012 milliseconds of the predicted displacement time history of the new design with the original geofoam setup under 11.55 kip load, d) Compares the first 0.012 milliseconds of the predicted displacement time history of the new design with the original geofoam setup under 14.68 kip load.

Figure C3. A cross-section in X direction for scenario 2-Geofoam EPS 19 (16 in. thick in Z direction).

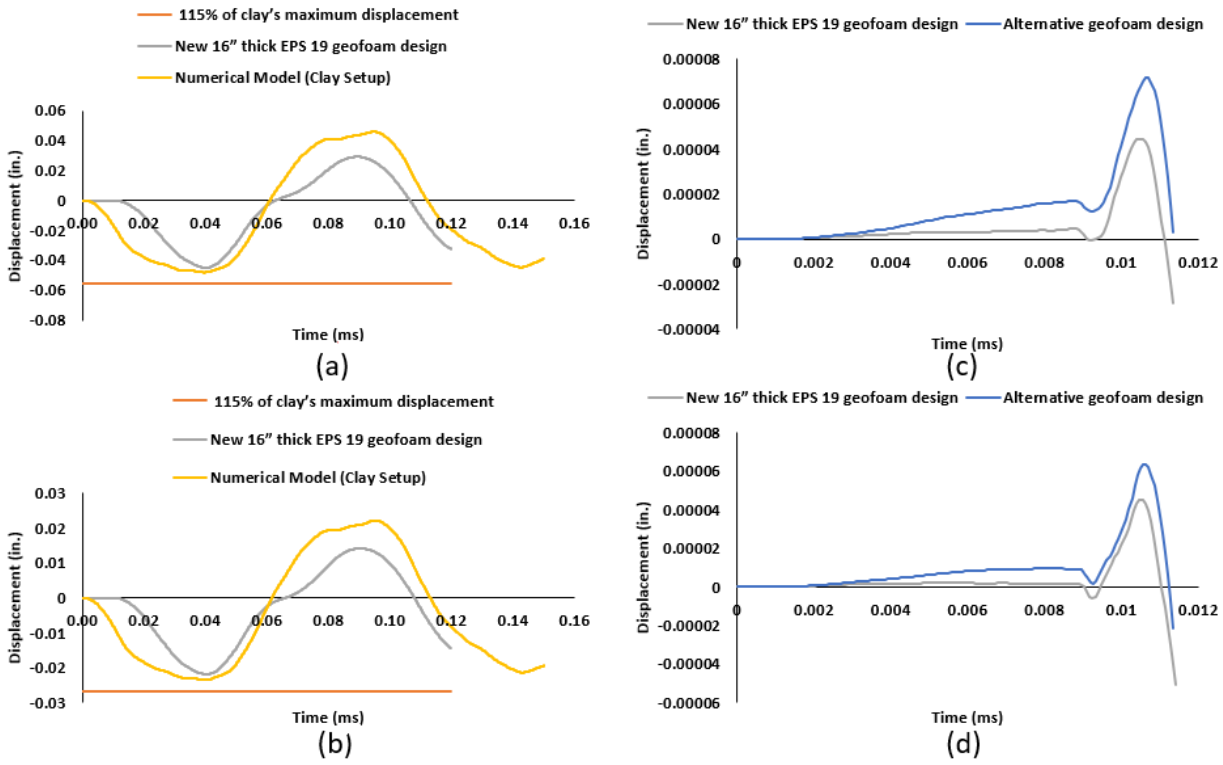

Figure C4. Scenario 2-a) Compares the predicted displacement time history of the new design with the clay setup under 11.55 kip load, b) Compares the predicted displacement time history of the new design with the clay setup under 14.68 kip load, c) Compares the first 0.012 milliseconds of the predicted displacement time history of the new design with the original geofoam setup under 11.55 kip load, d) Compares the first 0.012 milliseconds of the predicted displacement time history of the new design with the original geofoam setup under 14.68 kip load.

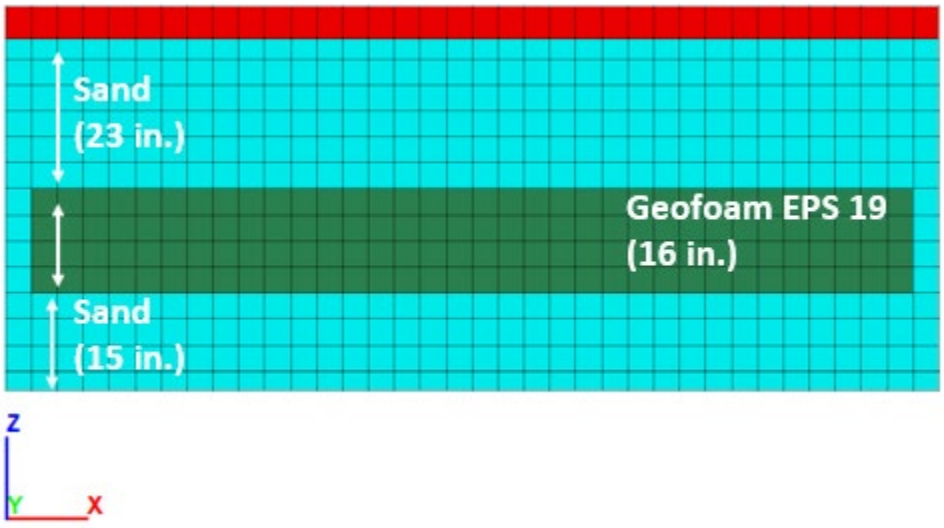

Figure C5. A cross-section in X direction for scenario 3-Geofoam EPS 19 (16 in. thick in Z direction).

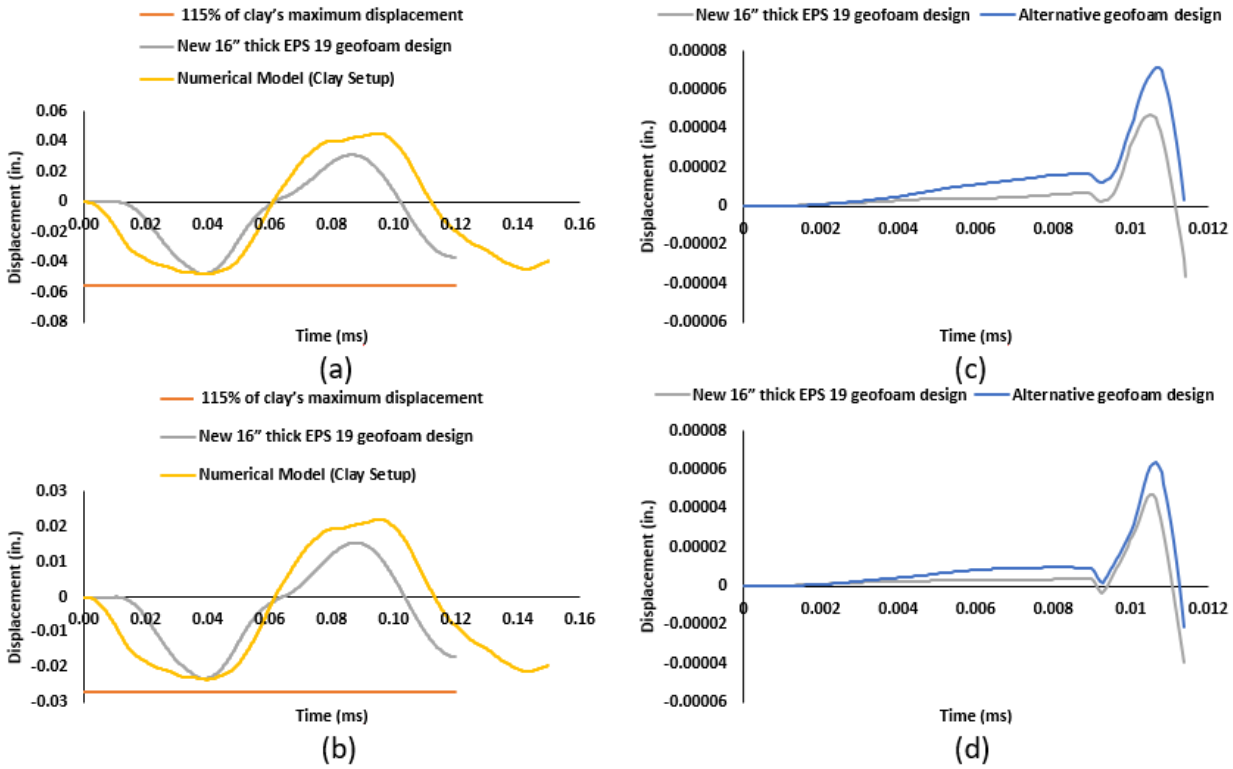

Figure C6. Scenario 3-a) Compares the predicted displacement time history of the new design with the clay setup under 11.55 kip load, b) Compares the predicted displacement time history of the new design with the clay setup under 14.68 kip load, c) Compares the first 0.012 milliseconds of the predicted displacement time history of the new design with the original geofoam setup under 11.55 kip load, d) Compares the first 0.012 milliseconds of the predicted displacement time history of the new design with the original geofoam setup under 14.68 kip load.

Figure C7. A cross-section in X direction for scenario 4-Geofoam EPS 19 (16 in. thick in Z direction).

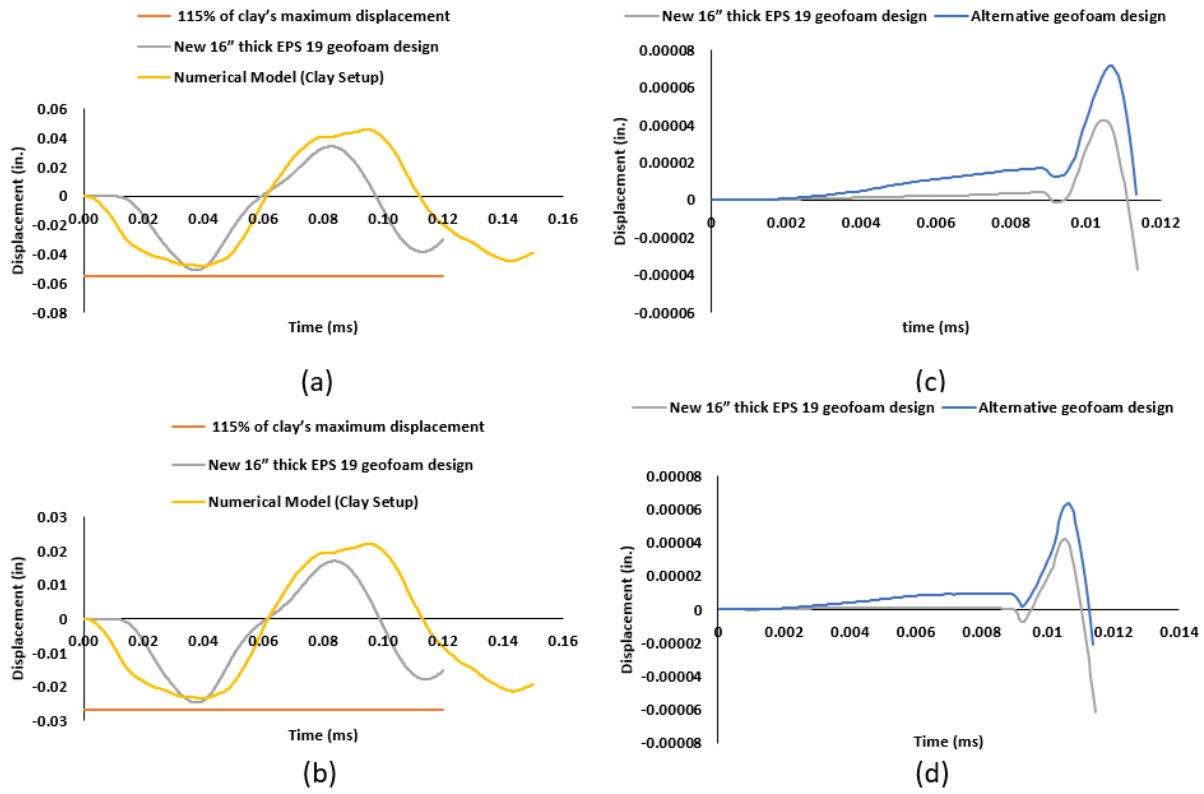

Figure C8. Scenario 4-a) Compares the predicted displacement time history of the new design with the clay setup under 11.55 kip load, b) Compares the predicted displacement time history of the new design with the clay setup under 14.68 kip load, c) Compares the first 0.012 milliseconds of the predicted displacement time history of the new design with the original geofoam setup under 11.55 kip load, d) Compares the first 0.012 milliseconds of the predicted displacement time history of the new design with the original geofoam setup under 14.68 kip load.

Figure C9. A cross-section in X direction for scenario 5-Geofoam EPS 19 (16 in. thick in Z direction).

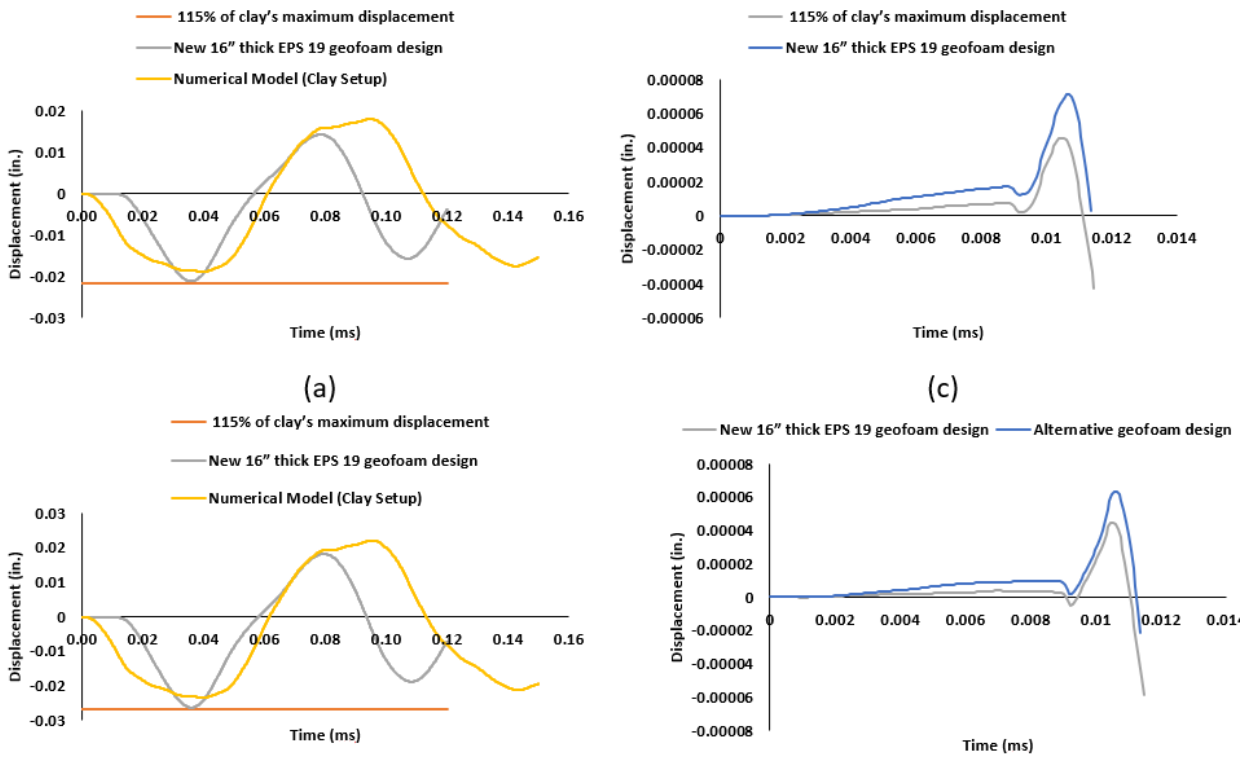

Figure C10. Scenario 5-a) Compares the predicted displacement time history of the new design with the clay setup under 11.55 kip load, b) Compares the predicted displacement time history of the new design with the clay setup under 14.68 kip load, c) Compares the first 0.012 milliseconds of the predicted displacement time history of the new design with the original geofoam setup under 11.55 kip load, d) Compares the first 0.012 milliseconds of the predicted displacement time history of the new design with the original geofoam setup under 14.68 kip load.

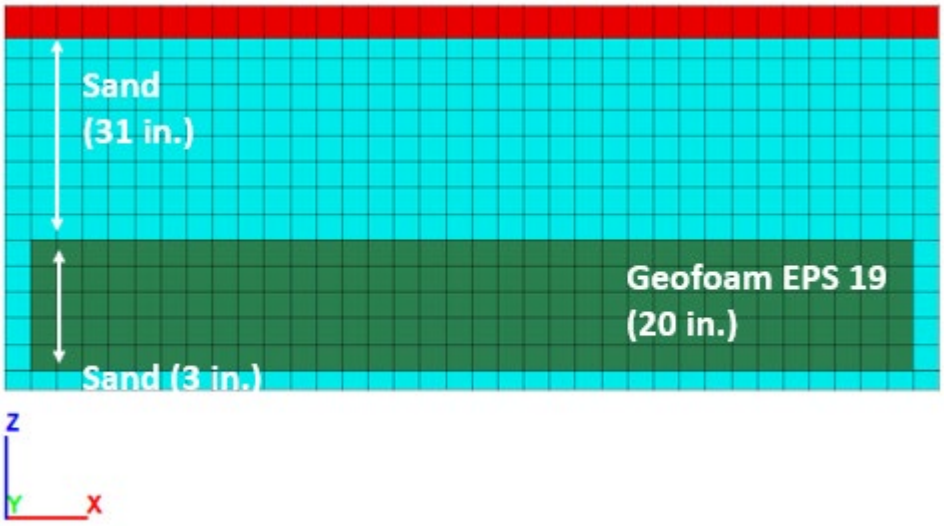

Figure C11. A cross-section in X direction for scenario 6-Geofoam EPS 19 (20 in. thick in Z direction).

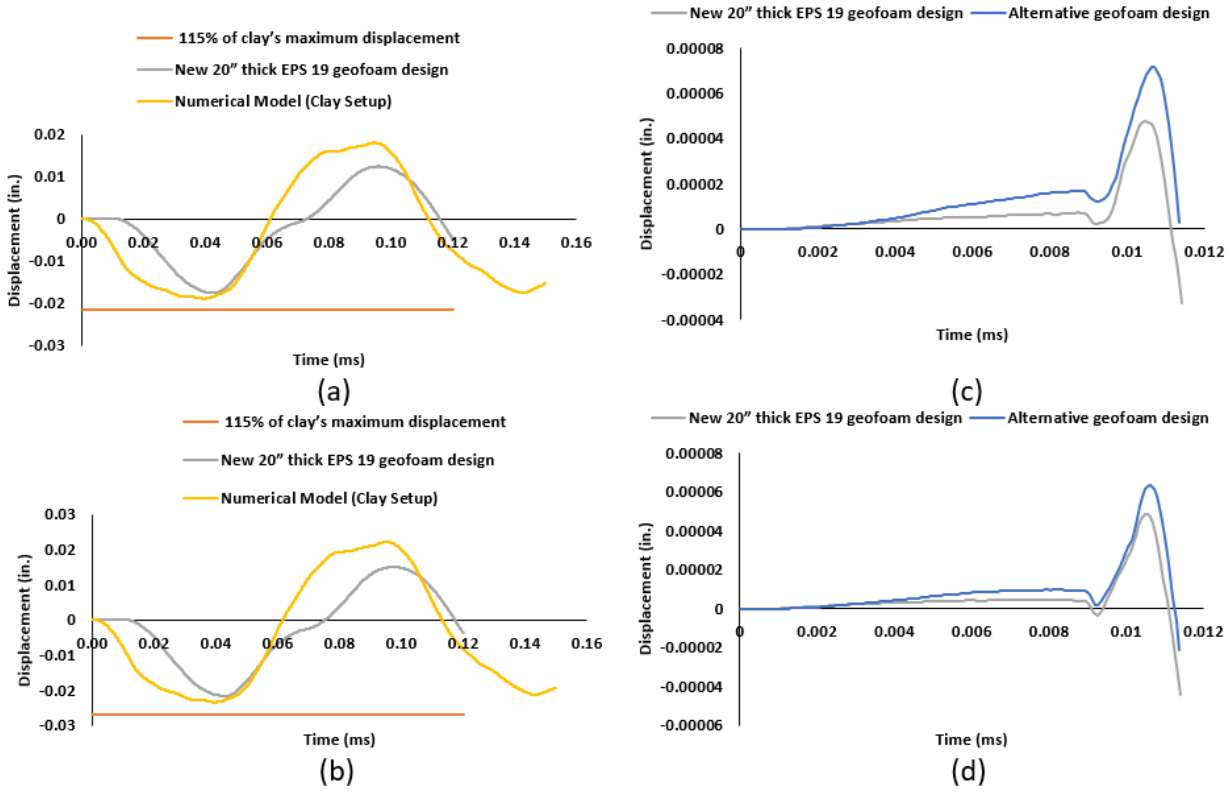

Figure C12. Scenario 6-a) Compares the predicted displacement time history of the new design with the clay setup under 11.55 kip load, b) Compares the predicted displacement time history of the new design with the clay setup under 14.68 kip load, c) Compares the first 0.012 milliseconds of the predicted displacement time history of the new design with the original geofoam setup under 11.55 kip load, d) Compares the first 0.012 milliseconds of the predicted displacement time history of the new design with the original geofoam setup under 14.68 kip load.

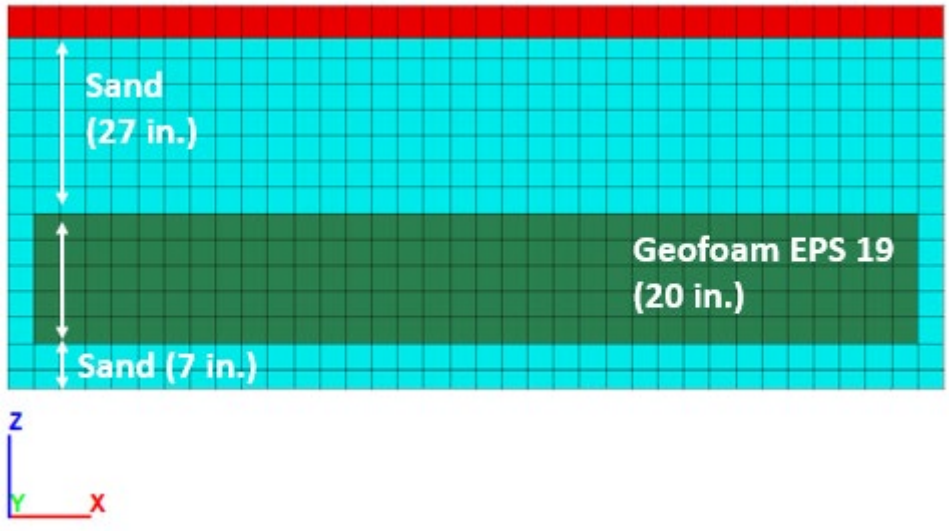

Figure C13. A cross-section in X direction for scenario 7-Geofoam EPS 19 (20 in. thick in Z direction).

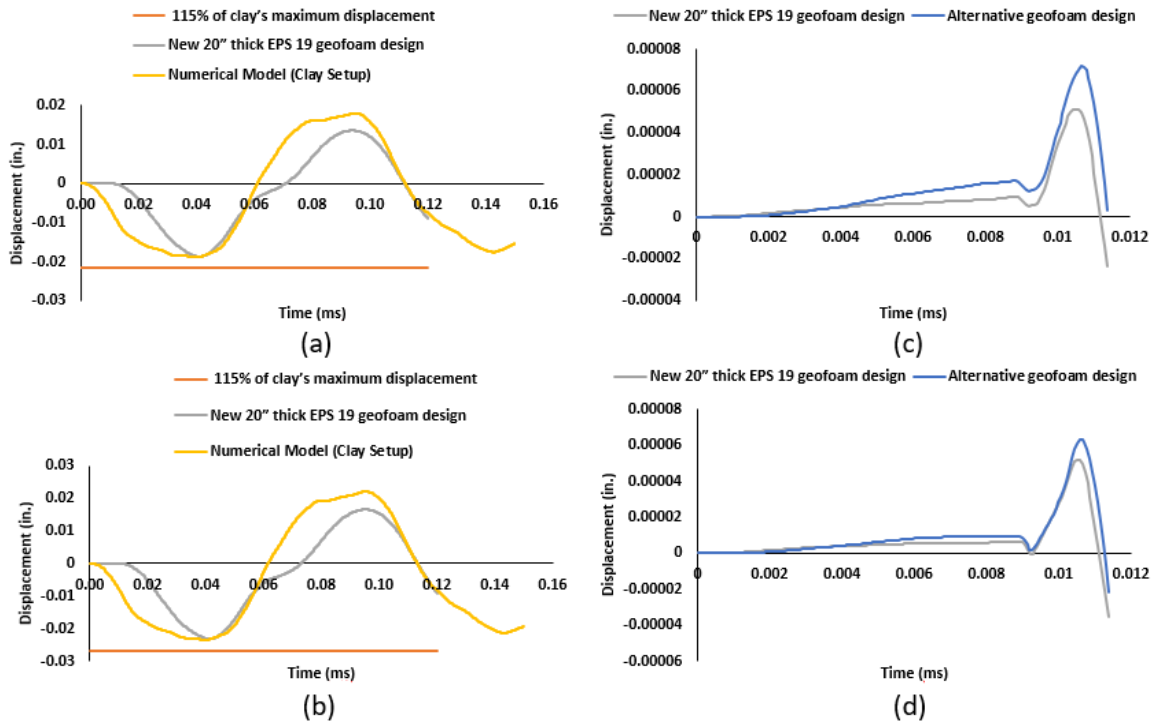

Figure C14. Scenario 7-a) Compares the predicted displacement time history of the new design with the clay setup under 11.55 kip load, b) Compares the predicted displacement time history of the new design with the clay setup under 14.68 kip load, c) Compares the first 0.012 milliseconds of the predicted displacement time history of the new design with the original geofoam setup under 11.55 kip load, d) Compares the first 0.012 milliseconds of the predicted displacement time history of the new design with the original geofoam setup under 14.68 kip load.

Figure C15. A cross-section in X direction for scenario 8-Geofoam EPS 19 (20 in. thick in Z direction).

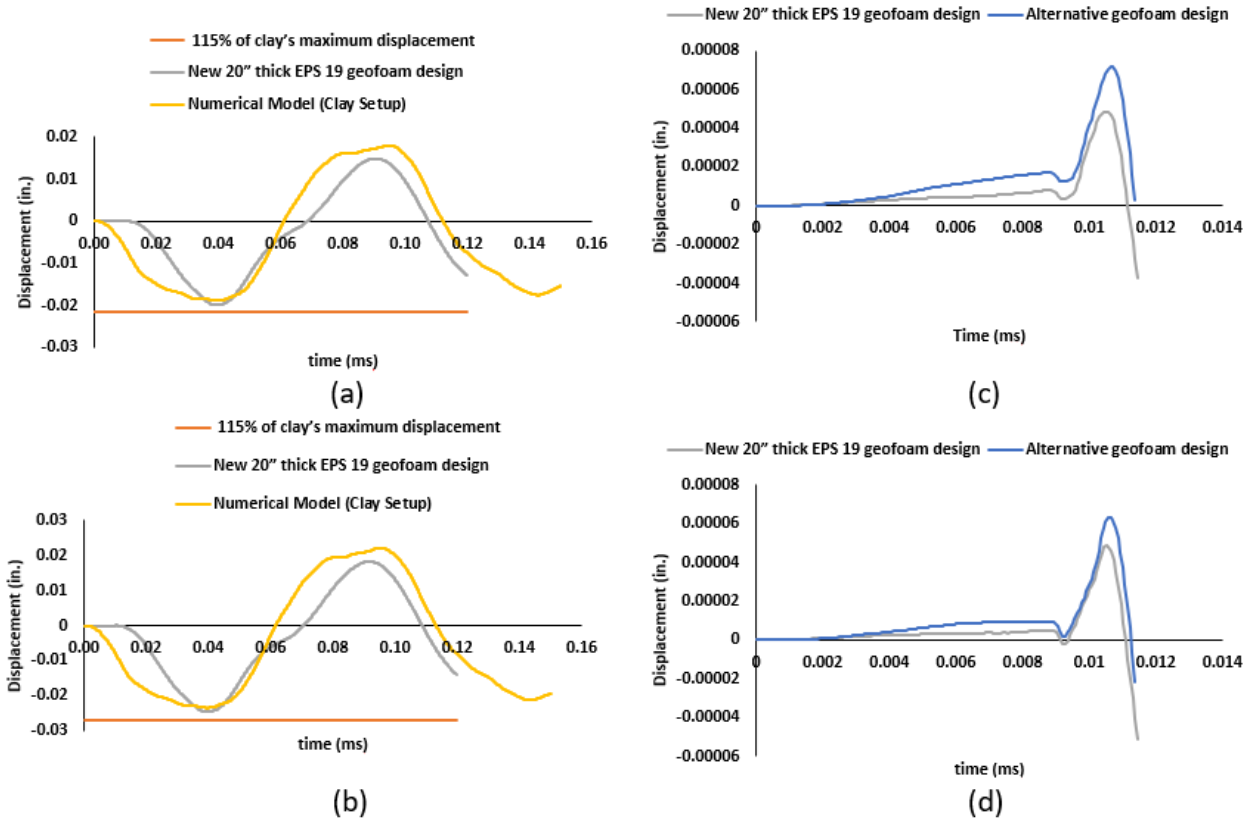

Figure C16. Scenario 8-a) Compares the predicted displacement time history of the new design with the clay setup under 11.55 kip load, b) Compares the predicted displacement time history of the new design with the clay setup under 14.68 kip load, c) Compares the first 0.012 milliseconds of the predicted displacement time history of the new design with the original geofoam setup under 11.55 kip load, d) Compares the first 0.012 milliseconds of the predicted displacement time history of the new design with the original geofoam setup under 14.68 kip load.

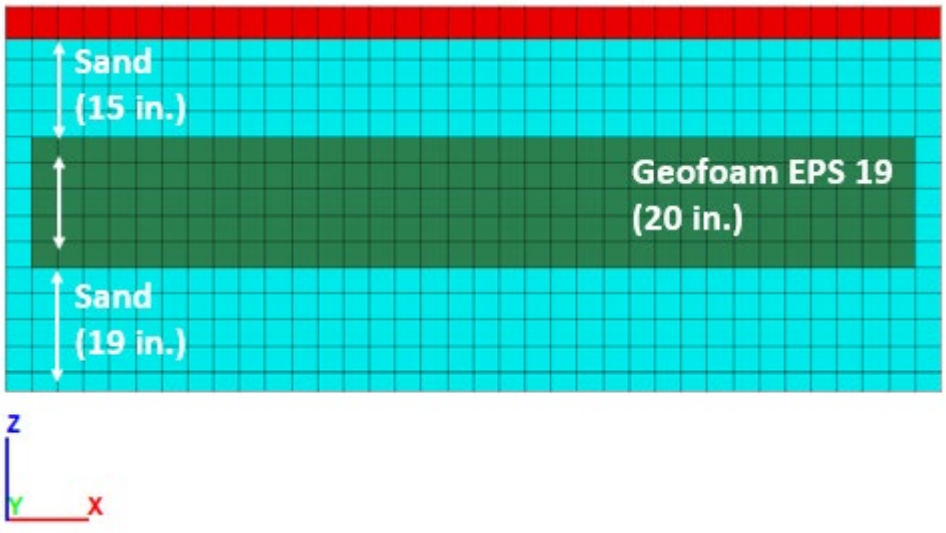

Figure C17. A cross-section in X direction for scenario 9-Geofoam EPS 19 (20 in. thick in Z direction).

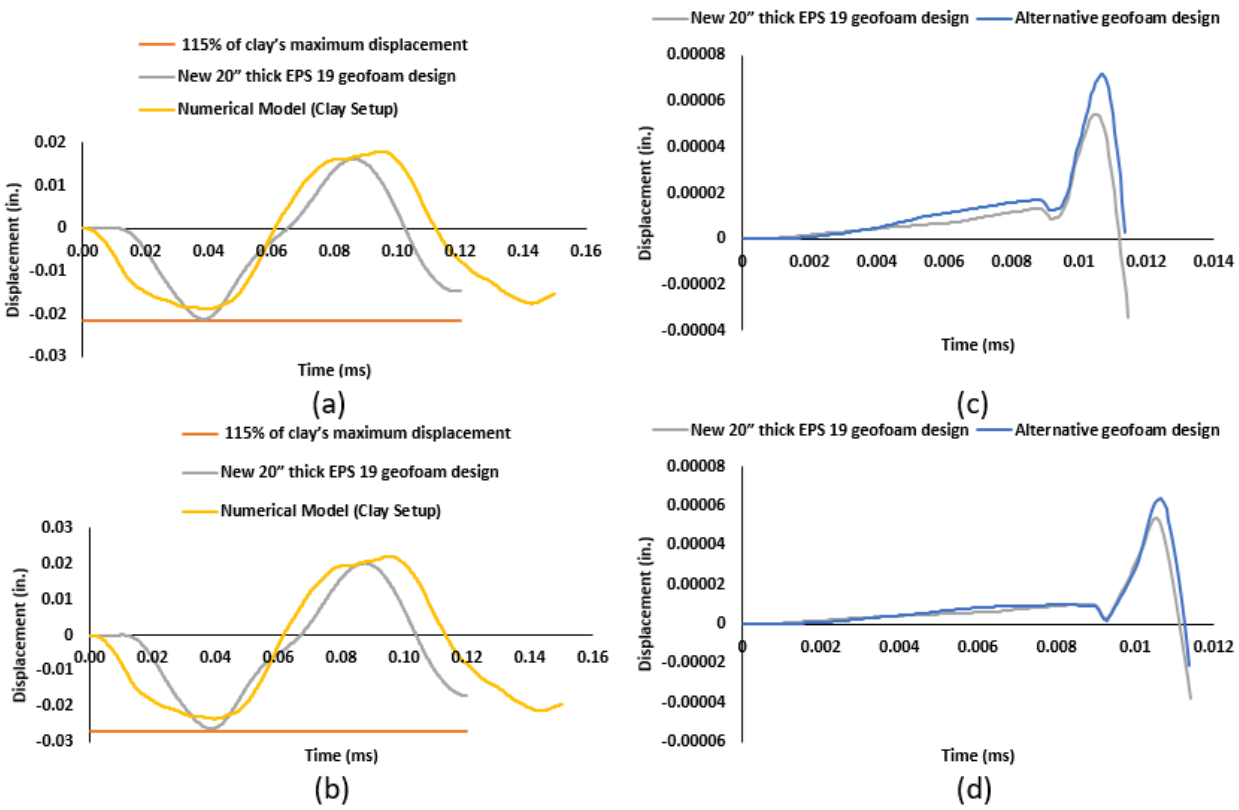

Figure C18. Scenario 9-a) Compares the predicted displacement time history of the new design with the clay setup under 11.55 kip load, b) Compares the predicted displacement time history of the new design with the clay setup under 14.68 kip load, c) Compares the first 0.012 milliseconds of the predicted displacement time history of the new design with the original geofoam setup under 11.55 kip load, d) Compares the first 0.012 milliseconds of the predicted displacement time history of the new design with the original geofoam setup under 14.68 kip load.

Figure C19. A cross-section in X direction for scenario 10-Geofoam EPS 19 (24 in. thick in Z direction).

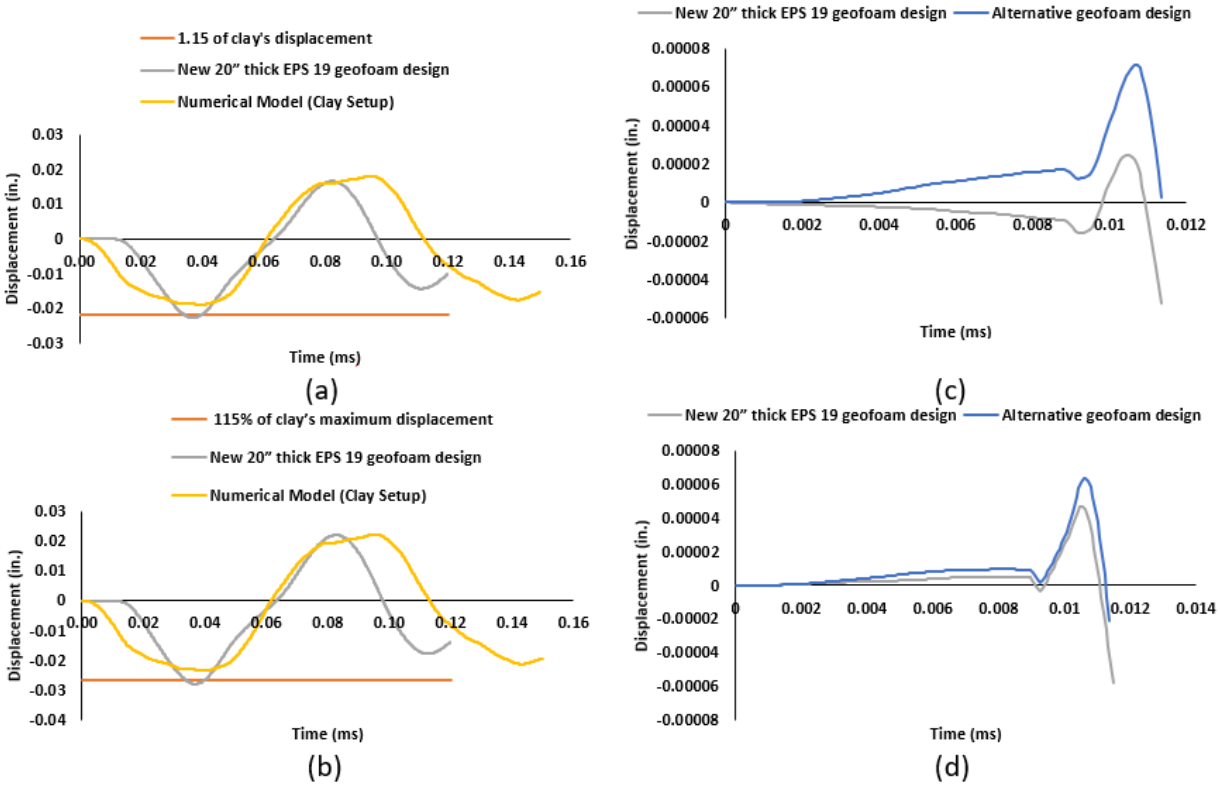

Figure C20. Scenario 10-a) Compares the predicted displacement time history of the new design with the clay setup under 11.55 kip load, b) Compares the predicted displacement time history of the new design with the clay setup under 14.68 kip load, c) Compares the first 0.012 milliseconds of the predicted displacement time history of the new design with the original geofoam setup under 11.55 kip load, d) Compares the first 0.012 milliseconds of the predicted displacement time history of the new design with the original geofoam setup under 14.68 kip load.

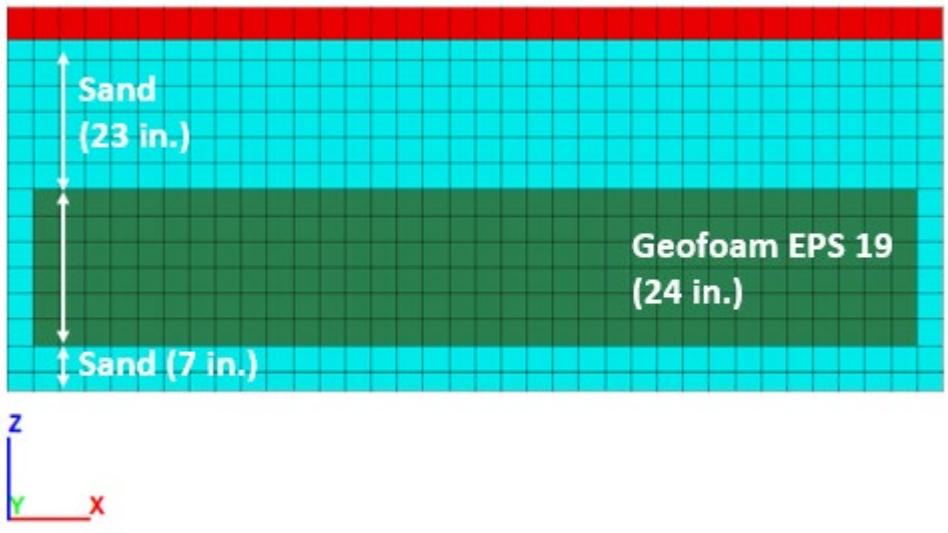

Figure C21. A cross-section in X direction for scenario 11-Geofoam EPS 19 (24 in. thick in Z direction).

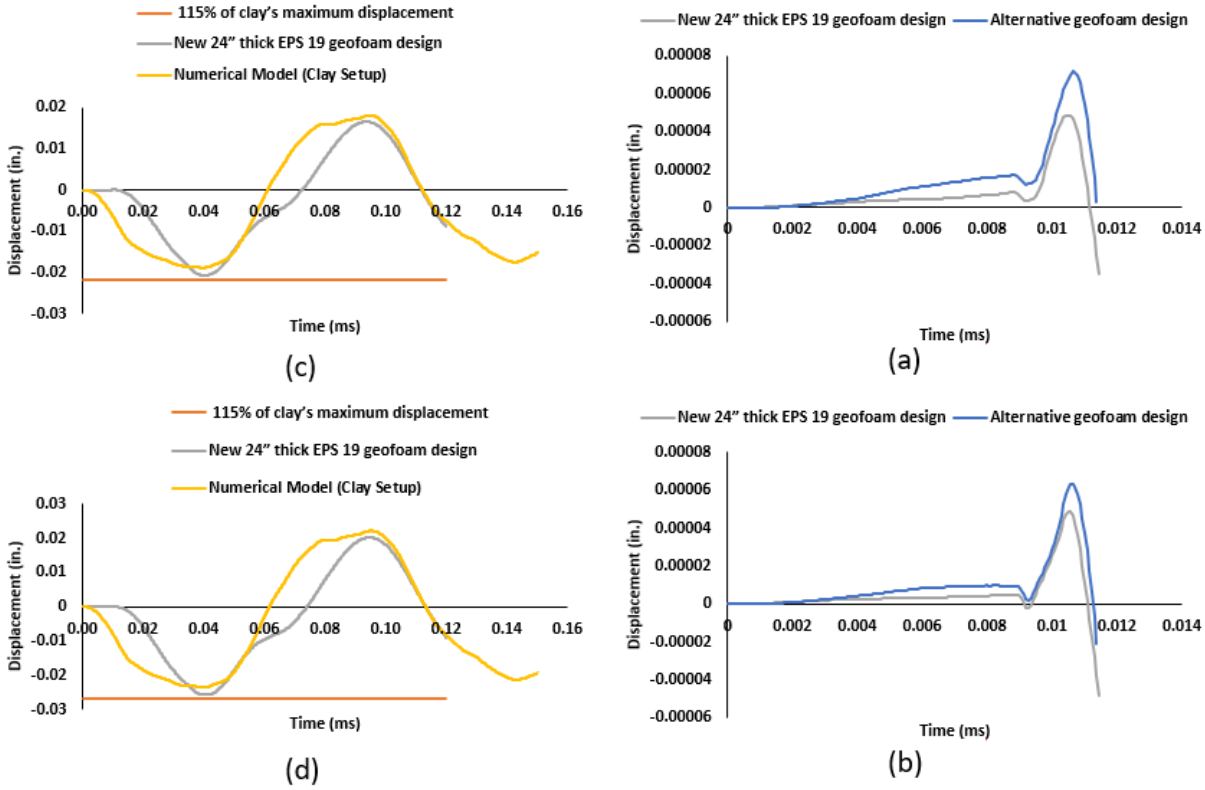

Figure C22. Scenario 11-a) Compares the predicted displacement time history of the new design with the clay setup under 11.55 kip load, b) Compares the predicted displacement time history of the new design with the clay setup under 14.68 kip load, c) Compares the first 0.012 milliseconds of the predicted displacement time history of the new design with the original geofoam setup under 11.55 kip load, d) Compares the first 0.012 milliseconds of the predicted displacement time history of the new design with the original geofoam setup under 14.68 kip load.

Figure C23. A cross-section in X direction for scenario 12-Geofoam EPS 19 (24 in. thick in Z direction).

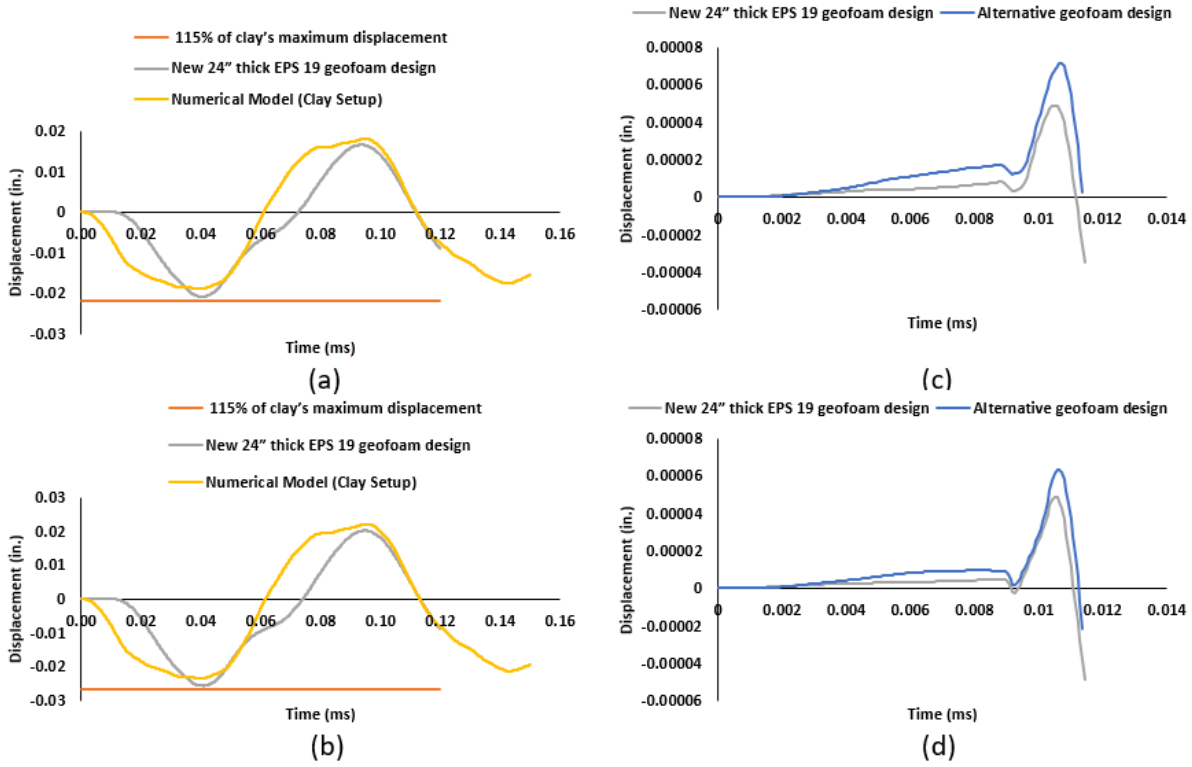

Figure C24. Scenario 12-a) Compares the predicted displacement time history of the new design with the clay setup under 11.55 kip load, b) Compares the predicted displacement time history of the new design with the clay setup under 14.68 kip load, c) Compares the first 0.012 milliseconds of the predicted displacement time history of the new design with the original geofoam setup under 11.55 kip load, d) Compares the first 0.012 milliseconds of the predicted displacement time history of the new design with the original geofoam setup under 14.68 kip load.

Figure C25. A cross-section in X direction for scenario 13-Geofoam EPS 19 (24 in. thick in Z direction).

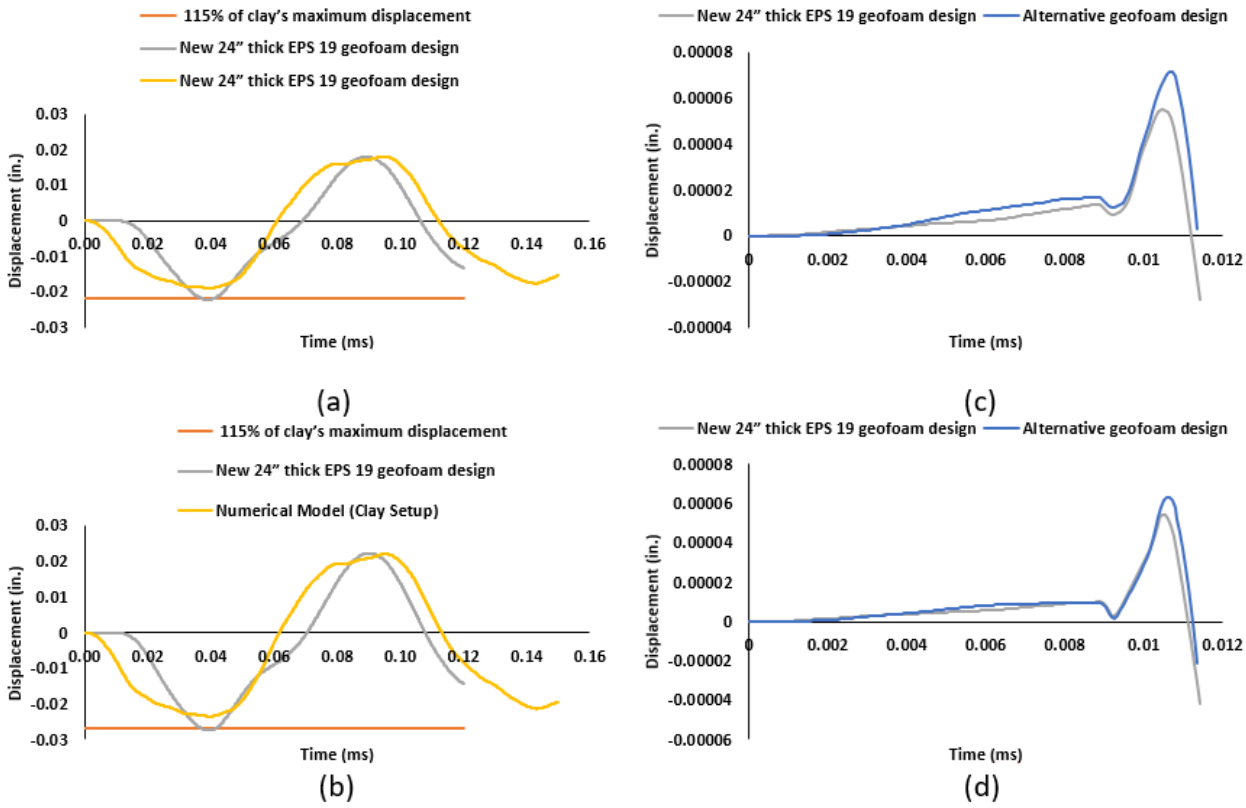

Figure C26. Scenario 13-a) Compares the predicted displacement time history of the new design with the clay setup under 11.55 kip load, b) Compares the predicted displacement time history of the new design with the clay setup under 14.68 kip load, c) Compares the first 0.012 milliseconds of the predicted displacement time history of the new design with the original geofoam setup under 11.55 kip load, d) Compares the first 0.012 milliseconds of the predicted displacement time history of the new design with the original geofoam setup under 14.68 kip load.

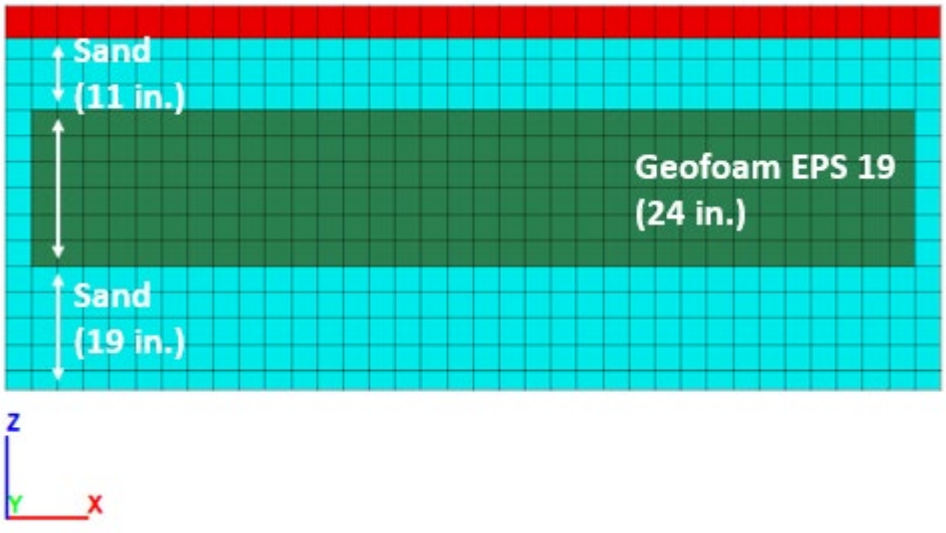

Figure C27. A cross-section in X direction for scenario 14-Geofoam EPS 19 (24 in. thick in Z direction).

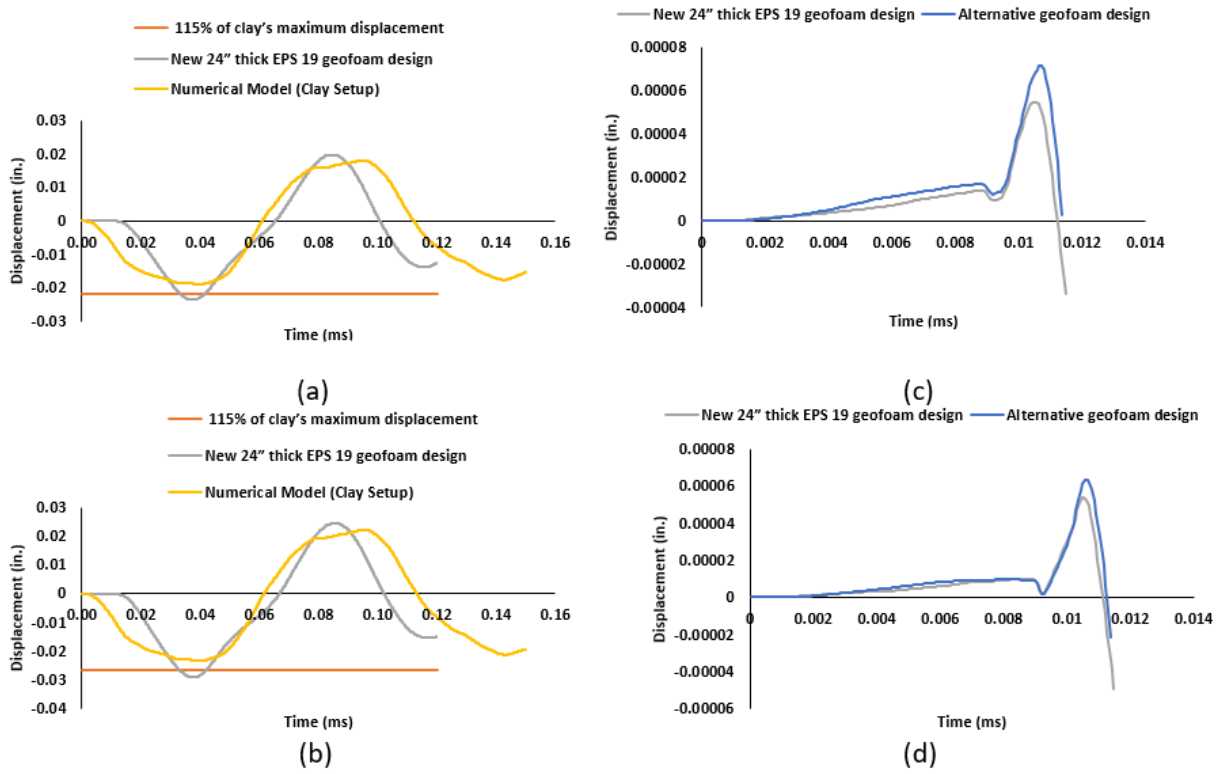

Figure C28. Scenario 14-a) Compares the predicted displacement time history of the new design with the clay setup under 11.55 kip load, b) Compares the predicted displacement time history of the new design with the clay setup under 14.68 kip load, c) Compares the first 0.012 milliseconds of the predicted displacement time history of the new design with the original geofoam setup under 11.55 kip load, d) Compares the first 0.012 milliseconds of the predicted displacement time history of the new design with the original geofoam setup under 14.68 kip load.

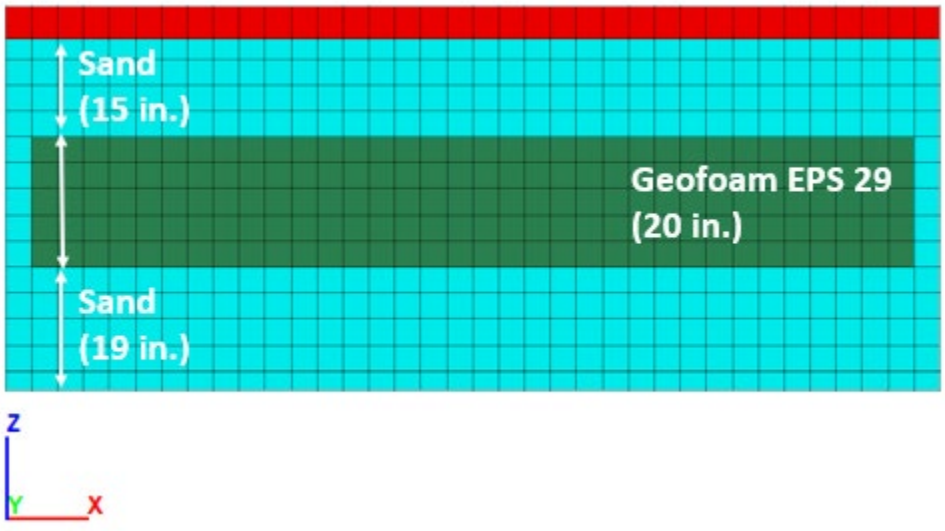

Figure C29. A cross-section in X direction for scenario 15-Geofoam EPS 19 (20 in. thick in Z direction).

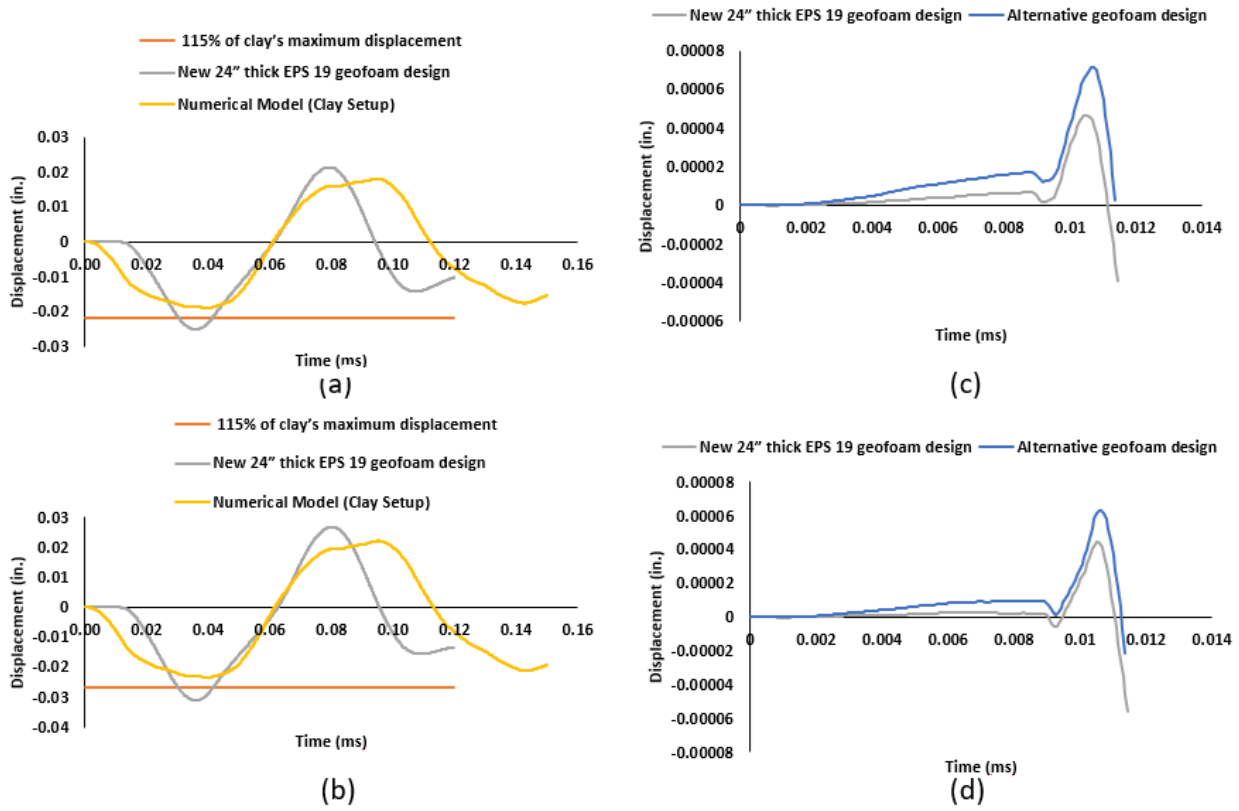

Figure C30. Scenario 15-a) Compares the predicted displacement time history of the new design with the clay setup under 11.55 kip load, b) Compares the predicted displacement time history of the new design with the clay setup under 14.68 kip load, c) Compares the first 0.012 milliseconds of the predicted displacement time history of the new design with the original geofoam setup under 11.55 kip load, d) Compares the first 0.012 milliseconds of the predicted displacement time history of the new design with the original geofoam setup under 14.68 kip load.

Figure C31. A cross-section in X direction for scenario 16-Geofoam EPS 29 (20 in. thick in Z direction).

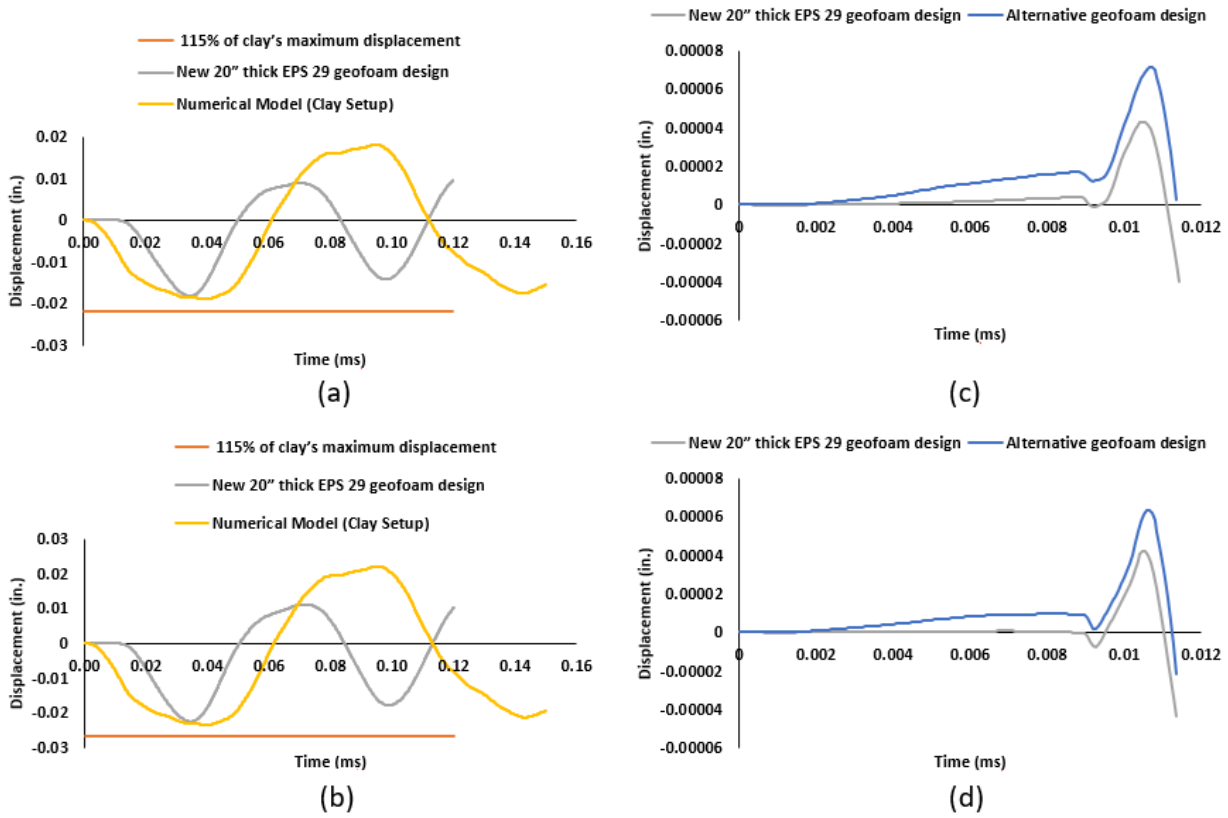

Figure C32. Scenario 16-a) Compares the predicted displacement time history of the new design with the clay setup under 11.55 kip load, b) Compares the predicted displacement time history of the new design with the clay setup under 14.68 kip load, c) Compares the first 0.012 milliseconds of the predicted displacement time history of the new design with the original geofoam setup under 11.55 kip load, d) Compares the first 0.012 milliseconds of the predicted displacement time history of the new design with the original geofoam setup under 14.68 kip load.

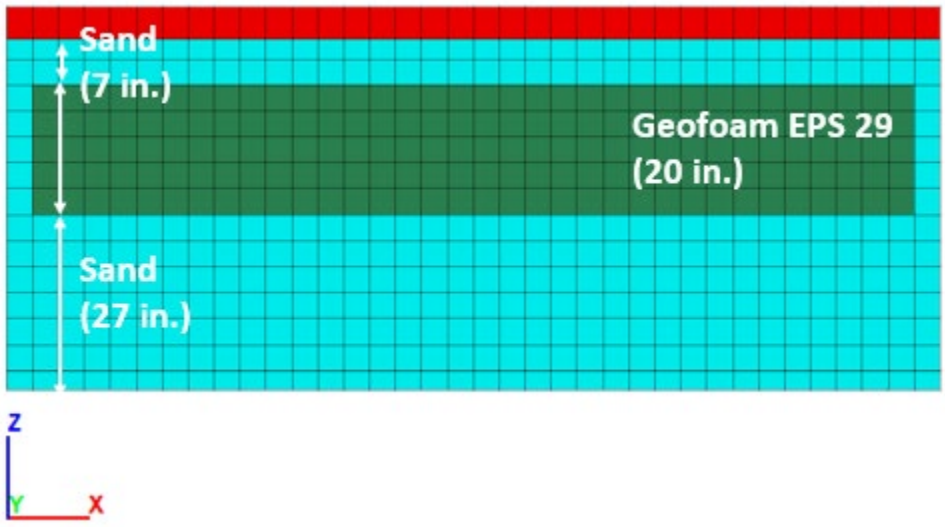

Figure C33. A cross-section in X direction for scenario 17-Geofoam EPS 29 (20 in. thick in Z direction).

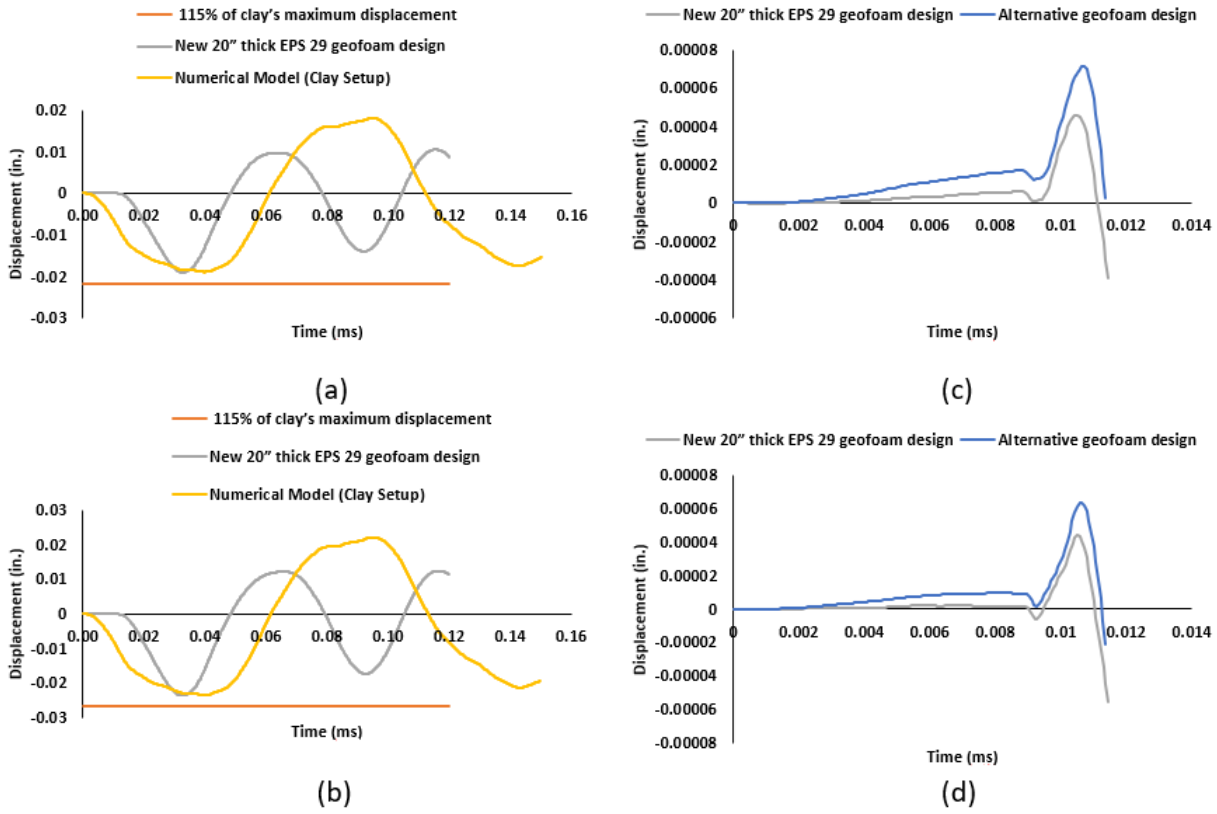

Figure C34. Scenario 17-a) Compares the predicted displacement time history of the new design with the clay setup under 11.55 kip load, b) Compares the predicted displacement time history of the new design with the clay setup under 14.68 kip load, c) Compares the first 0.012 milliseconds of the predicted displacement time history of the new design with the original geofoam setup under 11.55 kip load, d) Compares the first 0.012 milliseconds of the predicted displacement time history of the new design with the original geofoam setup under 14.68 kip load.

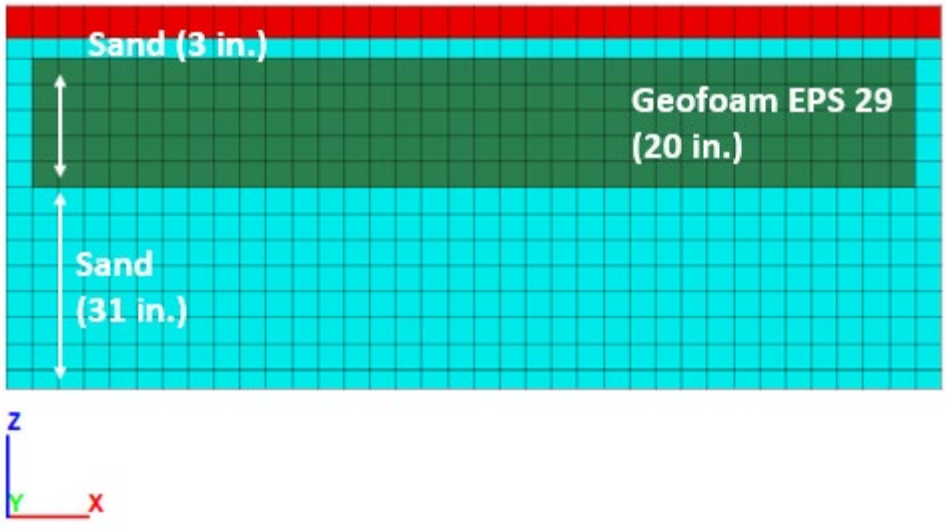

Figure C35. A cross-section in X direction for scenario 18-Geofoam EPS 29 (20 in. thick in Z direction).

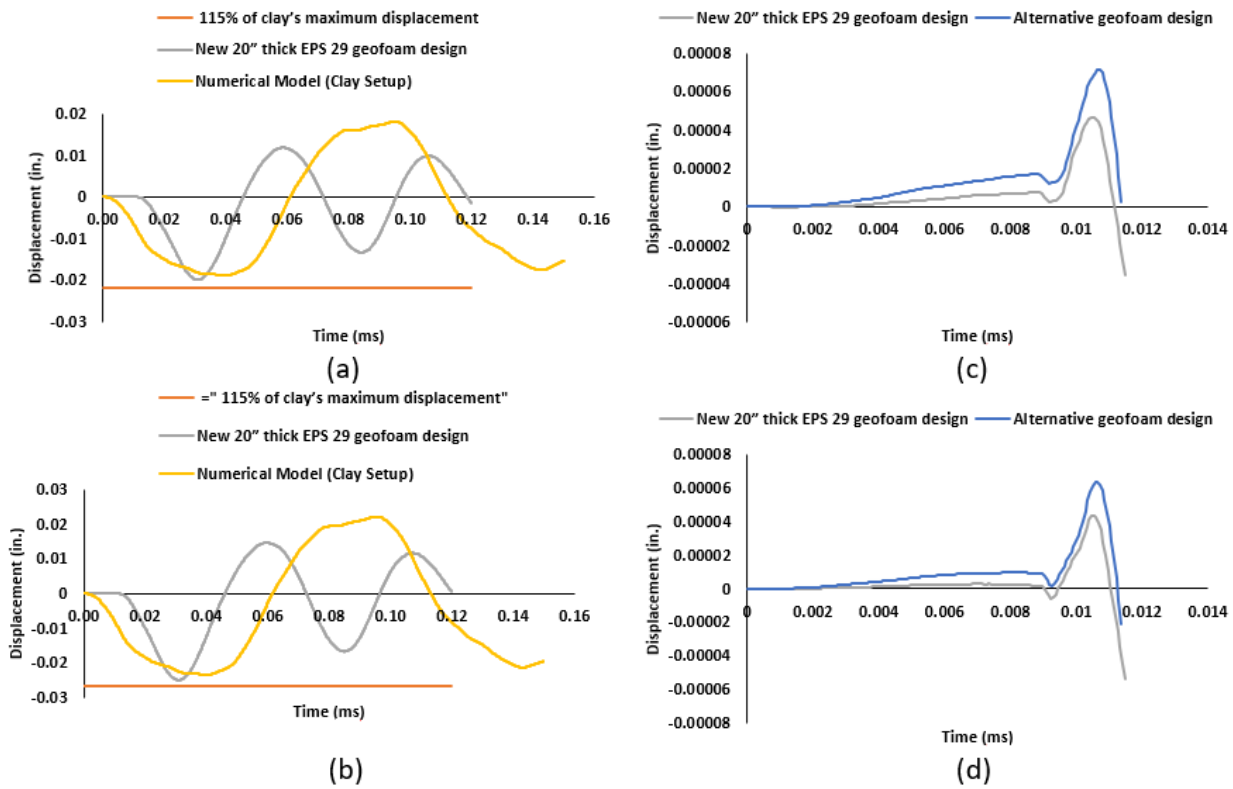

Figure C36. Scenario 18-a) Compares the predicted displacement time history of the new design with the clay setup under 11.55 kip load, b) Compares the predicted displacement time history of the new design with the clay setup under 14.68 kip load, c) Compares the first 0.012 milliseconds of the predicted displacement time history of the new design with the original geofoam setup under 11.55 kip load, d) Compares the first 0.012 milliseconds of the predicted displacement time history of the new design with the original geofoam setup under 14.68 kip load.

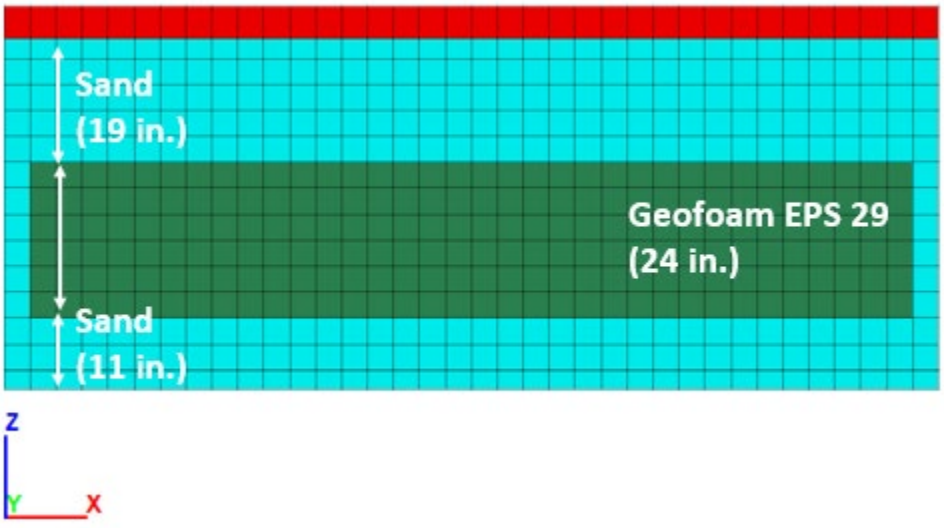

Figure C37. A cross-section in X direction for scenario 19-Geofoam EPS 29 (24 in. thick in Z direction).

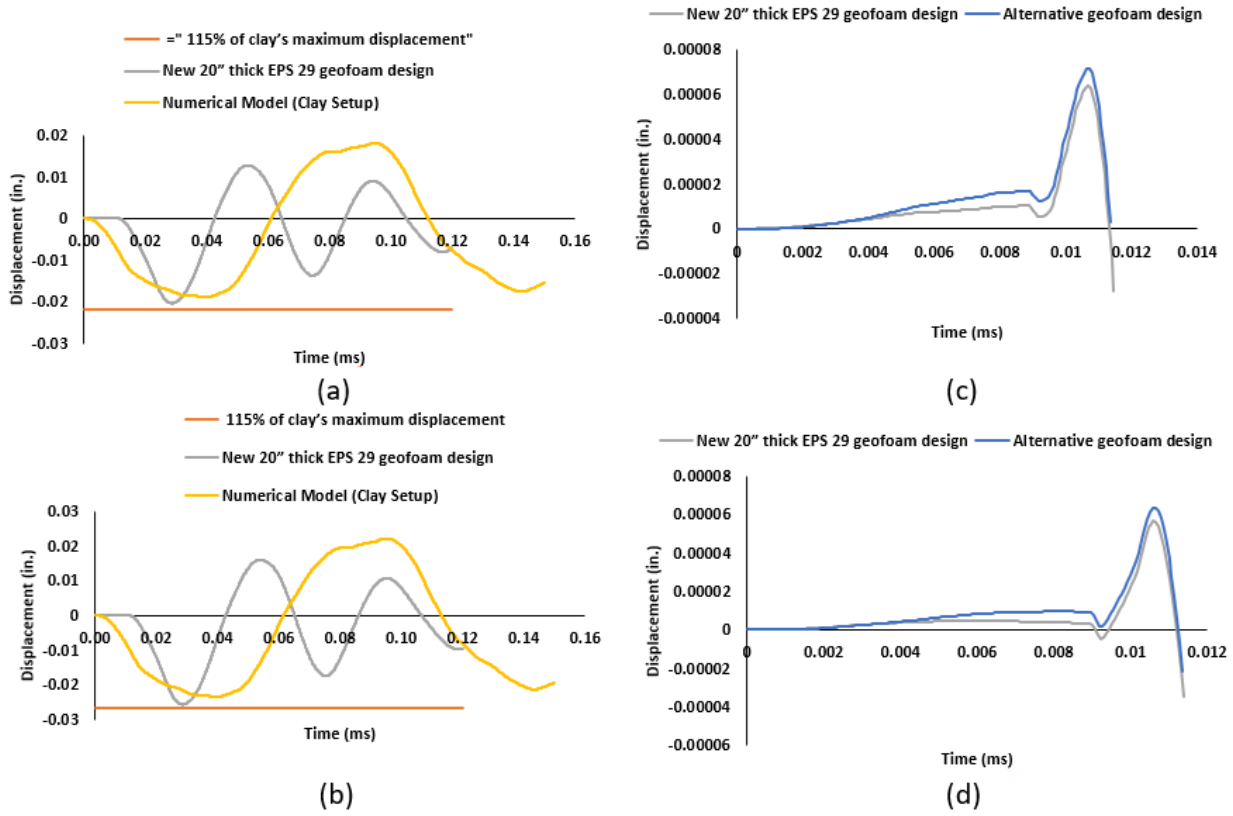

Figure C38. Scenario 19-a) Compares the predicted displacement time history of the new design with the clay setup under 11.55 kip load, b) Compares the predicted displacement time history of the new design with the clay setup under 14.68 kip load, c) Compares the first 0.012 milliseconds of the predicted displacement time history of the new design with the original geofoam setup under 11.55 kip load, d) Compares the first 0.012 milliseconds of the predicted displacement time history of the new design with the original geofoam setup under 14.68 kip load.

Figure C39. A cross-section in X direction for scenario 20-Geofoam EPS 29 (24 in. thick in Z direction).

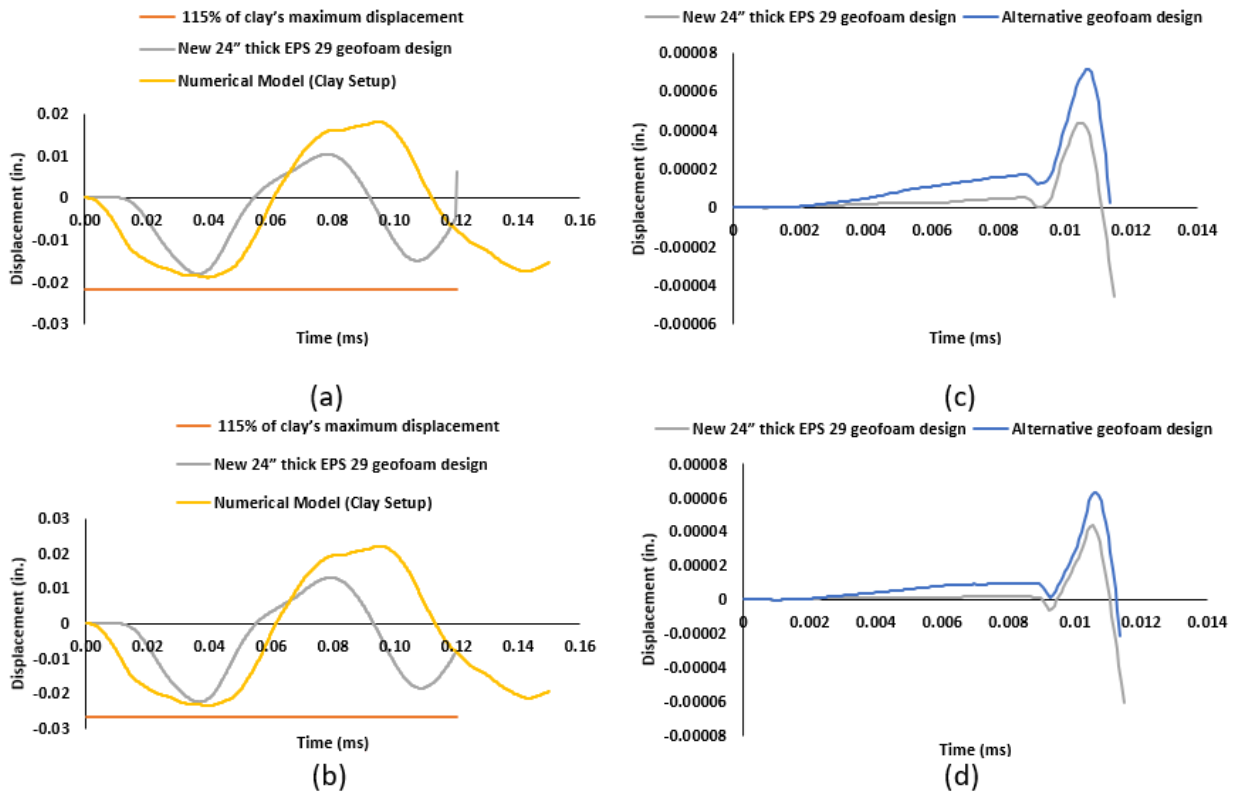

Figure C40. Scenario 20-a) Compares the predicted displacement time history of the new design with the clay setup under 11.55 kip load, b) Compares the predicted displacement time history of the new design with the clay setup under 14.68 kip load, c) Compares the first 0.012 milliseconds of the predicted displacement time history of the new design with the original geofoam setup under 11.55 kip load, d) Compares the first 0.012 milliseconds of the predicted displacement time history of the new design with the original geofoam setup under 14.68 kip load.

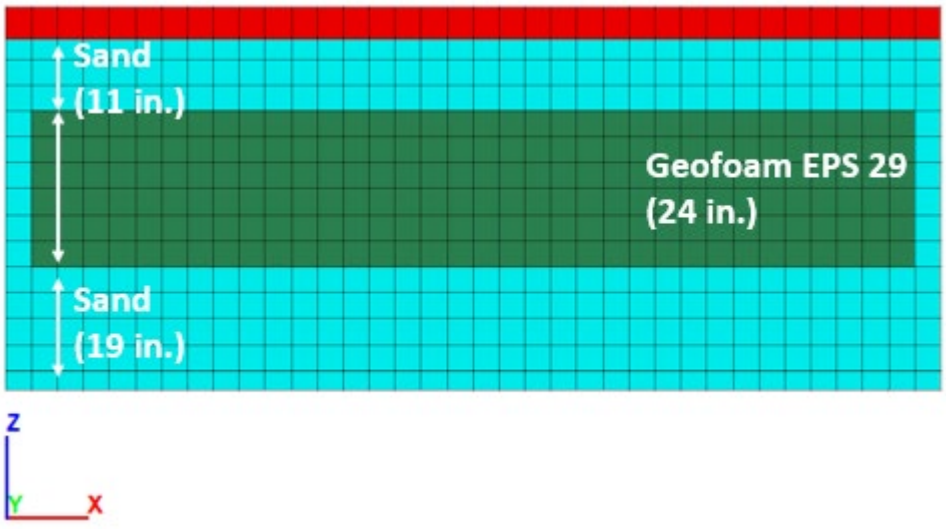

Figure C41. A cross-section in X direction for scenario 21-Geofoam EPS 29 (24 in. thick in Z direction).

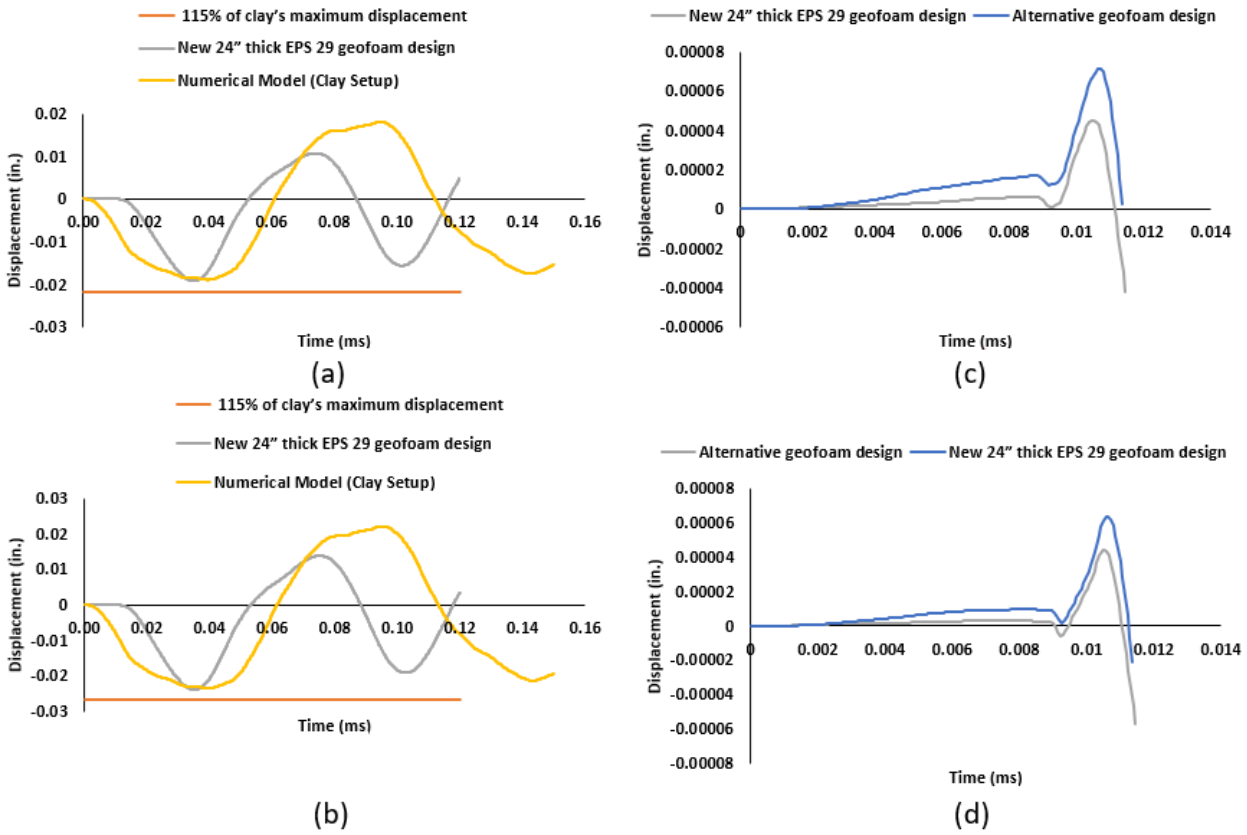

Figure C42. Scenario 21-a) Compares the predicted displacement time history of the new design with the clay setup under 11.55 kip load, b) Compares the predicted displacement time history of the new design with the clay setup under 14.68 kip load, c) Compares the first 0.012 milliseconds of the predicted displacement time history of the new design with the original geofoam setup under 11.55 kip load, d) Compares the first 0.012 milliseconds of the predicted displacement time history of the new design with the original geofoam setup under 14.68 kip load.

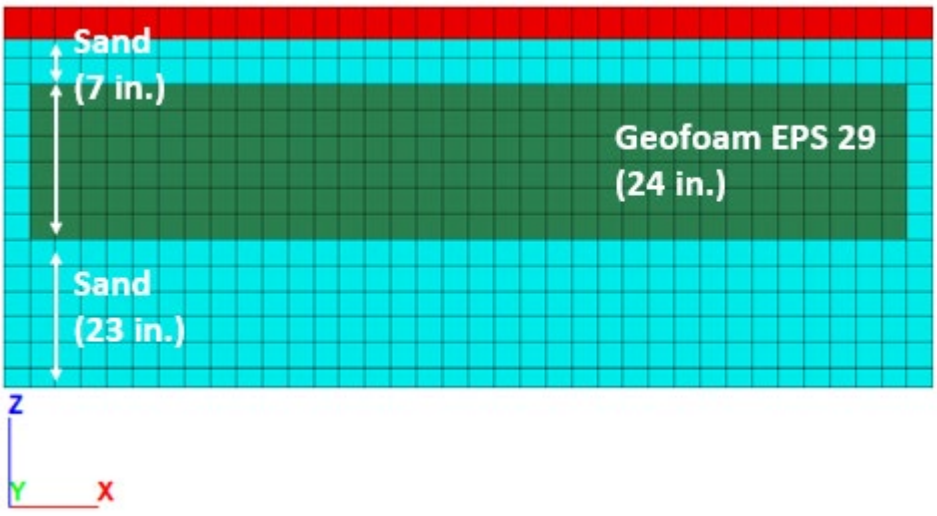

Figure C43. A cross-section in X direction for scenario 22-Geofoam EPS 29 (24 in. thick in Z direction).

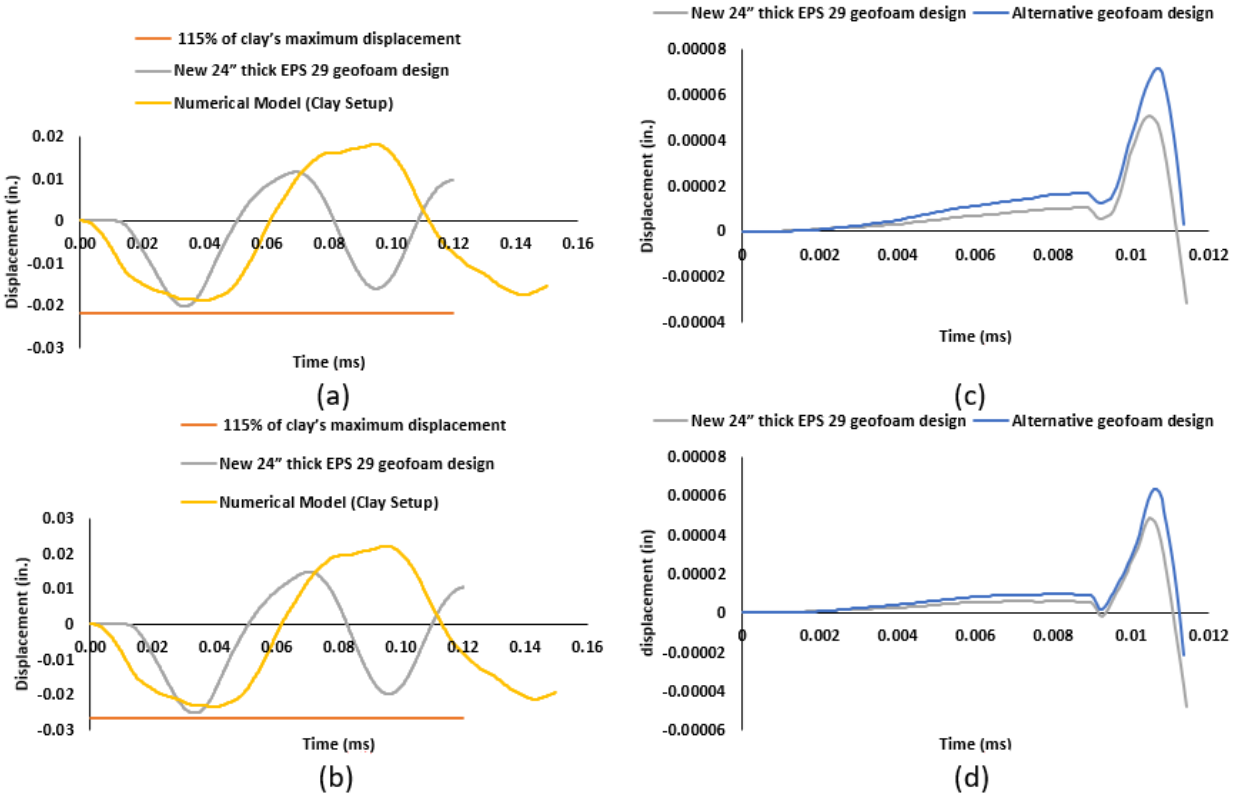

Figure C44. Scenario 22-a) Compares the predicted displacement time history of the new design with the clay setup under 11.55 kip load, b) Compares the predicted displacement time history of the new design with the clay setup under 14.68 kip load, c) Compares the first 0.012 milliseconds of the predicted displacement time history of the new design with the original geofoam setup under 11.55 kip load, d) Compares the first 0.012 milliseconds of the predicted displacement time history of the new design with the original geofoam setup under 14.68 kip load.

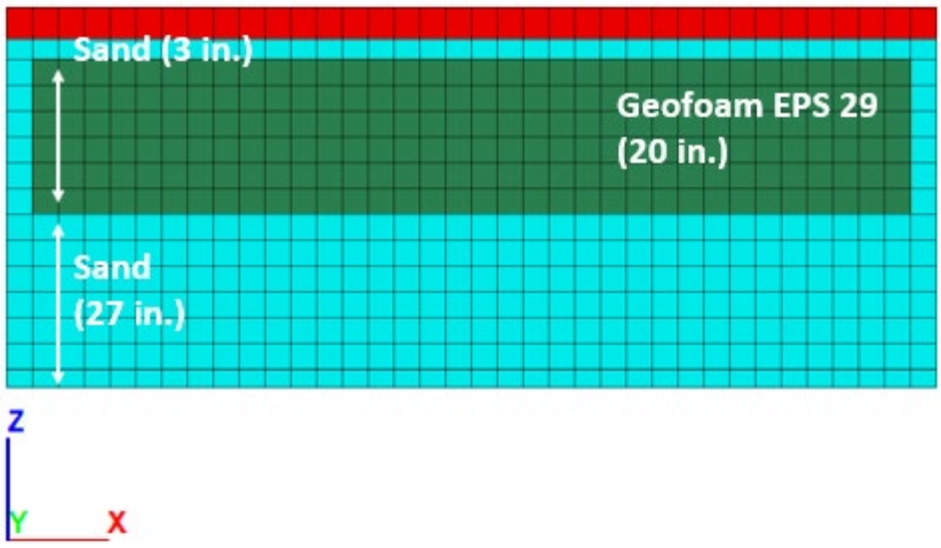

Figure C45. A cross-section in X direction for scenario 23-Geofoam EPS 29 (20 in. thick in Z direction).

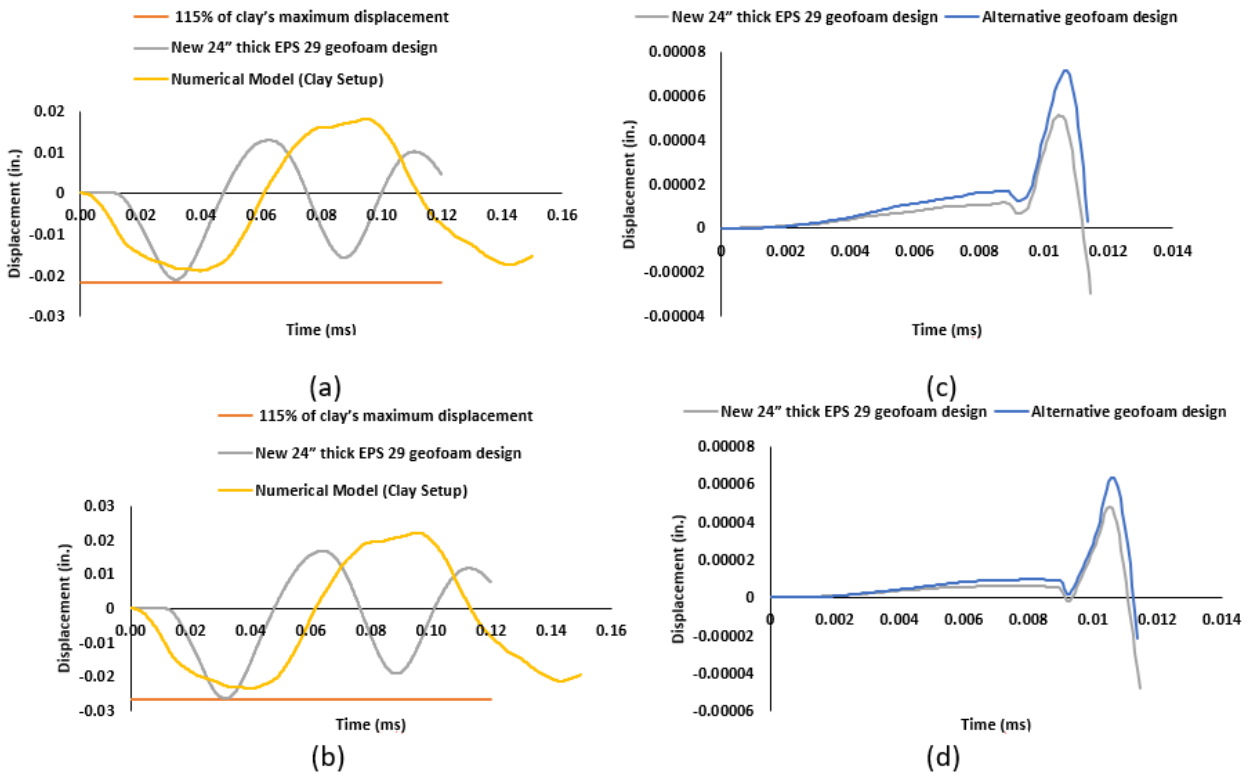

Figure C46. Scenario 23-a) Compares the predicted displacement time history of the new design with the clay setup under 11.55 kip load, b) Compares the predicted displacement time history of the new design with the clay setup under 14.68 kip load, c) Compares the first 0.012 milliseconds of the predicted displacement time history of the new design with the original geofoam setup under 11.55 kip load, d) Compares the first 0.012 milliseconds of the predicted displacement time history of the new design with the original geofoam setup under 14.68 kip load.

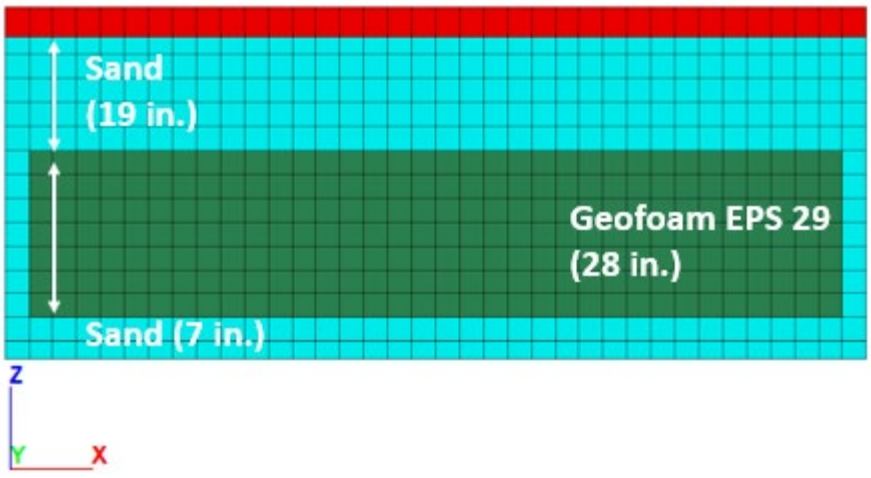

Figure C47. A cross-section in X direction for scenario 24-Geofoam EPS 29 (28 in. thick in Z direction).

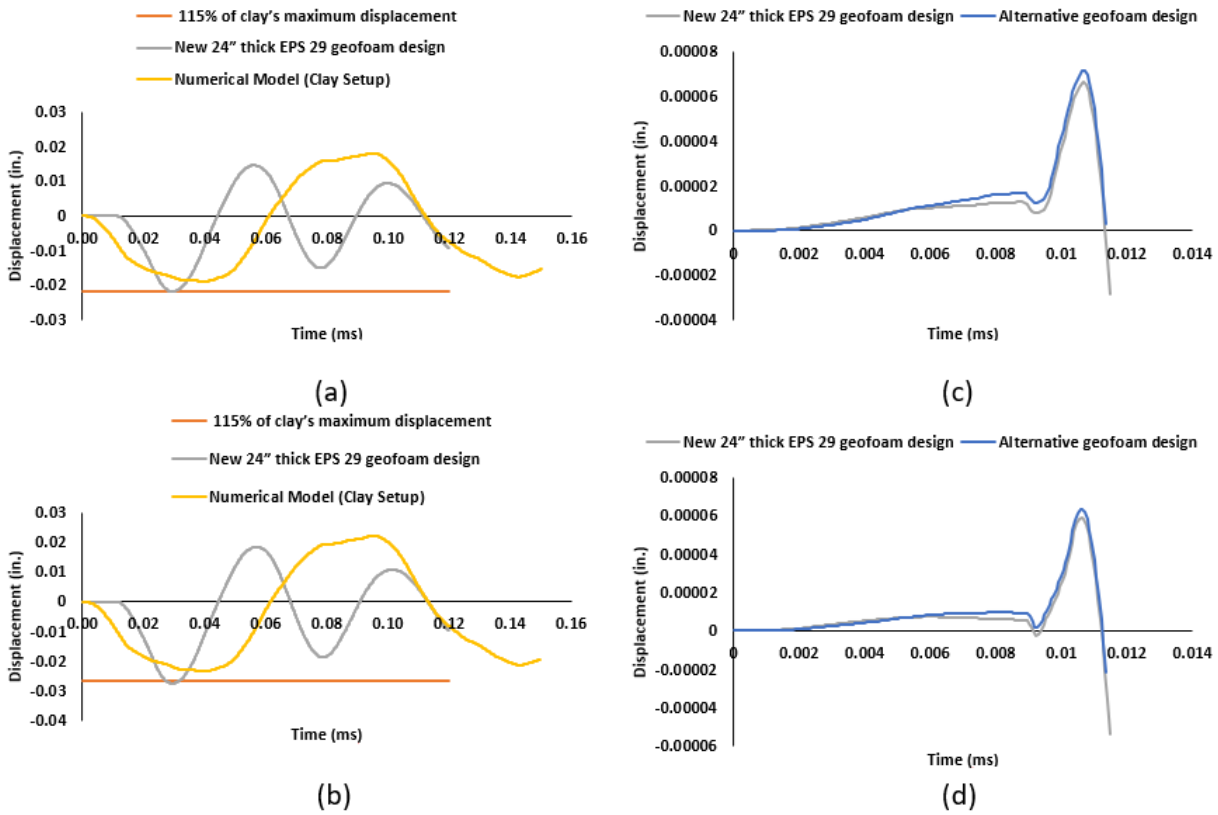

Figure C48. Scenario 24-a) Compares the predicted displacement time history of the new design with the clay setup under 11.55 kip load, b) Compares the predicted displacement time history of the new design with the clay setup under 14.68 kip load, c) Compares the first 0.012 milliseconds of the predicted displacement time history of the new design with the original geofoam setup under 11.55 kip load, d) Compares the first 0.012 milliseconds of the predicted displacement time history of the new design with the original geofoam setup under 14.68 kip load.

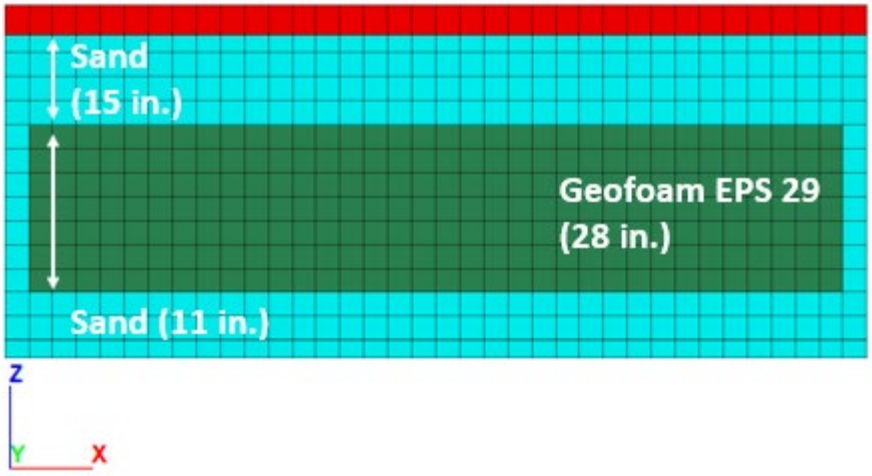

Figure C49. A cross-section in X direction for scenario 25-Geofoam EPS 29 (28 in. thick in Z direction).

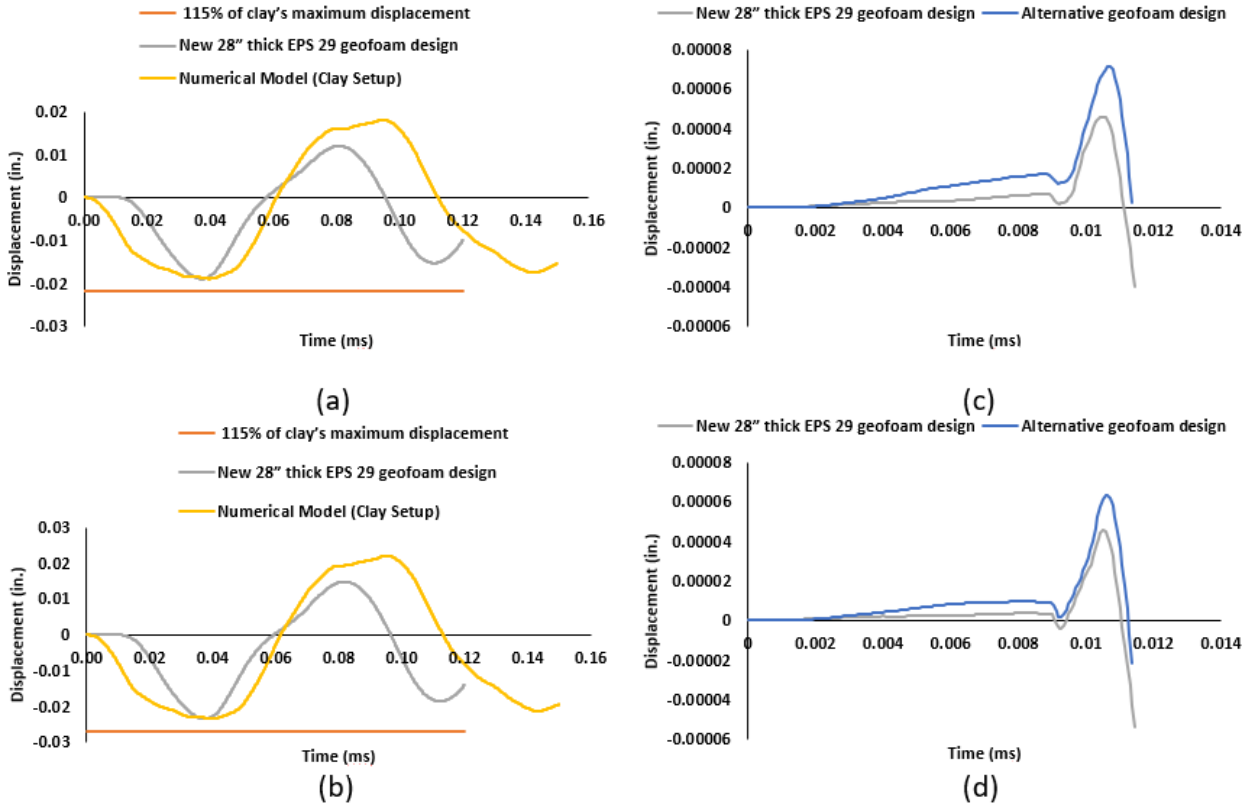

Figure C50. Scenario 25-a) Compares the predicted displacement time history of the new design with the clay setup under 11.55 kip load, b) Compares the predicted displacement time history of the new design with the clay setup under 14.68 kip load, c) Compares the first 0.012 milliseconds of the predicted displacement time history of the new design with the original geofoam setup under 11.55 kip load, d) Compares the first 0.012 milliseconds of the predicted displacement time history of the new design with the original geofoam setup under 14.68 kip load.

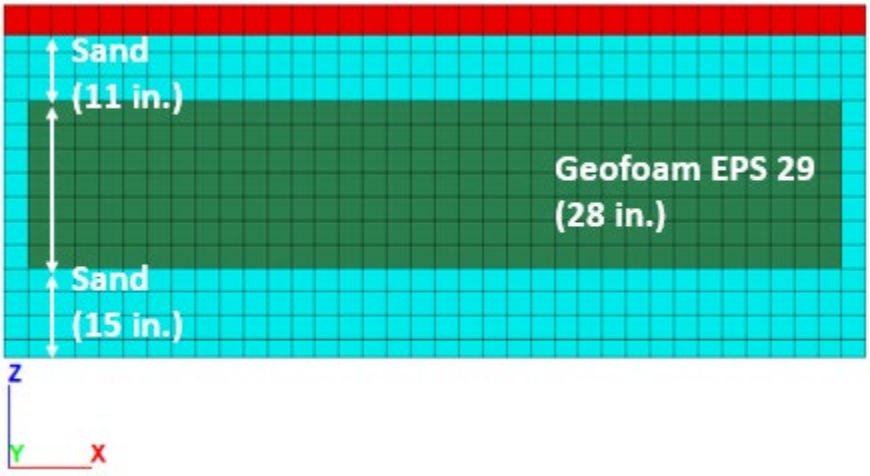

Figure C51. A cross-section in X direction for scenario 26-Geofoam EPS 29 (28 in. thick in Z direction).

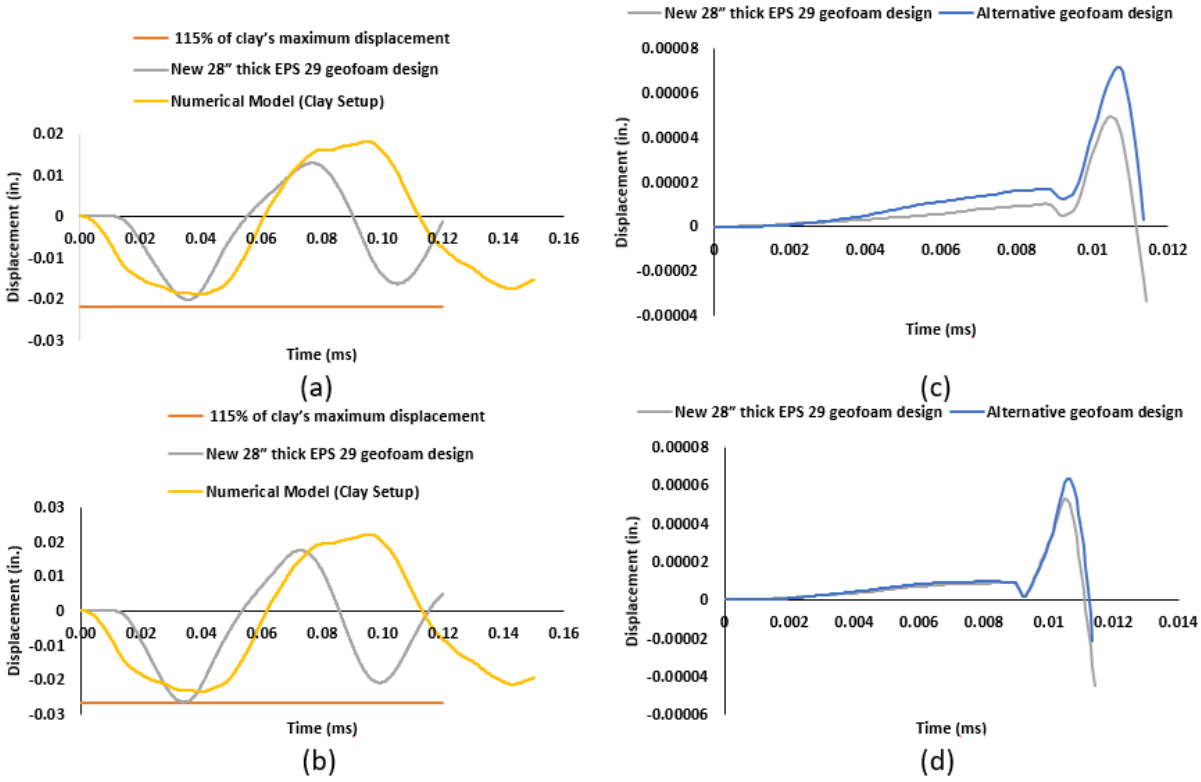

Figure C52. Scenario 26-a) Compares the predicted displacement time history of the new design with the clay setup under 11.55 kip load, b) Compares the predicted displacement time history of the new design with the clay setup under 14.68 kip load, c) Compares the first 0.012 milliseconds of the predicted displacement time history of the new design with the original geofoam setup under 11.55 kip load, d) Compares the first 0.012 milliseconds of the predicted displacement time history of the new design with the original geofoam setup under 14.68 kip load.